INFLUENCE OF DETAILING ON RESPONSE OF DAPPED END BEAMS

by

Ting Peng

April 2009

Department of Civil Engineering and Applied Mechanics

McGill University

Montréal, Canada

A thesis submitted to the Faculty of Graduate Studies

and Research in partial fulfillment of the requirements

for the degree of Master of Engineering

To my parents

Influence of Detailing on Response of Dapped End Beams

Abstract

This research investigated the behaviour of disturbed regions in dapped end beams. In this experimental research programme, two dapped end beams with similar geometry were designed and tested. Each had a span of 3 m, but each of the four different dapped ends utilized a different reinforcing detail. The main parameters studied in this research were the anchorage of the hanger reinforcement and the flexural reinforcement. The dapped ends were detailed in accordance with the provisions of the 2004 CSA Standard A23.3, as well as the 1971 and 1999 PCI Design Handbooks. Strut-and-tie models were used for the design and strength predictions.

The results from the experimental programme are compared with strut-and-tie model predictions. It was concluded that: (1) proper anchorage is essential; (2) the anchorage and the details of hanger steel and longitudinal reinforcement have a great influence on shear capacity and ductility; (3) design using strut-and-tie models for dapped end beams provides a conservative approach; and (4) the early versions of the 1971 and 1999 PCI Design Handbooks gave poor design and detailing requirements.

Influence de la modélisation sur le comportement de poutres à extrémités embouties

Résumé

Cette étude a porté sur le comportement de poutres à extrémités embouties sous contrainte. Dans le cadre de ce programme de recherche expérimentale, deux poutres à extrémités embouties ayant une géométrie similaire ont été conçues et mises à l'essai. Chaque poutre avait une portée de trois mètres, mais l'armature de chacune des quatre extrémités embouties était différente. Les principaux paramètres étudiés dans le cadre de cette recherche étaient l'ancrage principal l'armature de suspente et l'armature de flexion. Les extrémités embouties ont été modélisées conformément aux dispositions de la norme ACNOR A23.3 2004 ainsi que des manuels de conception du PCI. Le modèle de contrefiches et de tirants a servi aux prédictions de conception et de résistance.

Les résultats du programme expérimental sont comparés aux prédictions du modèle de contrefiches et de tirants. Il est conclu que : 1. un ancrage adéquat est essentiel; 2. l'ancrage et les détails de l'acier de suspension et l'armature longitudinale ont une grande influence sur la résistance au cisaillement et la ductilité; 3 la conception utilisant des modèles de contrefiches et de tirants pour des poutres à extrémités embouties représente une approche conservatrice; et 4. les exigences en matière de conception et de modélisation enchâssées dans les versions antérieures (1971 et 1999) des manuels de conception du PCI étaient peu contraignantes.

Acknowledgements

The author would like to express profound gratitude to her supervisor Prof. Denis Mitchell, for his invaluable encouragement, guidance and patient throughout this research work. The author also highly thanks Dr. William D. Cook for his invaluable assistance and suggestions, especially for his technical supervision during the experimental programme.

The experimental programme presented in this research was carried out in the Jamieson Structure Laboratory at McGill University. The author would like to acknowledge technicians Marek Przykorski and John Bartczak for their assistance in the laboratory, especially Ron Sheppard for all his help in the construction. The author also would like to thank her colleagues Michael Egberts and Erin Redl for their help in the construction and useful advice.

The author acknowledges the secretaries of Civil Engineering Department, especially Sandy Shewchuk-Boyd, and Anna Tzagourni.

The author would like to sincerely thank her parents, Mr. Xuewu Peng and Mrs. Jianhua Tong, for their support and encouragement to pursue this degree and their love throughout her life. Finally, the author wishes to express appreciation to her friends: Qian Peng, Helene Tischer and Marc Gregoire for their support.

Ting Peng

April, 2009

Table of Contents

List of Figures

CHAPTER 1 Introduction and Literature Review

CHAPTER 2 Experimental Programme

CHAPTER 3 Test Results

List of Tables

List of Symbols

a shear span of dapped end beams (a distance between vertical reaction force and gravity line of the vertical hanger reinforcement)

A_h horizontal shear reinforcement in the nib of dapped end beams

A_n axial tension reinforcement in the nib

A_s flexural reinforcement in the nib

A_{sh} shear reinforcement at the full-depth beam (vertical hanger reinforcement)

$A_{sh}^{'}$ anchorage reinforcement for the vertical hanger reinforcement

A_v vertical shear reinforcement in the nib of dapped end beams

A_{vf} equal to $A_s + A_n$

A_{vh} the same as A_h

d effective depth of the nib

D effective depth of the full-depth beam

E_s modulus of elasticity of non-prestressed reinforcement

$f_{2\max}$ limiting compressive stress in concrete strut

$f_c^{'}$ specified compressive strength of concrete

f_{cu} limiting compressive stress in concrete strut

f_t tensile stress in reinforcement

f_r	modulus of rupture of concrete
f_u	ultimate tensile strength of reinforcement
f_y	specified yield strength of non-prestressed reinforcement
f_{ys}	yield strength for A_{sh}
f_{yv}	yield strength for A_{vf}
F_i	force in strut or tie i
h	depth of the nib
H	full-depth of the dapped end beam
l_d	development length of reinforcement
l_i	the length of strut of tie i
l_v	shear span of dapped end beams (a distance between vertical reaction force and the face of dapped-ends) in 1971 PCI Design Handbook
T_u	axial force acted on dapped end beam
V_c	shear at diagonal tension cracking
V_n	nominal shear strength
V_p	vertical component of prestress force for tendon anchored in the dapped end
V_s	shear force in web reinforcement near end face of beam
V_u	vertical force acted on dapped end beam
α_s	smallest angle between compressive strut and adjoining tensile ties

ε_1	principal tensile strain in cracked concrete
$\varepsilon_c^{'}$	concrete strain corresponding to specified compressive strength of concrete
ε_{mi}	mean strain in strut or tie i
ε_s	tensile strain in tension tie
ε_{sh}	strain of reinforcement at strain hardening
ε_{rupt}	rupture strain of reinforcement
ε_y	yield strain of reinforcement
μ	coefficient of friction
λ	factor to account for low-density concrete
ϕ	resistance factor applied to a specified material property of to the resistance of a member, connection, or structure, which for the limit state under consideration takes into account the variability of dimensions and material properties, quality of work, type of failure, and uncertainty in the prediction of resistance
θ_s	resistance factor for concrete
ϕ_c	smallest angle between compressive strut and adjoining tensile ties

CHAPTER 1

Introduction and Literature Review

1.1 Introduction

Dapped end beams enable a reduction in the depth of a precast floor or roof structure but the reduced depth part results in a severe stress concentration at the re-entrant corner. It is important to understand the behaviour of dapped end beams such that serviceable and safe designs are attained. In this research programme, two reinforced concrete dapped end beams with four ends were designed and tested to investigate the influence of detailing on the behaviour of disturbed regions. Each end of the dapped end beams has different details, designed using the 2004 CSA Standard A23.3 as well as the 1971 and 1999 PCI Design Handbooks. The main parameters studied in this research were the anchorage of the hanger reinforcement and the flexure reinforcement. Strut-and-tie models were used for designing these specimens. This research shows that dapped end beams designed and detailed in accordance with the provisions of the 1971 and 1999 PCI Design Handbooks resulted in beams with lower shear capacity and ductility.

This chapter gives a brief overview of the 2006 Concorde Bridge collapse, previous research on dapped end beams, design using strut-and-tie models and a review of design requirements in different codes.

1.2 Case Study - Concorde Bridge Collapse

On September 30, 2006, the southern span, a 20-meter-long section, of the overpass on the Boulevard de la Concorde collapsed in Laval (Québec, Canada). The collapse killed five motorists and injured six others. This collapse shocked both the general public and the engineering profession.

1.2.1 Details of Reinforcement

The Concorde Bridge was built in 1970 and was expected to have a life span of 75 years. The design of the Concorde Bridge was carried out in accordance with the codes and standards in effect at that time. They are: (1) Standard Specifications for Highway Bridges, the 8th Edition (American Association of State Highway Officials, AASHO 1961); (2) Design of Highway Bridges (Canadian Standards Association, CAN/CSA-S6-1966); and (3) Design Handbook (Concrete Reinforcing Steel Institute, CRSI 1952).

The design of the de la Concorde overpass was innovative at the time. The use of prestressed concrete box girders made it possible to cross Autoroute 19 with a single span without an intermediate support. The box girders were supported on beam seats and located at the ends of cantilevers (see Fig. 1.1). The innovative design made it nearly impossible to inspect the dapped end thoroughly, as the entire deck would have had to be removed for such an inspection.

The region of the beam seat has a complex flow of stresses due to the concentrated load and the abrupt change in cross section. It is noted as a disturbed region which should be designed using a strut-and-tie model. Figure 1.2 shows the layout of the reinforcing bars in the east abutment cantilever. The U-shaped No.8 hanger bars play a key role in providing a tension tie to lift the load from the pad reaction to the top of the cantilever section. The Canadian Standards Association CSA Standard S6-1966 “Design of Highway Bridges” did not have design provisions for D-regions with a complex flow of stresses. The vertical #8 U-shaped hanger bars act as tension bars near the beam seat and were designed to have sufficient area to provide the necessary tension tie force but were inadequately anchored at the top and bottom of this hanger reinforcement. The hooks of the #8 hanger bars are not anchored around the longitudinal #14 bars (see Fig. 1.2). Mitchell and Cook (2007) indicated that this inadequate anchorage created a weak plane in a crucial part of the cantilever.

The 2007 Commission of Inquiry revealed that certain reinforcing bars of the abutments had not been installed in accordance with the design. Figure 1.3 shows the layout of the reinforcement in the beam seat for the “as designed” and “as-built” cases in the cantilever of the east abutment. In the figure, it illuminates the differences between the “as designed” and “as built” structure, and particularly showed that the hooks of the U-shaped No.8 hanger bars, and the diagonal reinforcing bars were not placed at the same plane as the No.14 bars, but instead were placed under these bars.

1.2.2 The Causes of the Failure

The Commission of Inquiry (2007) concluded that the overpass collapsed due to shear failure in the southeast abutment. This was due to a horizontal plane fracture that had slowly grown over the years. The fracture allowed the part of the abutment below it to break away from the part above, causing the collapse. The three main causes of the fracture and subsequent collapse were:

1 During design, the hanger reinforcement was not properly anchored, causing a weak plane. This did not contravene the code provisions of the time.

2 During construction, the hanger reinforcement was misplaced, exacerbating the design weakness. The contractors and inspecting engineers were blamed by the commission for this cause.

3 A low quality concrete was used in the abutments, causing poor freeze-thaw behaviour, particularly in the presence of de-icing salts.

Three other contributing causes were identified by the committee.

1 All thick reinforced concrete slabs should have shear reinforcing, and this is a deficiency in the existing bridge design code.

2 Proper waterproofing was never installed, even during the bridge repairs done in 1992.

3 Extensive concrete removal and rebar exposure caused during the 1992 repairs caused weakening of the structure.

The Commission of Inquiry (2007) concluded that no single entity or individual can be assigned the responsibility for the collapse. None of the defects or omissions identified could have in itself caused the collapse, which resulted from a chain of causes. The tragic event of September 30, 2006, results from an accumulation of shortcomings: the design codes applicable at the time which would be considered inadequate today; the design itself; the construction work; and the management of the structure during its useful life.

Due to the significant role of the poor detailing in the beam seat region of the Concorde Bridge it was decided to carry out this research study to evaluate the influence of the detailing on the response of dapped end beams.

1.3 B- and D- Regions

In the design of reinforced and prestressed concrete structures, there are two types of regions: flexural (bending) regions (B-regions) and regions near discontinuities (D-regions) (Collins and Mitchell, 1986; Schlaich et al., 1987).

B-regions stand for beam or Bernoulli regions allowing a linear strain distribution which beam theory could apply. D-regions are regions near sections with a discontinuity or disturbance. These discontinuities are caused by abrupt change in cross-sectional dimensions or cross-sectional forces. In these disturbed regions, beam theory does not apply. For D-regions, their strain distribution is significantly nonlinear such as near concentrated loads, corners, bends, openings and other discontinuities (see Fig. 1.4). Figure 1.5 shows the smooth stress trajectories in B-regions have, compared with the rather turbulent stress trajectories in D-regions. This figure also illustrates that the stress intensities decrease rapidly with the distance from the stress concentration. Schlaich, J., Schäfer, K., and Jennewein, M, (1987) reported that B and D regions in a structure could be identified by this behaviour and proposed a procedure to find the division lines between B- and D- regions. Figure 1.6 shows the results of the identification of B- and D-regions with respect to their load bearing behaviour. In this method, it demonstrates that both geometry and loads must be considered for proper classification. Whereas, St. Venant's principle suggests that the localized effect of a disturbance dies out in about one member depth from the point of the disturbance.

Clause 11.2.1.1 of the 1984 CSA Standard CAN3-A23.3-M84 (CSA, 1984) indicates that for B-regions, the members shall be designed for shear either by the simplified method of Clause 11.3 or the general method of Clause 11.4. In Clause 11.4.7 it states that regions, where shear stresses could not be assumed to be uniformly distributed over the depth, shall be idealized as trusses consisting of concrete compressive struts and reinforcing steel tension ties interconnected by nodal zones. AASHTO LRFD Specifications in section 5.8.1.1(AASHTO, 2004) permit the use of either traditional sectional models (section 5.8.3) or the strut and tie model (section 5.6.3) for B-regions, and require the use of the strut and tie model (section 5.8.1.2) for D-regions. Schlaich, J., Schäfer, K., and Jennewein, M, (1987) stated that the preferred concept of D-region design is to use the strut-and-tie model approach. The B-regions are designed with truss models as a special case of a strut-and-tie model. The analysis method for B- and D-regions and some guidance for the design of statically indeterminate structures were proposed (see Tables 1.1 and 1.2).

Table 1.1 Analysis leading to stresses or strut-and-tie forces (Schlaich et al, 1987)

<table>
<tr><td colspan="2" rowspan="2">Structure
Analysis</td><td colspan="3">Structure consisting of:</td></tr>
<tr><td colspan="2">B- and D- regions
e.g., linear structures, slabs and shells</td><td>D-regions only
e.g., deep beams</td></tr>
<tr><td colspan="2" rowspan="3">Overall structural analysis
(Table 1.2) gives:</td><td>B-regions</td><td>D-regions</td><td>D-regions</td></tr>
<tr><td rowspan="2">Sectional effects
M, N, V, M_r</td><td colspan="2">Boundary forces:</td></tr>
<tr><td>Sectional effects</td><td>Support reactions</td></tr>
<tr><td rowspan="3">Analysis of
Inner forces
Or stresses
In individual regions</td><td>State I
(uncracked)</td><td>Via sectional values
$A, J_{B,} J_T$</td><td colspan="2">Linear elastic analysis*
(with redistributed stress peaks)</td></tr>
<tr><td rowspan="2">State II
(cracked)</td><td colspan="3">Strut-and-tie models
and/or nonlinear stress analysis*</td></tr>
<tr><td>Usually tress</td><td colspan="2"></td></tr>
</table>

*maybe combined with overall analysis

Table 1.2 Overall structural behaviour and method of overall structural analysis of statically indeterminate structures. (Schlaich et al, 1987)

<table>
<tr><td rowspan="2">Limit state</td><td>Overall structural behaviour</td><td colspan="2">Corresponding method of analysis of sectional effects and support reactions</td></tr>
<tr><td></td><td>Most adequate</td><td>acceptable</td></tr>
<tr><td rowspan="2">serviceability</td><td>Essentially uncracked</td><td>Linear elastic</td><td></td></tr>
<tr><td>Considerably cracked, with steel stresses below yield</td><td>Nonlinear</td><td>Linear elastic (or plastic if design is oriented at elastic behaviour</td></tr>
<tr><td>Ultimate capacity</td><td>Widely cracked, forming plastic hinges</td><td>Plastic with limited rotation capacity or elastic with redistribution</td><td>Linear elastic or nonlinear or perfectly plastic with structural restrictions</td></tr>
</table>

1.4 The Strut-and-Tie Model Design Approach

The strut-and-tie model is a system of forces in equilibrium with a given set of loads consisting of concrete compressive struts, steel tension ties, and nodal zones (see Fig 1.7). It permits a clearer understanding of the behaviour of structural concrete, and codes based on such an approach would lead to improved structures. There is no unique strut-and-tie model and the most direct path for loads to travel to the supports will be the most efficient model.

1.4.1 Development of the Strut-and-Tie Model Approach

At the beginning, Ritter (1899) and Mörsch (1909) introduced the truss analogy method for shear design of B-Regions. The truss model idealizing the flow of force in a cracked concrete beam has also been used as the design basis for torsion. This method was later further refined by Kupfer (1964) and Thurlimann et al (1983). Schlaich et al (1984) and Marti (1985) promoted the use of truss model in D-Regions. Marti (1985) created its scientific basis for a rational application in tracing the concept back to the theory of plasticity. Collins and Mitchell developed the first general design approach using strut-and-tie models for the 1984 CSA Standard. The strut-and-tie model first appeared in codes in 1984, with the strut-and-tie design provisions in Clause 11.4.7 of the 1984 CSA Standard CAN3-A23.3-M84 (CSA, 1984) and this method was introduced in the following editions: 1994 CSA Standard (CSA, 1994) and 2004 CSA Standard (CSA, 2004). The first complete design examples using the strut-and-tie model approach of the 1984 CSA Standard were given by Collins and Mitchell in the CPCA Concrete Design Handbook (1985). This design method was also adopted by the AASHTO LRFD Bridge Design Specifications in 1994 (AASHTO, 1994) and 2004 (AASHTO, 2004). Mitchell et al (2004) provided complete design examples of disturbed regions in bridge structures, including dapped end beams. The strut-and-tie model has been included as an alternative design procedure in Appendix A of the 2002 ACI code (ACI, 2002).

Table 1.3 shows stress limits defined in 2002 ACI Code and 1984 CSA Specifications, respectively. Due to uncertainties associated with defining the characteristics of an idealized truss, they have different rules in their provisions and guidelines.

Table 1.3 Stress limits according to 1984 CSA and 2002 ACI

<table>
<tr><td></td><td colspan="2">Stress limits</td></tr>
<tr><td></td><td>1984 CSA</td><td>2002 ACI</td></tr>
<tr><td>Nodal zones</td><td>For CCC node: $0.85\phi_c f_c^{'}$
For CCT node: $0.75\phi_c f_c^{'}$
For CCC node: $0.65\phi_c f_c^{'}$
ϕ_C =0.6 for concrete</td><td>$f_{cu} = 0.85\beta_n f_c^{'}$
For CCC node: $\beta_n = 1.0$
For CCT node: $\beta_n = 0.8$
For CCC node: $\beta_n = 0.6$</td></tr>
<tr><td>Compression struts</td><td>$f_{cu} = \frac{f_c^{'}}{0.8 + 170\varepsilon_1} \leq 0.85 f_c^{'}$
$\varepsilon_1 = \varepsilon_s + (\varepsilon_s + 0.002)\cot^2\alpha_s$
α_s is the smallest angle between the compressive strut and the tension tie
ε_s can be conservatively taken as f_y / E_s</td><td>$f_{cu} = 0.85\beta_s f_c^{'}$
β_s =1.00 for prismatic struts in uncracked compression zones
β_s =0.40 for struts in tension members
β_s =0.75 struts may be bottle shaped and crack control reinforcement is included
β_s =0.60 struts may be bottle shaped and crack control reinforcement is not included
β_s =0.60 for all other cases</td></tr>
</table>

1.4.2 Previous Research on Strut-and-Tie Models

Mörsch (1909) proposed the concept of using uniaxially stressed truss members to model the complex stress flow in cracked reinforced concrete. Schlaich, Schäfer and Jennewein (1987) studied the elastic stress fields in D-regions and investigated the use of strut-and-tie model to present these elastic stress flows. Marti (1985) indicated that it is important to formulate the actual dimension of the compressive struts and tension ties in strut and tie models. Collins and Mitchell (1986) developed a simple design approach for D-regions based on a strut-and-tie model. They modelled the regions of high unidirectional compressive stress in concrete as compressive struts and modelled principal reinforcement as tension ties. The regions where struts and ties meet were modelled as nodal zones (see the example of strut-and-tie model for deep beam in Fig. 1.8). They also summarized the main steps for design of a D-region using strut-and-tie model as follows:

1. Sketch the flow of forces and locate the nodal zone;
2. Determine the truss model;
3. Choose the required area of tension tie reinforcement;
4. Check nodal zone stresses (see Fig. 1.8);
5. Check compressive stress ($f_{2\max}$) limits using strain compatibility and strain softening of the concrete in compression:

$$f_{2\max} = \frac{\lambda \phi_c f_c^{'}}{0.8 + 170\varepsilon_1} \leq \lambda \phi_c f_c^{'}$$

$$\varepsilon_1 = \varepsilon_s + (\varepsilon_s + 0.002)\cot^2 \theta_s$$

   Figure 1.9 illustrates the manner in which $f_{2\max}$ changes as θ_s changes. From this figure, it is noted that $f_{2\max}$ reduces as θ_s decreases.

6. Provide adequate anchorage and secondary reinforcement to control cracking and insure ductility.

Schlaich et al (1987) concluded that it was important to ensure the load transfer between struts by checking the nodal regions. Modelling and dimensioning is an iterative process. They also proposed three types of struts (C), ties (T) and four types of nodes based on the combination of C and T. The four types of nodes are: CCC, CCT, CTT, and TTT (see Fig. 1.10). Figure 1.11 illustrates three typical configurations for compression fields: the “fan”;

the “bottle” and the “prism” or parallel stress field (special case of shear span a = 0 or a/d = 1).

The AASHTO LRFD Specifications (AASHTO, 2004) prescribed simple straight-line struts instead of using curved compressive struts to model the flow of compression, and used additional uniformly distributed horizontal and vertical reinforcement (section 5.6.3.6) (see Fig. 1.12) to control cracking in the D- regions. The straight-line compressive struts are assumed to act along the center of the flow of the compressive stresses. Each vertical tension tie represents the tension forces in a number of stirrups over a certain length. This code used the strut-and-tie model from the CSA Standard A23.3. A number of design examples of disturbed regions in bridge structures are given by Mitchell et al (2004).

Schlaich et al (1987) proposed the load path method to develop strut-and-tie model and also developed strut-and-tie models for complicated cases which is the combination of an elastic finite element method analysis with the load path method. Figure 1.13 presents an example of this combined approach. They proposed a formulation as a criterion to determine the optimal strut-and-tie model, which is

$$\sum F_i l_i \varepsilon_{mi} = Minimum$$

(Where F_i is the force in strut or tie i, l_i is the length of member i, ε_{mi} is the mean strain of member i). This criterion could be helpful to eliminate less desirable models (see Fig. 1.14).

Cook and Mitchell (1988) compared the analyses of disturbed regions using strut-and-tie models with the predictions of nonlinear finite element analyses and with test results. The results showed that the strut-and-tie models provided conservative estimates of the D-regions at ultimate stress. Collins and Mitchell (1990) summarized the design of D-regions including the design approach and examples using strut-and-tie models.

1.5 Dapped End Beams - Research and Design

1.5.1 Research on Dapped End Beams

Werner and Dilger (1973) proposed that the shear could be predicted at which diagonal tension cracking would occur at the re-entrant corner and the shear strength of the dapped end could be calculated using:

$$V_n = V_c + V_p + V_s$$

Where,

V_c = shear at diagonal tension cracking

V_p = vertical component of prestress force for tendon anchored in the dapped end

V_s = shear force in web reinforcement near end face of beam

Hamondi and Phang (1974) conducted six prototype prestressed concrete T-beams with variables included: (1) geometry of the dapped ends; (2) type of web reinforcement in dapped regions; (3) ratio of shear span to depth of beam; and (4) prestress level. The results indicated that shear strength of prestressed concrete beams can be predicted with reasonable accuracy, and that dapped regions with inclined prestressed high-strength steel bars could control shear cracking at the working load.

Mattock and Chan (1979) provided an improved understanding of the behaviour of dapped-end beams both at service load and at ultimate and developed a rational design procedure. Eight dapped ends were designed and tested. Four specimens were being subjected to vertical load only, and the other four being subjected to a combination of vertical and horizontal loads. The conclusions given by Mattock and Chan (1979) are summarized below:

1. The dapped end of the beam may be designed as a corbel. The shear span, a, was defined as the distance from the centre of action of the vertical load to the center of gravity of the hanger reinforcement of area, A_{vh}.
2. Closed stirrups should be placed close to the end of the full-depth beam to resist the vertical component of the inclined compression force in the nib and must be positively anchored at both top and bottom.
3. Sufficient reinforcement must satisfy moment and force equilibrium requirements across two potential inclined cracks AY and BZ in Fig. 1.15.
4. The main nib reinforcement, A_s, should be provided with a positive anchorage and extend into the beam with a distance of $H - D + l_d$ beyond the re-entrant corner to develop its yield strength at the diagonal tension crack BZ.
5. The horizontal stirrups of area, A_h, in the nib should be positively anchored near the end face of the beam and as recommended in the 1978 PCI Design Handbook, the effective length should extend beyond the re-entrant corner a distance of $1.7\,l_d$.

Mattock and Theryo (1986) investigated five dapped end reinforcement details to attain a better understanding of the behaviour of dapped ends and to develop simple reinforcing details that are economical and easy to fabricate. The experimental results showed that the reinforcing details using inclined hanger reinforcement provided better control of cracking than using vertical hanger reinforcement. It was found that draping half of the prestressing strands through the nib of the dapped end significantly reduced reinforcement stresses and associated cracking at service load. They recommended that not less than half the prestressing strands be draped though the nib. The hanger reinforcement was effectively anchored with a 180 degree loop and having a minimum bend diameter of six bar diameters. Mattock and Theryo (1986) suggested that it is preferred to ensure a concentric or near concentric arrangement of hanger reinforcement. Mattock and Theryo (1986) also proposed that the nominal shear strength V_n is taken equal to V_c for the full depth section adjacent to a dapped end (where V_c is the lesser of V_{ci} and V_{cw}, calculated for the section distance h/2 from the end of the full depth section. The results indicated that the effect of the horizontal tension force in the nib must be added into account when calculate V_{ci} and V_{cw} in the 1977 ACI Code.

Cook and Mitchell (1988) presented experimental results from a number of tests on disturbed regions, including results for dapped end beams. They also provided strut-and-tie models for the design of these regions. These experimental results provided verification of the strut-and-tie model design approach proposed by Collins and Mitchell (1986) that was included in the 1984 CSA A23.3 Standard (CSA 1984).

In 1998 ASCE-ACI Committee 445 (Ramirez et al 1998) published a state-of-the-art report titled “Recent Approaches to Shear Design of Structural Concrete”. Chapter 6 of this report summarizes the state-of-the-art for “Design with Strut-and-Tie Models”.

The 2002 ACI Special Publication on “Examples for the Design of Structural Concrete with Strut-and-Tie Models” provides experimental results for the behaviour of dapped end beams (Mitchell et al, 2002 and Sanders 2002). These examples show how strut-and-tie models are capable of predicting the responses of dapped end beams.

1.5.2 CPCI and PCI Handbook Design Requirements

The reinforcement detailing provided in 1971 PCI Design Handbook is presented in Fig.1.16. The design requirements are limited as following:

$$A_{vf} = \frac{1}{\phi f_{yv}}[\frac{V_u}{\mu} + T_u]$$

$$A_{sh} = \frac{A_{vf}(f_{yv})}{\mu f_{ys}}$$

Where $T_u \geq 0.2V_u$; $\phi = 0.85$

f_{yv} = yield strength for A_{vf}

f_{ys} = yield strength for A_{sh}

Additional precautions that should be taken were: A_{vf} should have positive anchorage by welded cross bars or by welding to confinement angles; additional horizontal bars, $A_{vh} = A_{vf} / 2$; the closed ties should be placed by paralleling to both the top and the bottom longitudinal reinforcement as shown in the Fig. 1.16; the effective length for the A_{vh} is $1.5 l_d$; the shear span ratio of l_v /d should not exceed 0.4; and h should not be less than one half the overall depth of the beam.

1978 PCI Design Handbook states that the design requirement for dapped-end connections should investigate several potential failure modes. See Fig. 1.17, the reinforcement requirement were listed for each consideration,

1. Flexure reinforcement A_s and axial tension reinforcement A_n should be used to provide flexure and axial tension in the dapped ends.
2. Shear friction reinforcement A_s , A_{vh} and axial tension reinforcement A_n should be used to provide direct shear at the junction of the dap and the main body of the member.
3. Shear reinforcement $A_{sh} = \frac{V_u}{\phi f_{ys}}$ should be provided to resist diagonal tension cracking starting from the re-entrant corner.

4. Shear reinforcement A_{vh} and A_v should be used to provide diagonal tension in the dapped ends.
5. If plain concrete bearing strength is exceeded, shear friction reinforcement A_s should be used.

Note: the reinforcement requirements are not cumulative but the greater among all considerations.

Additional precautions that should be taken were: horizontal bars A_s and A_n should have a minimum effective length of $1.7\,l_d$ past the end of the dap and require to be anchored at the end of the beam by welding to cross bars, angles or plates; horizontal bars A_{vh} should be extended a minimum of $1.7\,l_d$ past the end of the dap and anchored at the end of the beam by hooks or other suitable means; vertical hanger bars A_{sh} and shear reinforcement A_v should be properly anchored by hooks as required by ACI 318-77; the depth of the dapped end should not be less than one-half the depth of the beam; vertical hanger bars, A_{sh}, should be placed as closely as practical to the re-entrant corner.

The design requirements of dapped end beams from the 1982 CPCI have slightly changed from the 1978 PCI Design Handbook. In the codes, shear reinforcement A_v is not included in the design requirements. The shear span, a, is the distance between the vertical action force with the gravity centerline of hanger reinforcement and $\frac{a}{d} \le 1$. Additional consideration in the 1982 CPCI is that the hanger reinforcement, A_{sh}, must be positively anchored at the top and bottom and the bottom longitudinal reinforcement at the full-depth section should have a total area not less than that of the hanger reinforcement. Moreover, these bottom longitudinal bars should be positively anchored at their outer ends and extend $1.7\,l_d$ into the beam (see Fig. 1.18). Another difference from

1978 PCI Design Handbook is that the effective lengths for A_s and A_n have changed to $H-d+l_d$ instead of 1.7 l_d .

The 1985 PCI Design Handbook added an alternative effective length of the horizontal bars A_s to be l_d past crack 5 on the design requirements compared to 1978 PCI Design Handbook (see Fig. 1.19).

In the 1999 PCI Design Handbook, the effective lengths have changed to l_d from 1.7 l_d (see Fig. 1.20). An alternative scheme proposed in the PCI Design Handbook: hanger reinforcement, A_{sh} , may be bent and continued parallel to the beam bottom, or separate horizontal reinforcement $A_{sh}^{'} \geq A_{sh}$ must be provided and extended at least l_d beyond crack 5 (see Fig. 1.20). The $A_{sh}^{'}$ may be anchored on the end of full-depth section by welding it to a plate, angle or cross bar.

1.6 Research Objectives

(1) To study the behaviour of dapped end beams with different detailing.

(2) To evaluate the effectiveness of proper anchorage.

(3)To investigate the proper hanger reinforcement details.

(4) To evaluate the design requirements and reinforcement details in older versions of standards and codes.

(5) To compare the experimental results with strut-and-tie predictions.

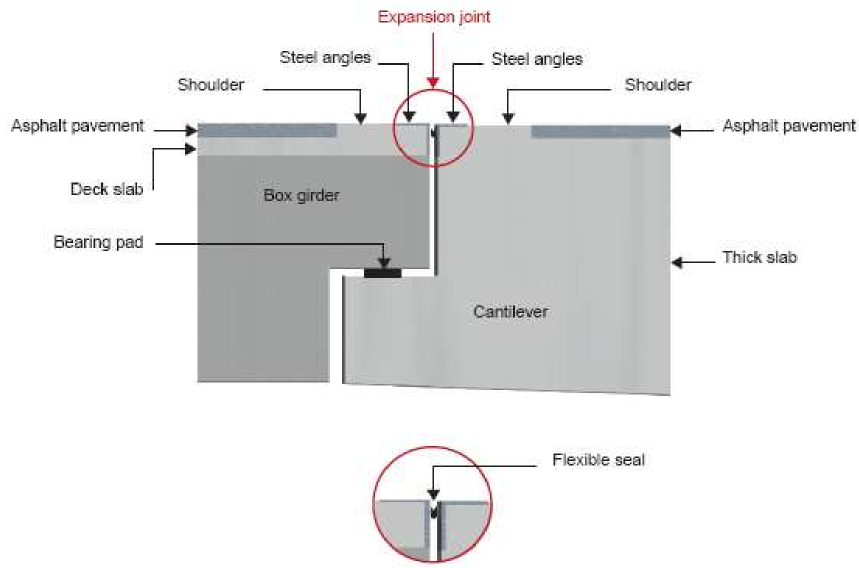

Figure 1.1 The expansion joints at the dapped end and beam seat
(Commission of Inquiry, 2007)

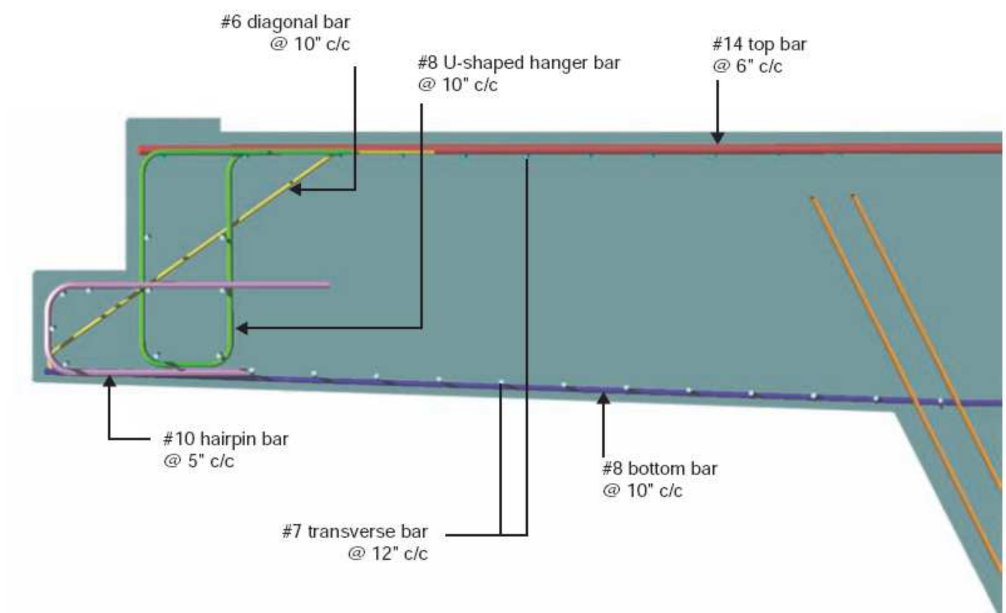

Figure 1.2 Layout of the reinforcing bars in the east abutment cantilever
as specified on the "as designed" drawings
(Commission of Inquiry, 2007)

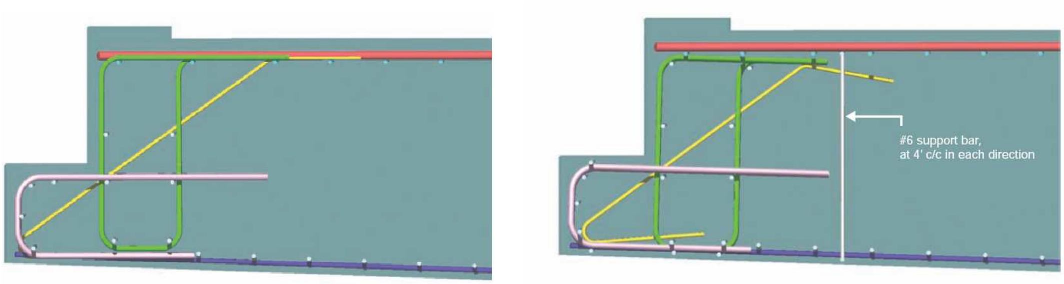

a) "As-designed" b) "As-built"

Figure 1.3 Layout reinforcement in the beam seat
(Commission of Inquiry, 2007)

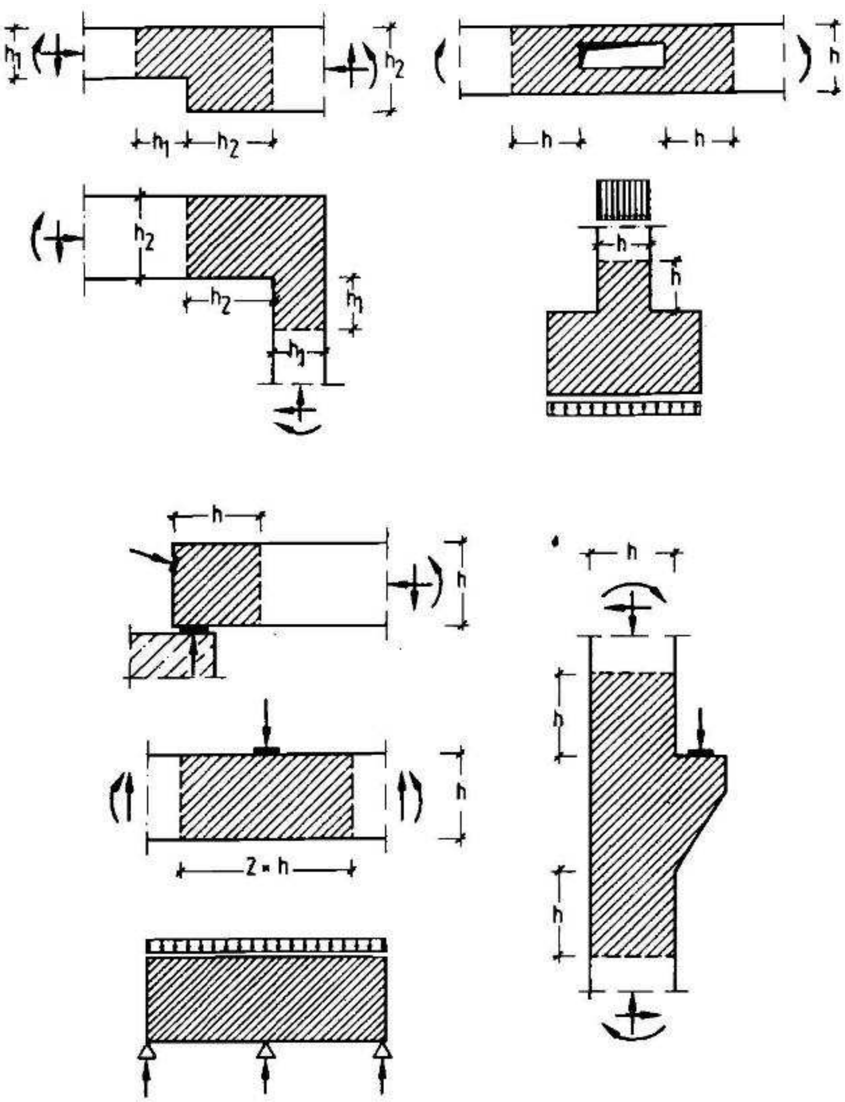

Figure 1.4 Examples of D-regions (Schlaich, 1987)

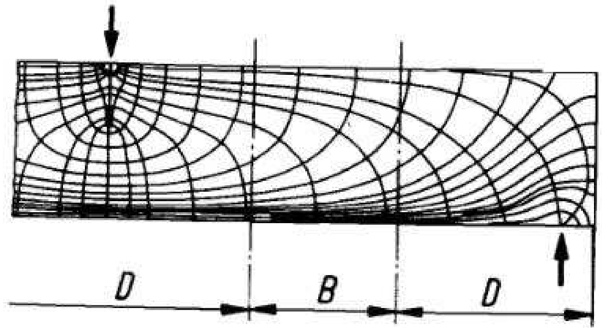

Figure 1.5 Stress trajectories in a B-region and near D- regions (Schlaich, 1987)

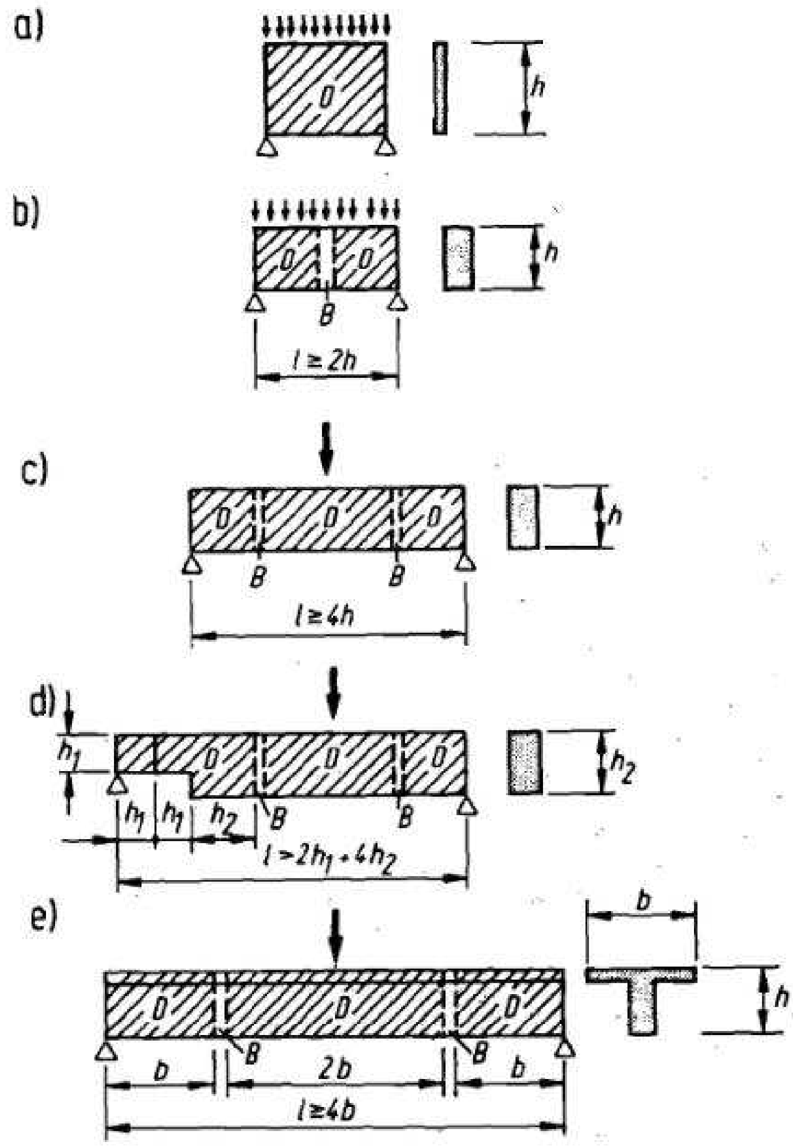

Figure 1.6 The identification of B- and D- regions (Schlaich et al, 1987)

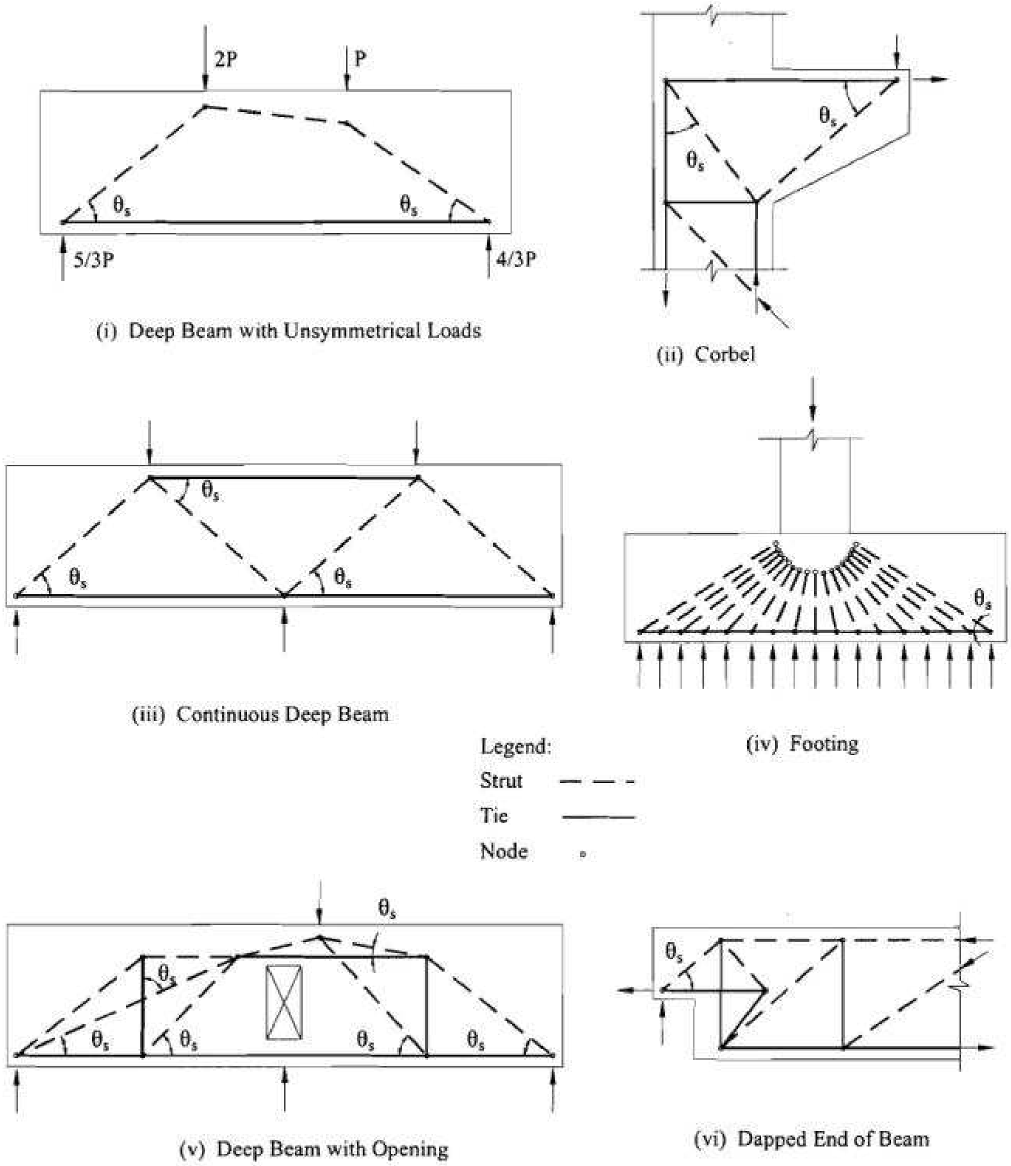

Figure 1.7 Examples of strut-and-tie models (CAC, 2005)

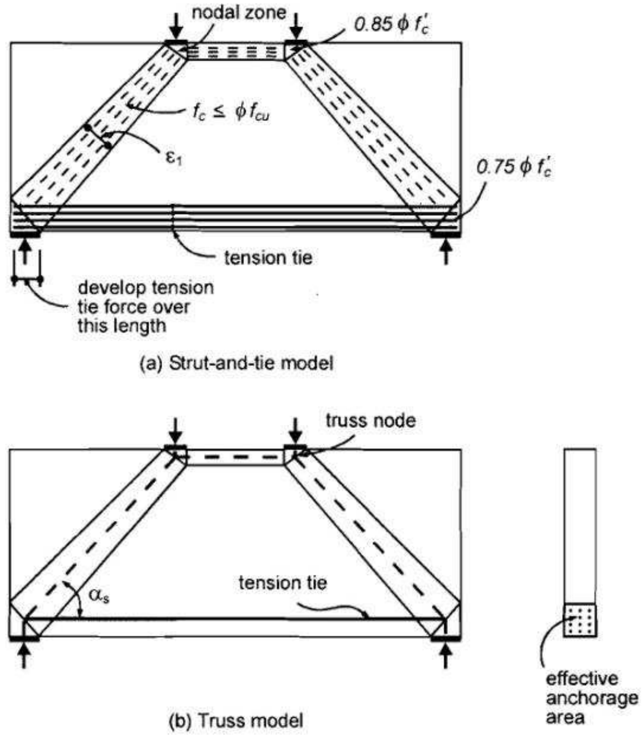

Figure 1.8 Strut-and-tie model and idealized truss model for deep beam (Collins and Mitchell, 1986)

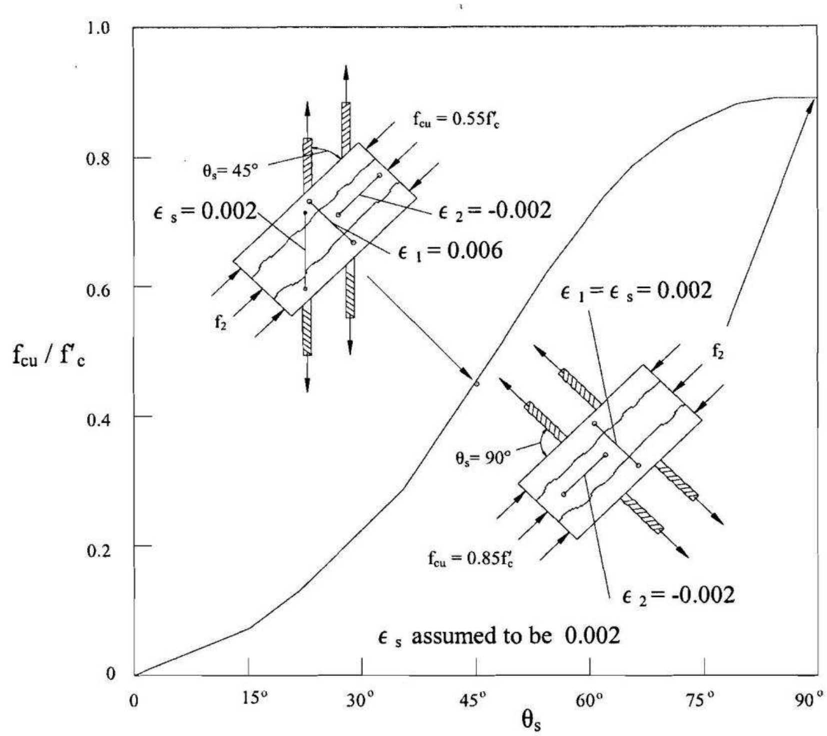

Figure 1.9 Crushing strength of compressive strut versus orientation of tension tie passing through strut (Collins and Mitchell, 1986)

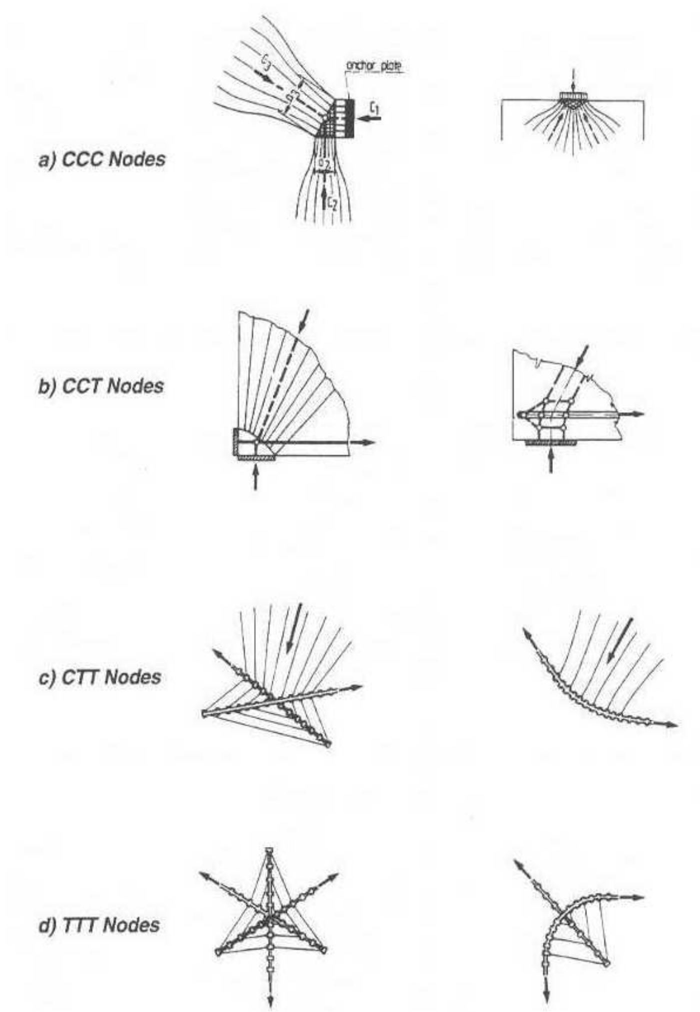

Figure 1.10 Types of singular nodes (Adapted from Schlaich et al, 1987)

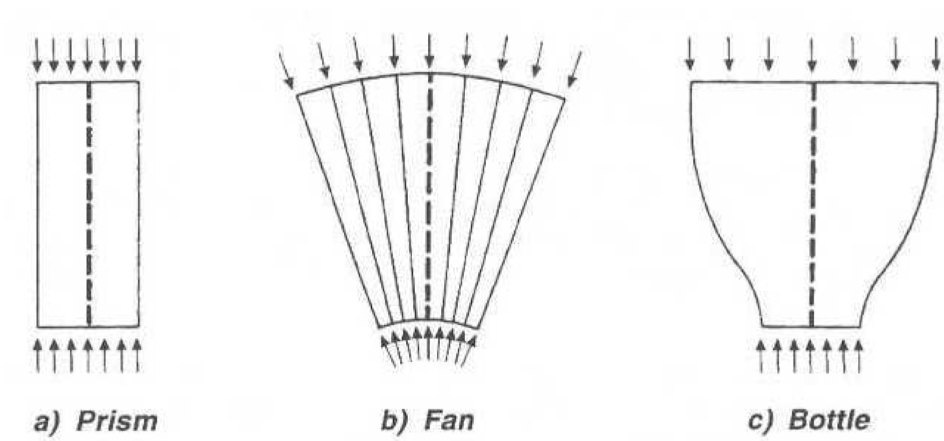

Figure 1.11 Types of Struts (Adapted from Schlaich et al, 1987)

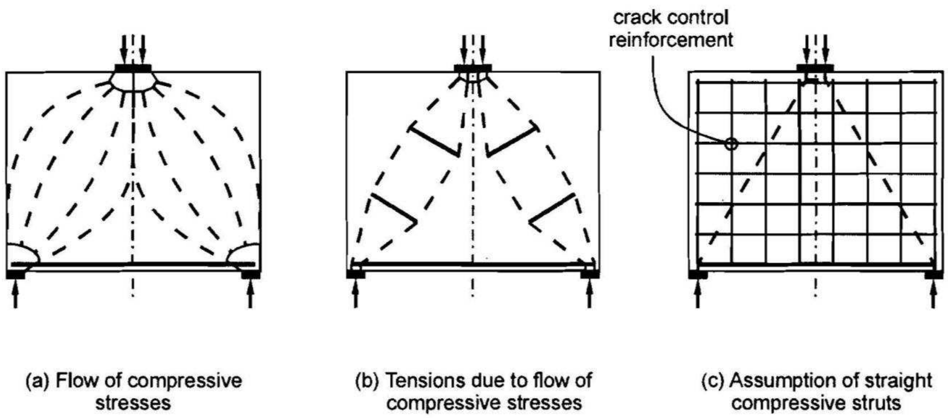

Figure 1.12 Straight-line struts and required crack control reinforcement (Adapted from Schlaich et al, 1987)

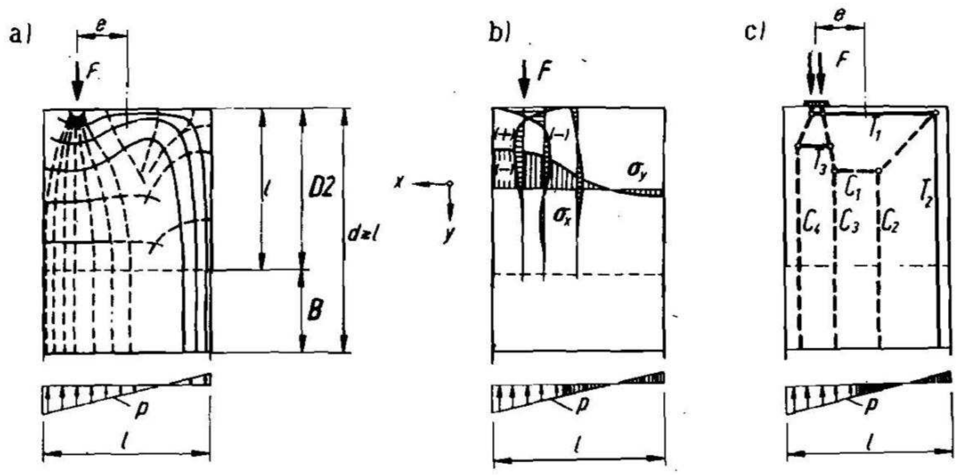

Figure 1.13 A typical D-region: (a) elastic stress trajectories; (b) elastic stresses; (3) strut-and-tie models. (Schlaich et al, 1987)

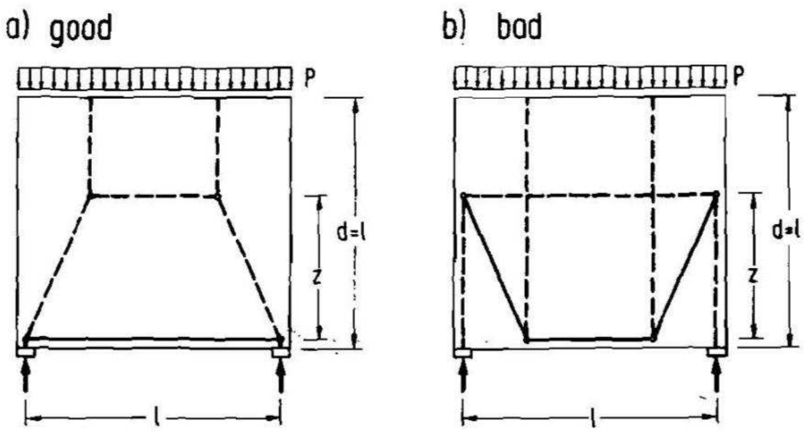

Figure 1.14 The good model (a) has shorter ties than the bad model (b) (Schlaich et al, 1987)

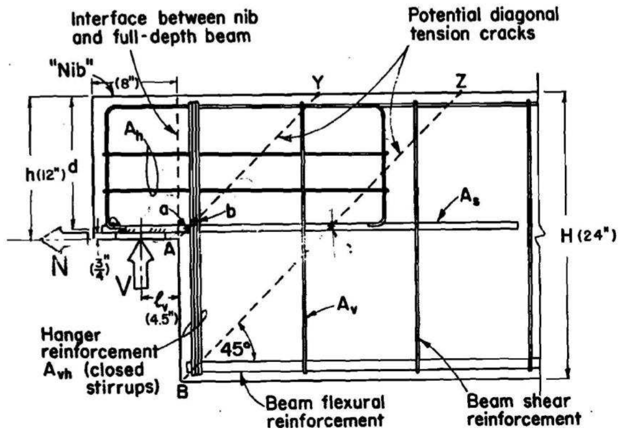

Figure 1.15 Typical dapped-end reinforcement and location of potential diagonal tension cracks (Mattock, 1979)

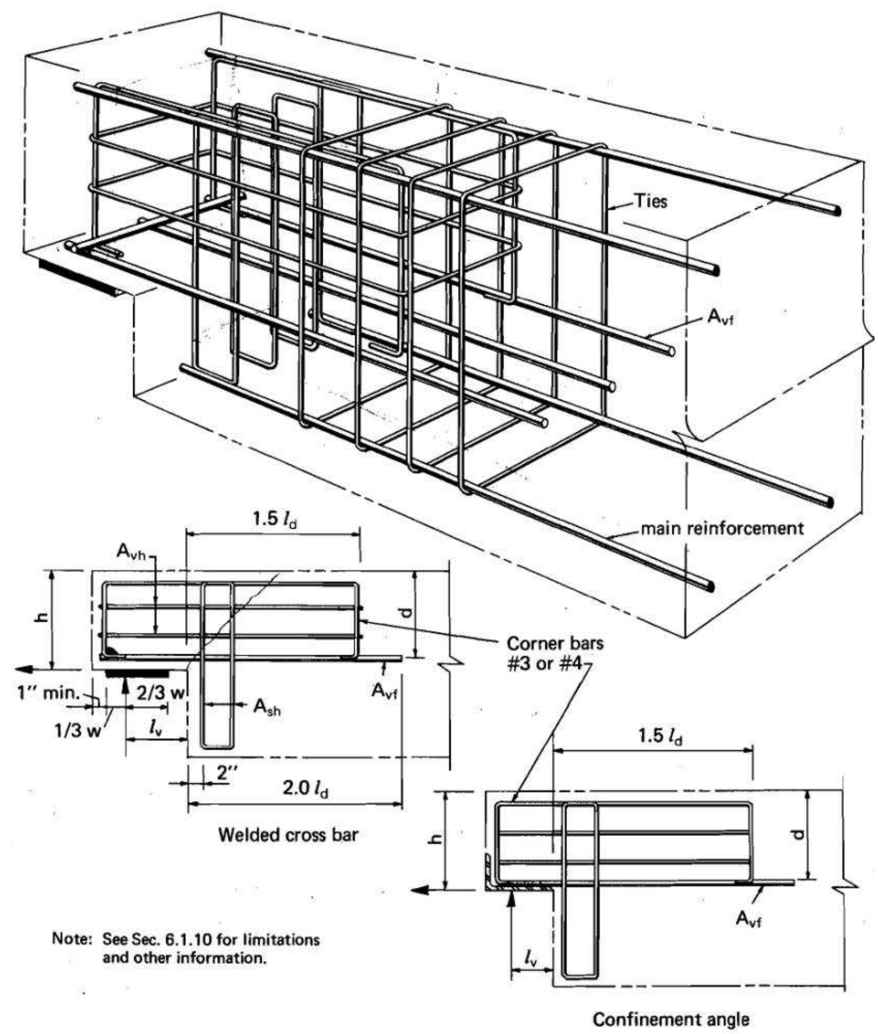

Figure 1.16 Reinforcement for dapped-end beam (PCI, 1971)

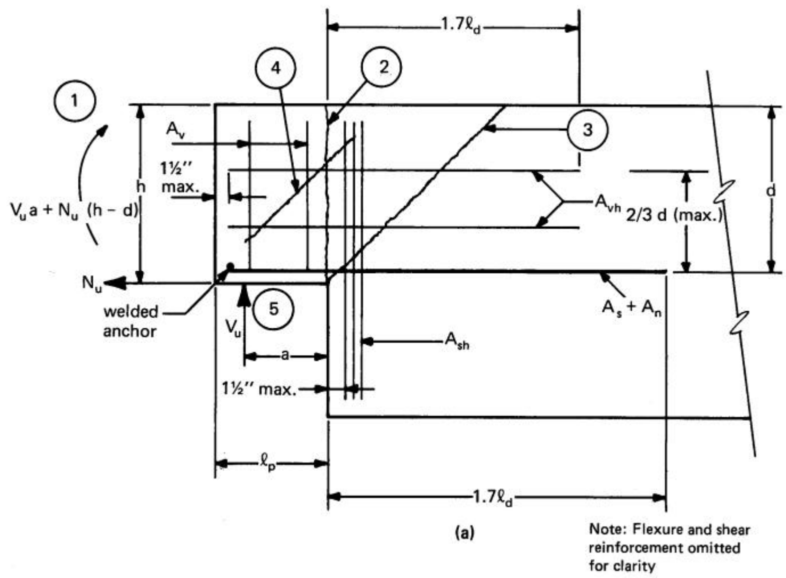

Figure 1.17 Reinforcement for dapped-end beam (PCI, 1978)

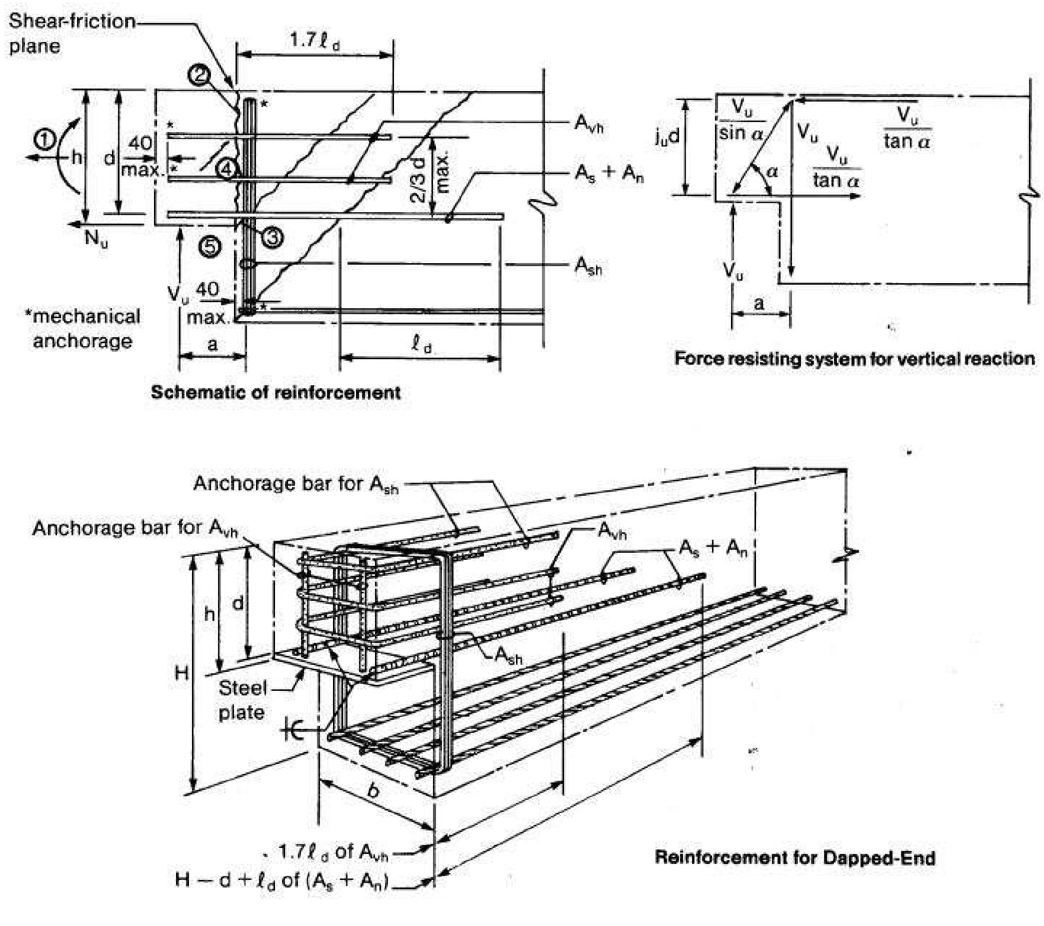

Figure 1.18 Reinforcement for dapped-end beam (CPCI, 1982)

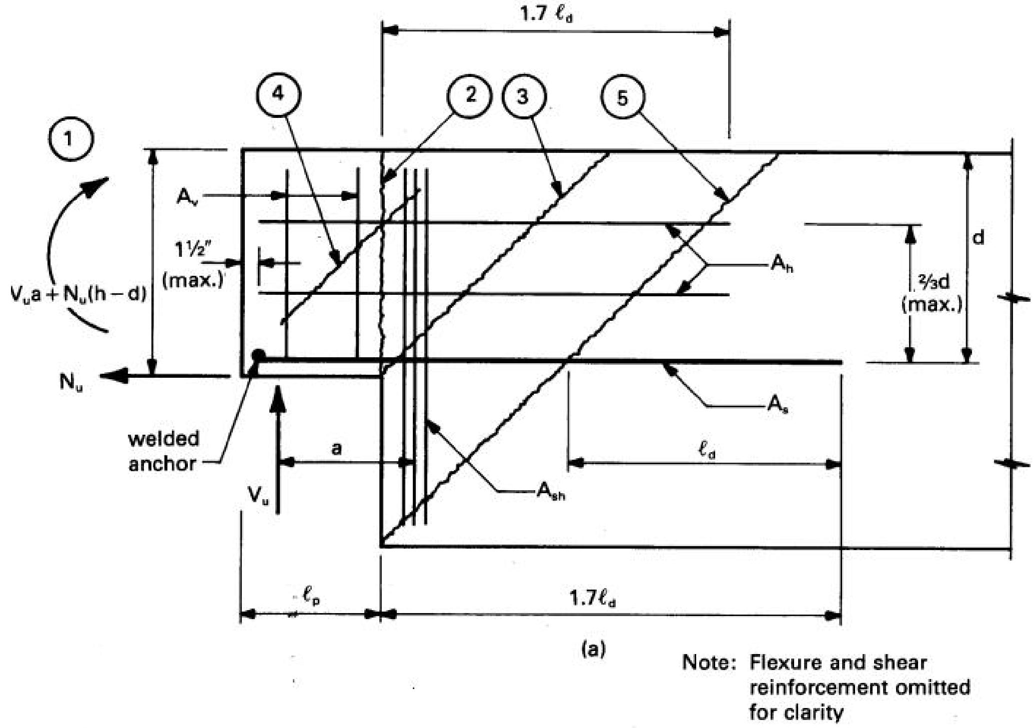

Figure 1.19 Reinforcement for dapped-end beam (PCI, 1985)

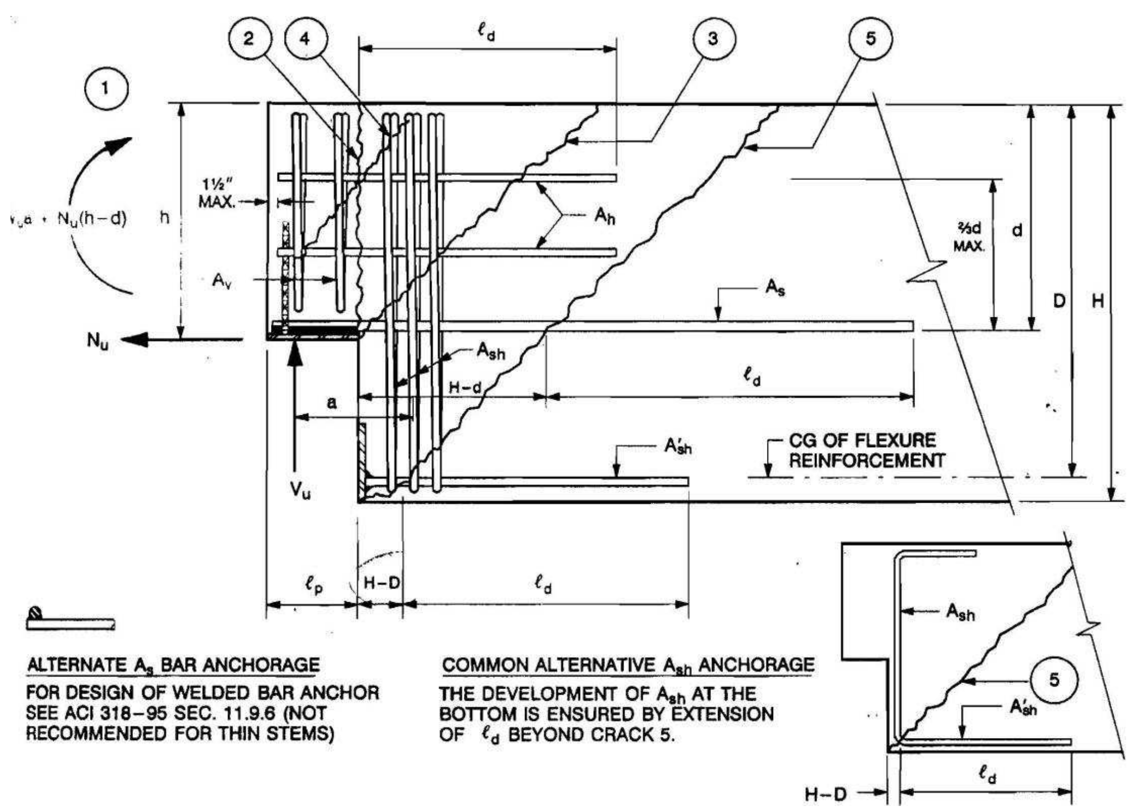

Figure 1.20 Reinforcement for dapped-end beam (PCI, 1999)

CHAPTER 2

Experimental Programme

Two reinforced concrete dapped end beams with similar geometry were constructed and tested in the Jamieson Structures Laboratory in the Department of Civil Engineering at McGill University. The target concrete compressive strength for the specimens was 30MPa. Both specimens used of three types of reinforcing steel: 10M, 15M and 25M bars. In addition, steel plates were used for reinforcement anchorage.

2.1 Design and Detail of the Test Specimens

To evaluate examples of different details for disturbed regions of dapped end beams, the design criterion from the PCI design handbooks (1971, 1978, 1985, and 1999) and CSA concrete design handbook (2005) were used. In this experimental programme, two dapped end beams, named DB1 and DB2 were constructed and tested. Both of these beams had two dapped-ends with different details. Each dapped end is 230 mm long with a cross section measuring 300 mm x 300 mm. The full depth section is 2700 mm long with a cross section size of 300 mm wide by 600 mm deep. The span of the beam was 3 m, so the supports are located 150 mm away from the end of the full depth beam.

2.1.1 Specimen DB1

This beam was designed and detailed according to the CSA Standard A23.3 “Design of Concrete Structures” (CSA, 2004) and using the design example in the CAC “Concrete Design Handbook” (CAC, 2005). Since the flow of the forces in the disturbed region of the beam can be visualized as struts of unidirectional compressive stresses together with ties provided by reinforcing bars, the strut and tie method is an appropriate method to design the beam. Figure 2.1 shows the strut and tie model of one-half the beam. It is in the form of a truss idealization, which consists of concrete compressive struts and reinforcing tension ties. The strut and tie model was designed to be a realistic force flow in the beam. The geometry for the strut and tie model was based on the following rules: (1) the bottom chord of the truss was located along the centerline of the bottom longitudinal reinforcement; (2) The top chord of the truss was located along the centerline of the top longitudinal reinforcement; (3) The tie BC defines the centerline of the hanger; and (4) The tie AD was located at the level along the centerline of horizontal bars at the bottom of dapped end. The structure was designed based on having three stirrups for the vertical hanger reinforcement.

As shown in Fig. 2.2, the south and north side of the beam have different reinforcing details. The north side was designed based on the 2004 CSA Standard, which required additional 2-15M horizontal U-bars with a 50 mm spacing to provide the anchorage of the bottom tension reinforcement at the end of the full-depth section. The south side was designed following the 1971 PCI Design Handbook (PCI, 1971) that did not have requirements for the anchorage of the bottom tension reinforcement at the end of the full-depth section and indicated hanger reinforcement that was not properly anchored around the longitudinal top and bottom bars (see Fig. 2.2). Photographs of the reinforcement details are shown in Figs. 2.15 to 2.19. The bottom flexural tension ties consist of four 25M reinforcing bars along the length of the full-depth portion of the beam. Three 10M closed stirrups were used to provide the required capacity for the main vertical tension hanger. In the rest of the shear span, double legged 10M stirrups were spaced at 231 mm centre-to-centre. Two 15M top bars were used to anchor the stirrups. For the tension tie AD, four 15M bars were used and extended a distance of ℓ_d beyond the anchor point of the strut-and-tie model. In addition, these four 15M bars were welded to a steel plate for tension anchorage. To improve the crack control and ductility, two 10M horizontal U-bars were placed parallel to four 15M horizontal bars in the region above the support.

2.1.2 Specimen DB2

Figure 2.3 shows the strut and tie model of one-half the beam DB2. As shown in Fig. 2.4, both ends of beam DB2 were designed and detailed based on the 1999 PCI Design Handbook (PCI, 1999). The south end used three 15M vertical hanger reinforcement which was anchored by horizontal bends at the top and bottom (see Fig. 2.4). The anchorage of the bottom flexural bars at the north end was provided by three 15M horizontal U bars welded to a 295 x 125 x 10 mm steel plate. Photographs of the reinforcing steel details are shown in Figs. 2.20 to 2.25. The bottom flexural tension reinforcement consists of four 25M reinforcing bars along the length of the full-depth beam. Three 10M closed stirrups were used to provide the required capacity for the main vertical tension hanger and had the same area as the vertical tension tie at the south ends. In the rest of the shear span, the 10M double-legged closed stirrups were spaced at 210 mm at the north end and 217 mm at the south end. Two 15M top bars were used to anchor the stirrups. For the horizontal tension tie AD, four 15M bars were used and extended a distance of ℓ_d beyond the assumed anchor point. In addition, these four 15M bars were welded to a steel plate for anchorage. Two 10M horizontal U-bars were placed parallel to the primary tensile tie reinforcement in the region above the support to provide crack control. The two horizontal U-bars in the nib were held in place by two vertical stirrups immediately above the support.

2.2 Material Properties

2.2.1 Reinforcing Steel

Three different sizes of reinforcing bars were used: 10M, 15M and 25M. The properties of these bars are given in Table 2.1. The values are the average values based on three randomly chosen specimens for each bar size. Figures 2.5, 2.6 and 2.7 provide typical stress-strain curves for these reinforcing bars.

Table 2.1 Reinforcing steel properties

Size designation	Area (mm^2)	f_y (MPa)	f_u (MPa)	ε_y (mm/mm)	ε_{sh} (mm/mm)	ε_{rupt} (mm/mm)
10M	100	494	618	0.00247	0.0199	0.1383
15M	200	442	720	0.00221	0.0063	0.1260
25M	500	423	677	0.00212	0.0043	0.1477

2.2.2 Concrete

The target concrete compressive strength was 30MPa, using normal strength concrete. Different batches of concrete were used for the two specimens. The properties of the fresh concrete are shown in Table 2.2. After casting, both specimens were moist cured for a period of one week by covering the beams with wet burlap and plastic sheets on the top. The mix design of the concrete was presented in Table 2.3. The expecting slump was 80$\pm$30 mm, and air content was 5-8%. The designed water cement ratio was 0.46.

Table 2.2 Fresh concrete properties

Properties	Slump (mm)	Air content (%)
DB1	105	6.75
DB2	128	6.40

Table 2.3 Mix design of the concrete

Ingredients	Type	Specified Quality
cement	Type GU/10	289 kg/m^3
	Type F Fly Ash	73 kg/m^3
Sand	Concrete sand	812 kg/m^3
Aggregate	10-20 mm limestone	635 kg/m^3
	5-14 mm limestone	343 kg/m^3
Water	Batch water	165 L
Air Entrainment Admixture	Microair	33.12 ml/100 kg
Water Reducing Admixture	Polyheed 997	350 ml/100 kg
Water Reducing & Accelerating Admixture	Pozzutec 20 plus	0.1 L/100 kg

Standard concrete cylinders, 100 mm in diameter and 200 mm long, were prepared for compressive strength and splitting tensile strength tests. Standard flexural beams, 100 x 100 x 400 mm, were used for modulus of rupture tests, using four-point loading. All these samples were cured under 100% humidity condition 24 hours after casting. At the time of testing the beams, the concrete samples were tested to determine the concrete compressive strength, f_c', the splitting tensile strength, f_t, and the modulus of rupture, f_r. The testing was carried out on three specimens from the two types of concrete for DB1, DB2, respectively. Table 2.3 gives the properties of the two types of concrete. The compressive stress-strain curves are presented in Figs. 2.8 and 2.9.

Table 2.4 Concrete properties

Concrete	f_c' (MPa)	ε_c' (x 10^{-6})	f_r (MPa)	f_t (MPa)
DB1	33.0	2093	5.84	3.86
DB2	32.9	2259	4.83	3.78

2.3 Testing Setup and Instrumentation

Both specimens were tested under a computer controlled MTS testing machine (see Fig. 2.10), having a compressive axial load capacity of 11,400 kN. The supports of the beam were composed of a steel roller of diameter of 90 mm, and W shaped steel beams. The rollers permitted the beams to elongate and rotate at their ends. For the bearing, one steel plate of 500 x 180 x 25 mm was set under the flat plate of MTS machine at the mid-span of the beam. The same size of steel plates as the anchorage steel plates in the nibs were located at the support points. Thin layers of high-strength capping compound were used at all contact surfaces between the beam and the steel plates. In order to minimize eccentricities, the bearing plates, rollers, and W shape beams were carefully positioned during test setup.

A total of 34 electrical resistance strain gauges were glued to the reinforcing bars to measure the strains for DB1, and 33 gauges were used for DB2. From Fig. 2.11 and 2.12, it can be seen that most of the strain gauges were located in regions of expected cracking. In addition, 22 Linear Voltage Differential Transducers (LVDTs) were installed to determine the vertical displacement of the beams and the strains in the concretes. The LVDTs were attached to threaded rods, which in turn were attached to the concrete by inserting the rods into 30 mm deep holes that were grouted with epoxy. Five LVDTs (NV1, NV4, MV1, SV1, and SV4) were used to measure the vertical displacement at the supports, at the full depth ends and at midspan (see Fig. 2.13 and 2.14).

2.4 Testing Procedure

Before the test, all the instruments were checked and zeroed. The testing commenced in load control, with a 25 kN/min loading rate. And then the loading control was switched to deflection control at 0.5 mm/min when the applied load reached 300 kN. Loading was stopped when failure of one end occurred. Then the beam was unloaded and prepared for the testing of the other end. In order to enable testing of the end that had not failed, the failed end was strengthened by using added post-tensioned stirrups and the support as moved 600 mm closer to midspan (see Figs. 2.26 and 2.27). The same deflection control rate was used in the subsequent loading to failure.

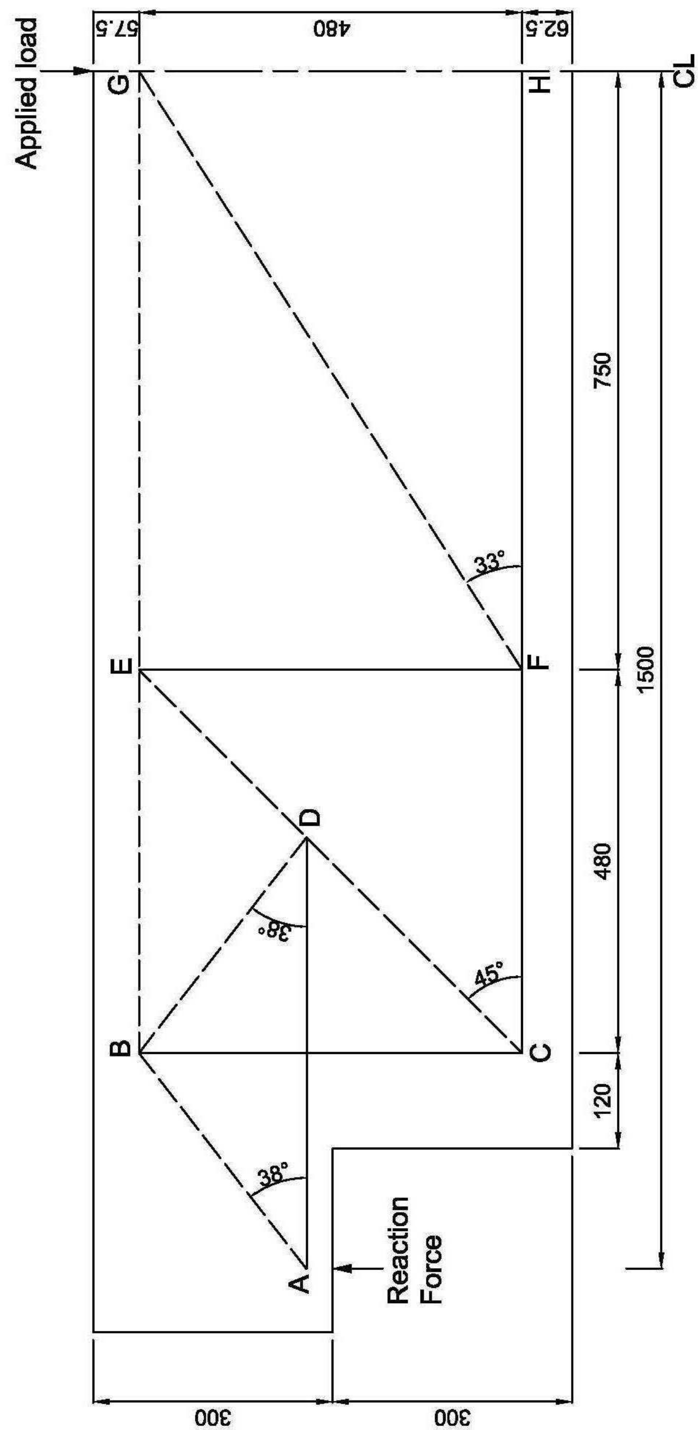

Figure 2.1 Strut and tie model for DB1

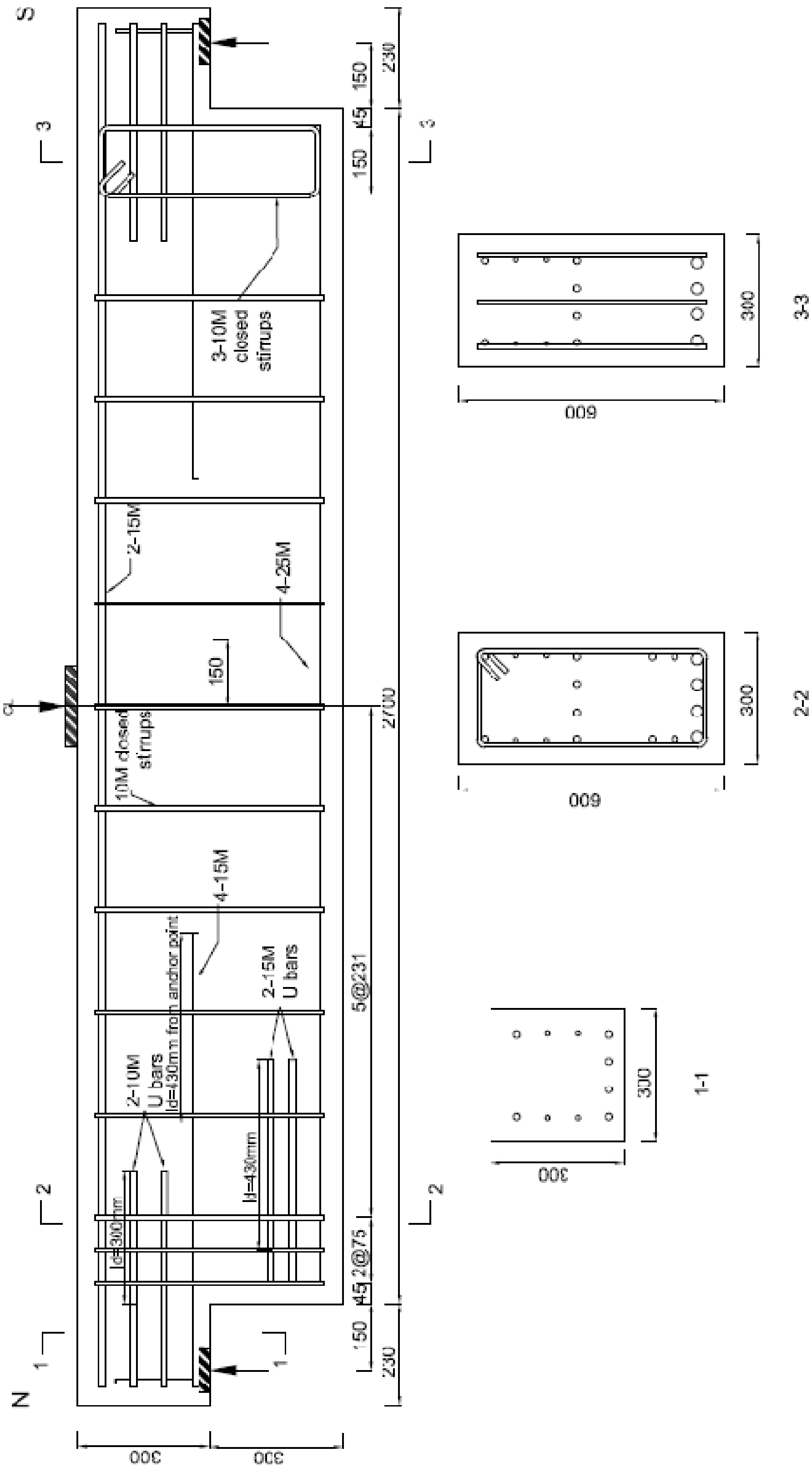

Figure 2.2 Reinforcing details for DB1

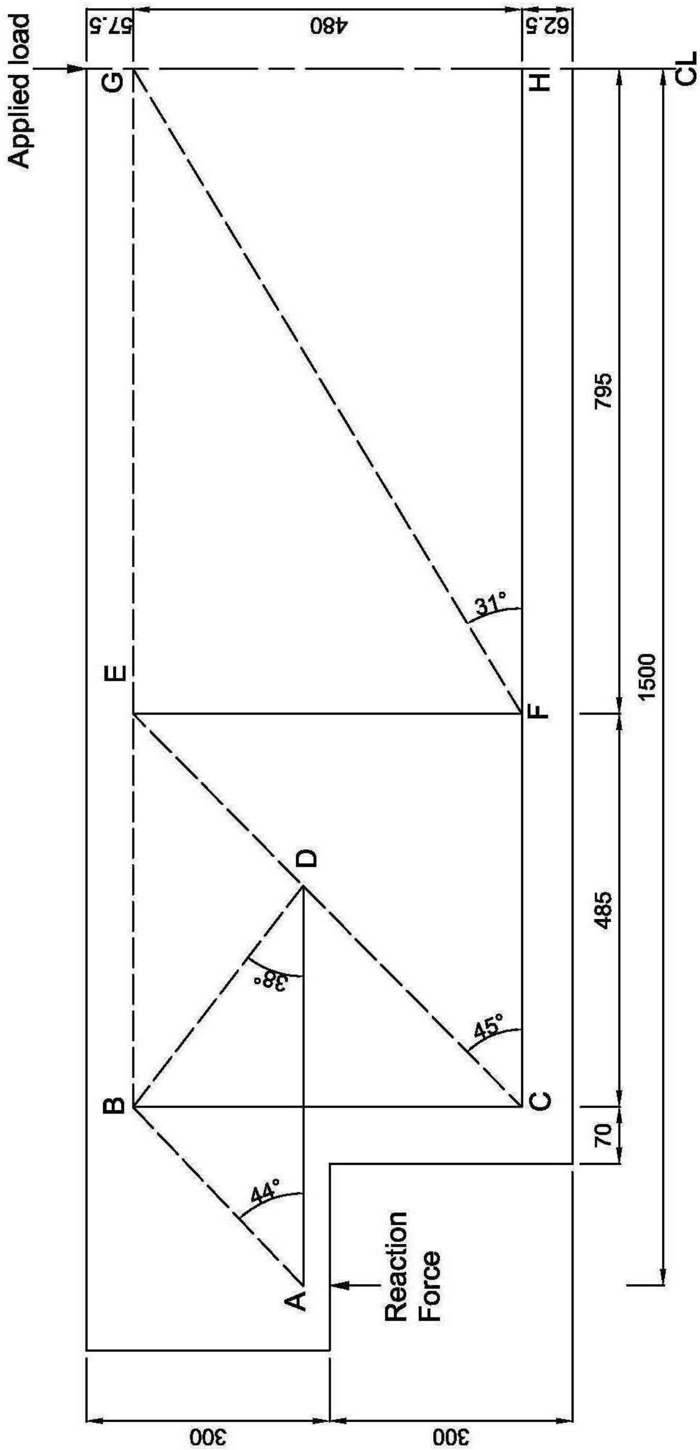

Figure 2.3 Strut and tie model for DB2

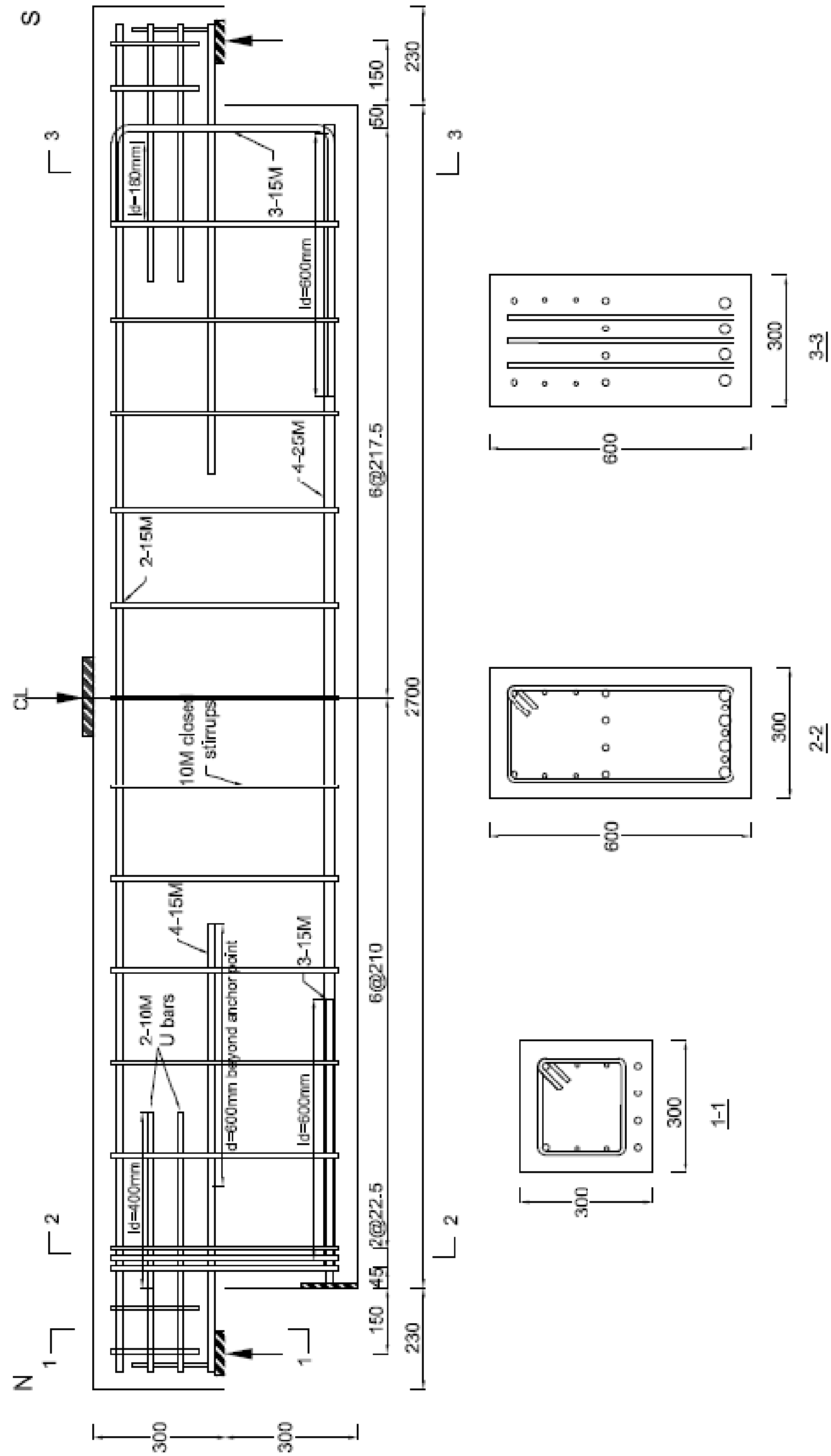

Figure 2.4 Reinforcing details for DB2

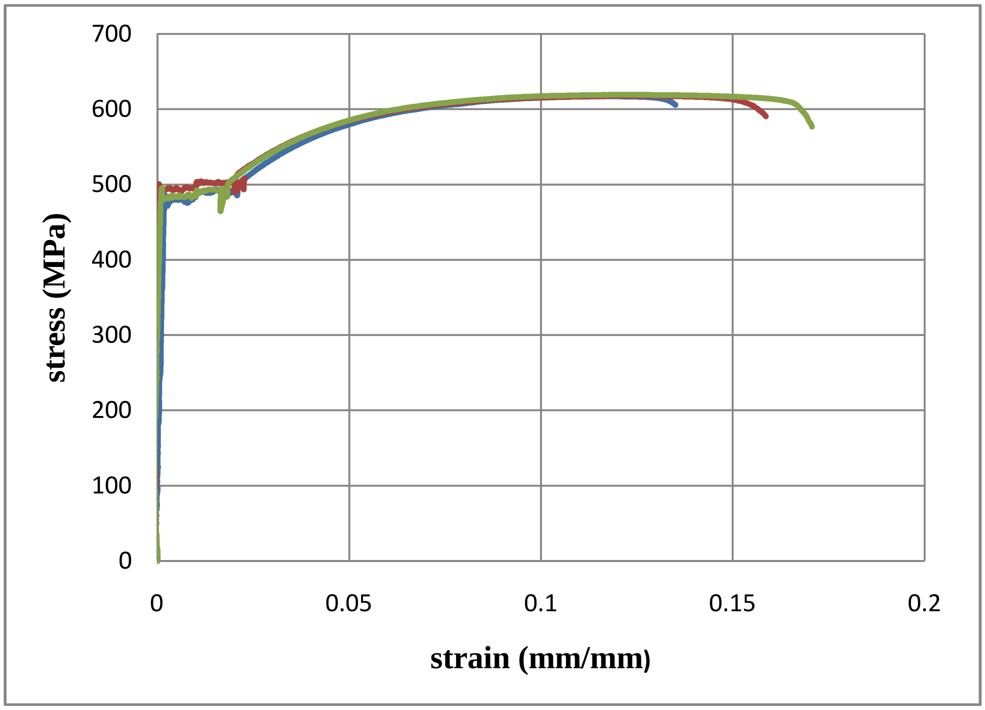

Figure 2.5 Tensile stress-strain curves for 10M bars

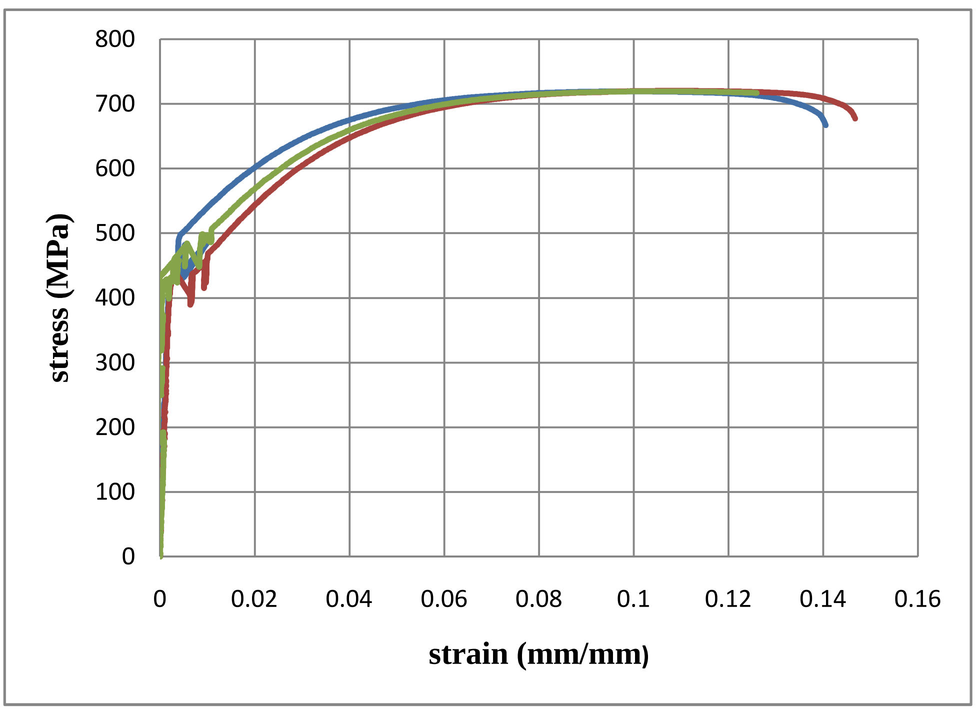

Figure 2.6 Tensile stress-strain curves for 15M bars

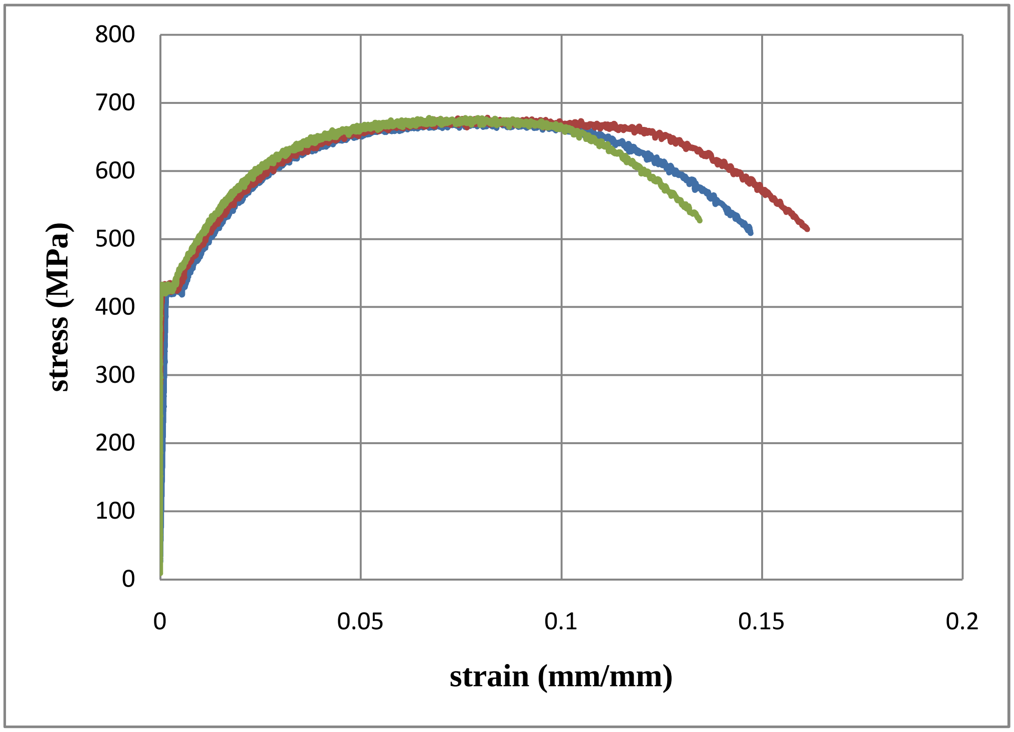

Figure 2.7 Tensile stress-strain curves for 25M bars

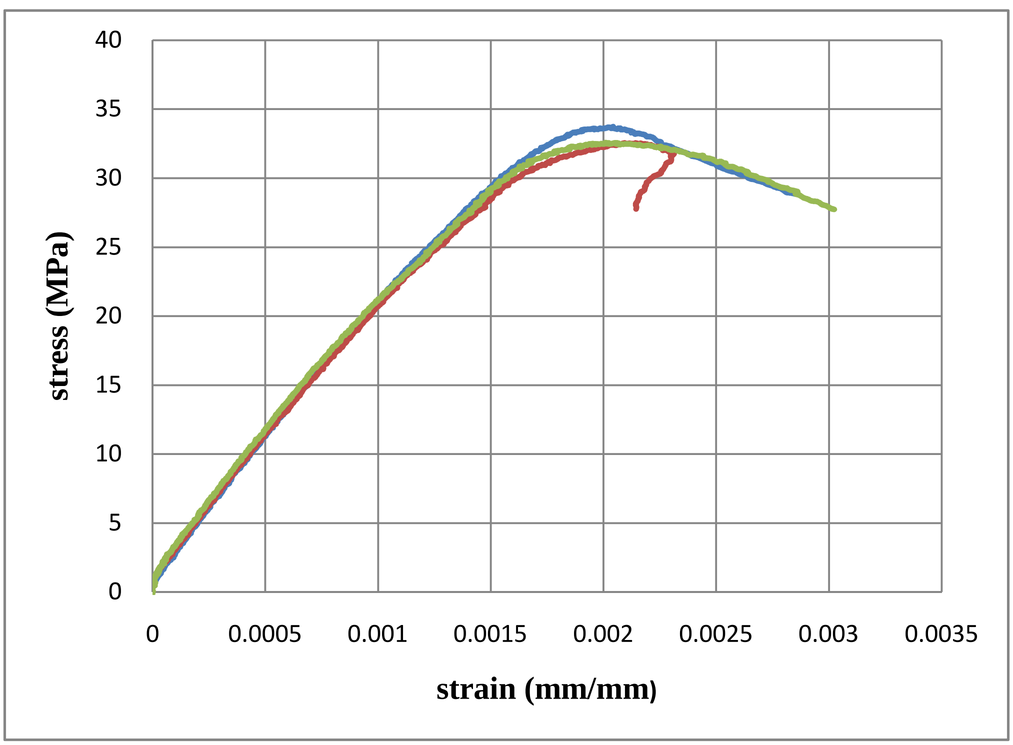

Figure 2.8 Compressive stress-strain curves for concrete in beam DB1

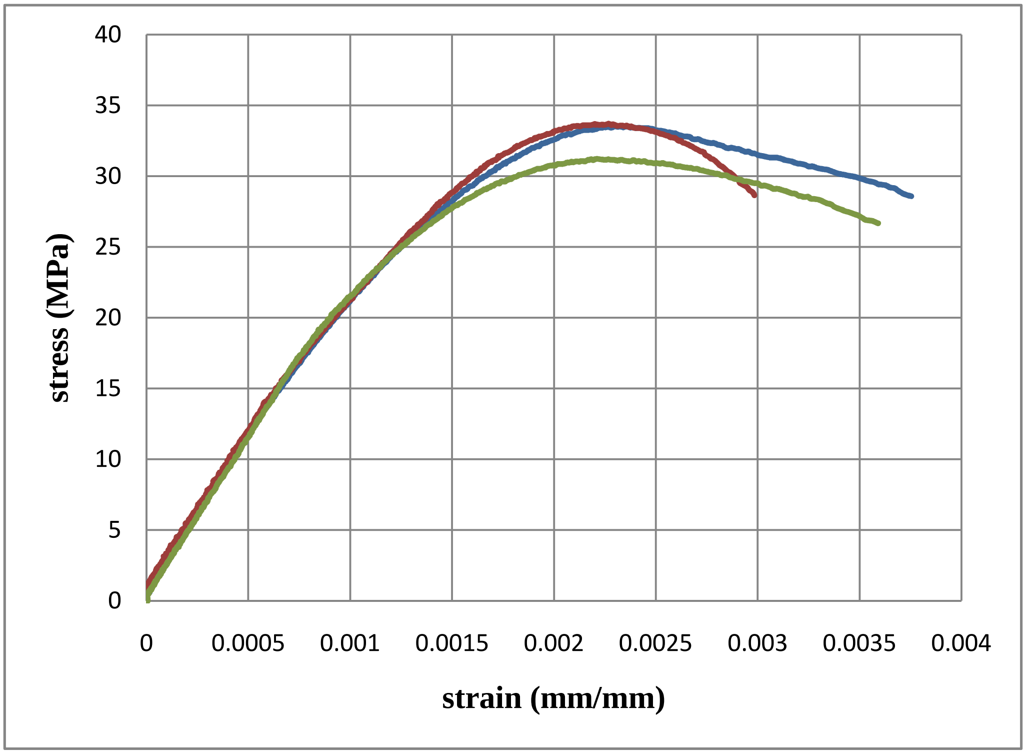

Figure 2.9 Compressive stress-strain curves for concrete in beam DB2

Figure 2.10 Overview of specimen under MTS machine

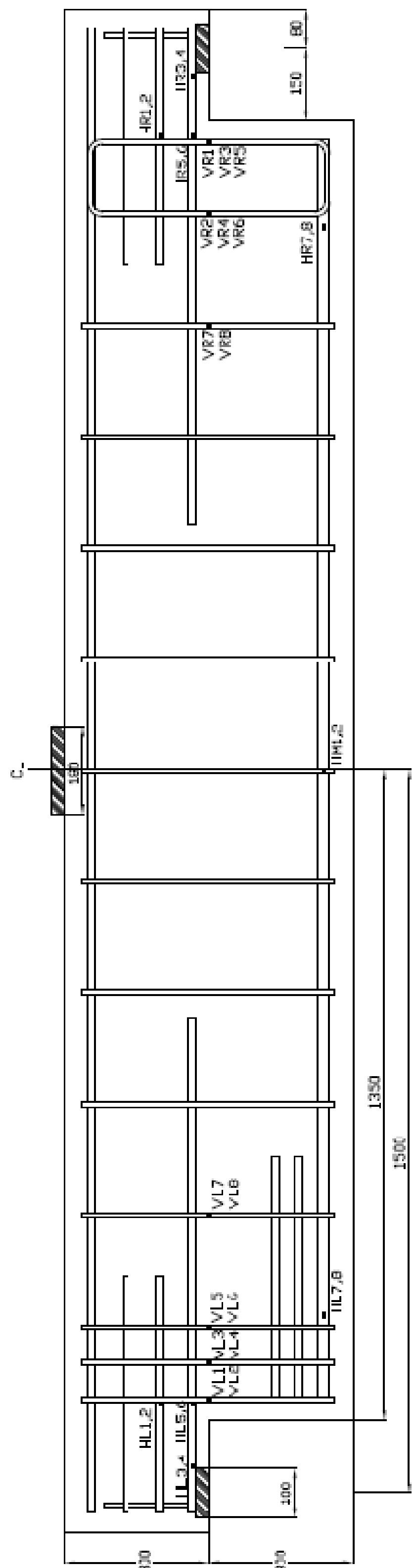

Figure 2.11 Strain gauges location of DB1

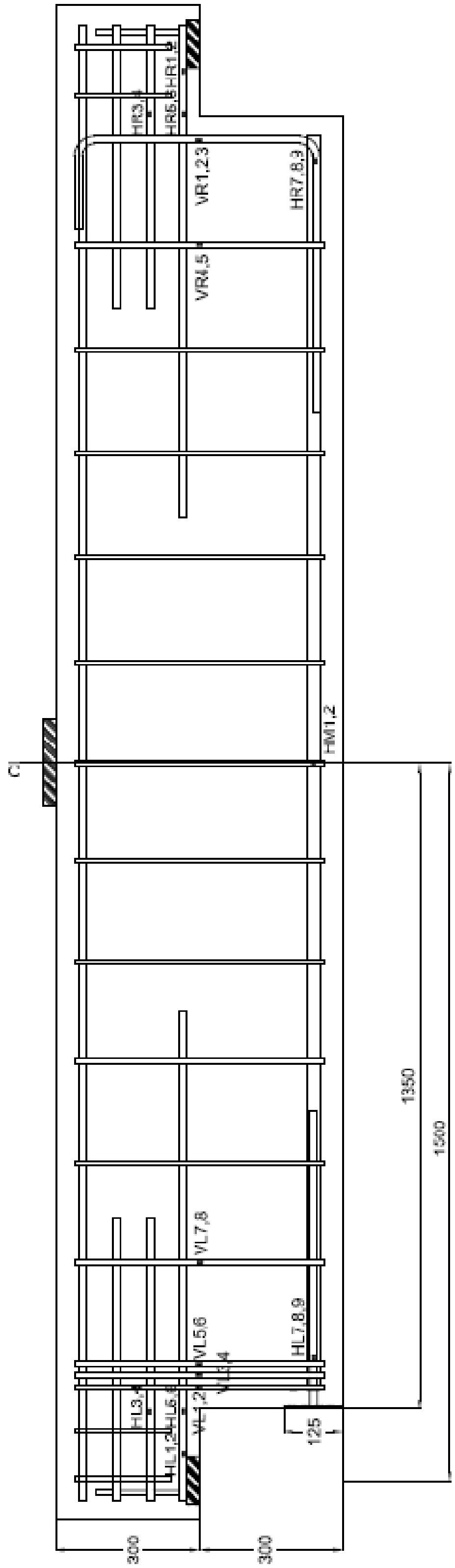

Figure 2.12 Strain gauge locations in beam DB2

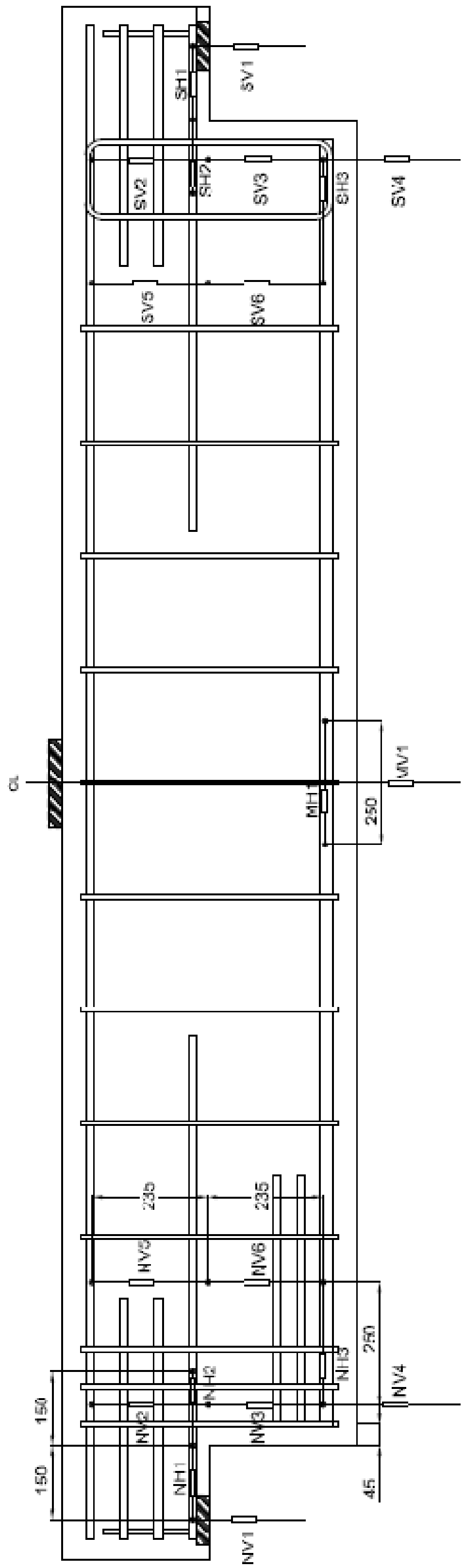

Figure 2.13 LVDT locations for beam DB1

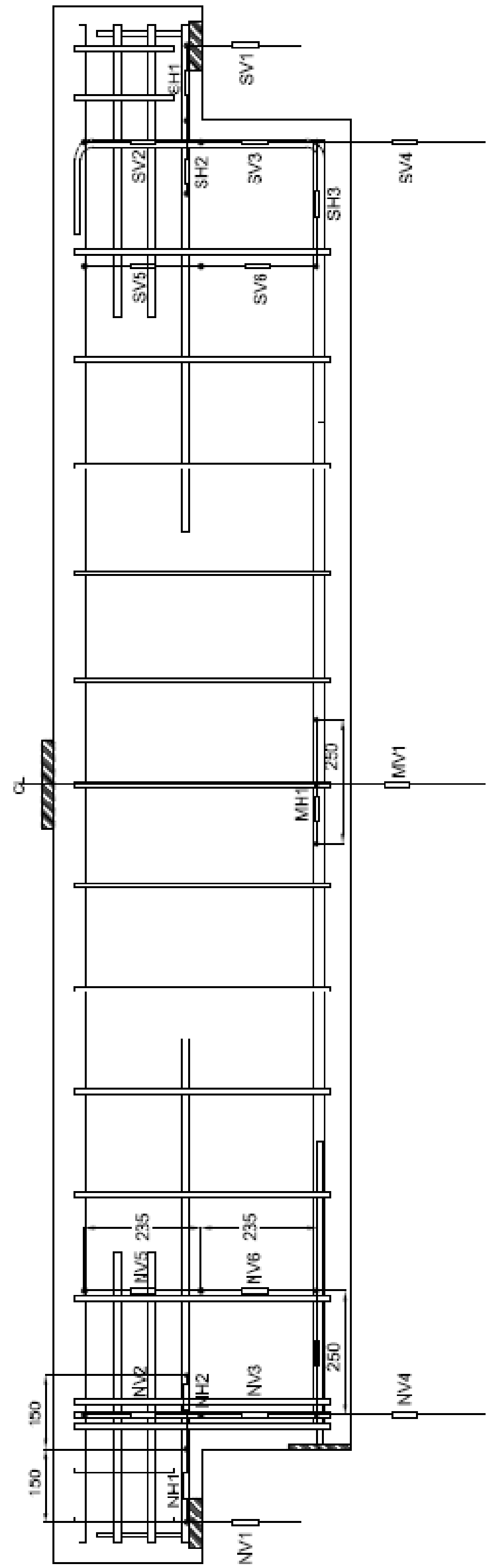

Figure 2.14 LVDT locations for beam DB2

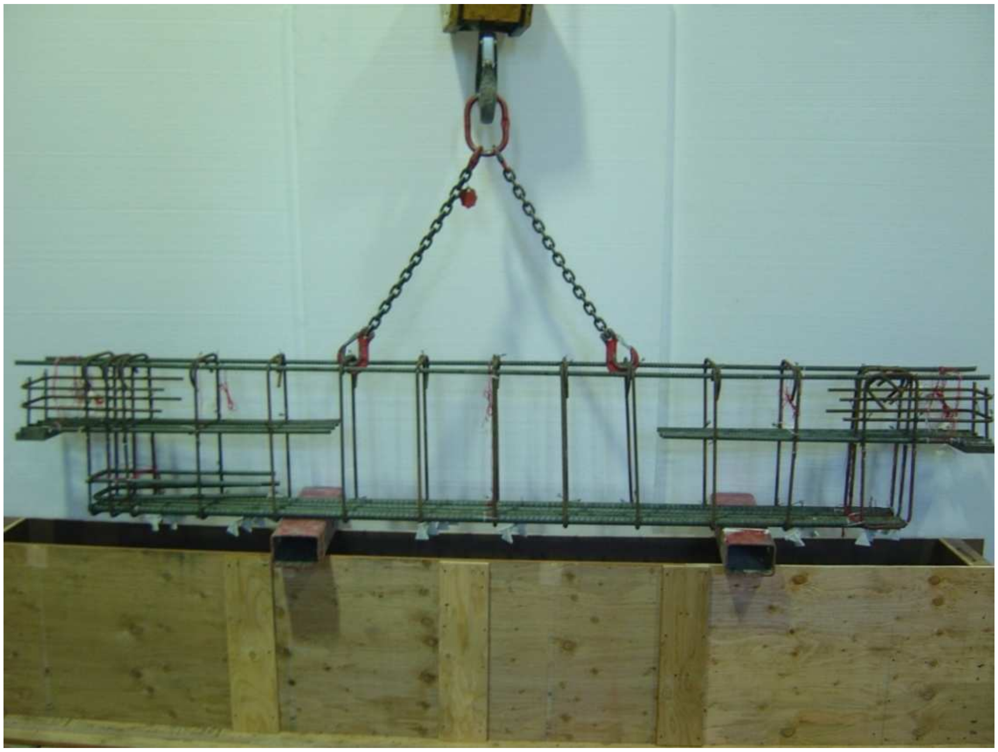

Figure 2.15 Overall view of reinforcement cage of DB1

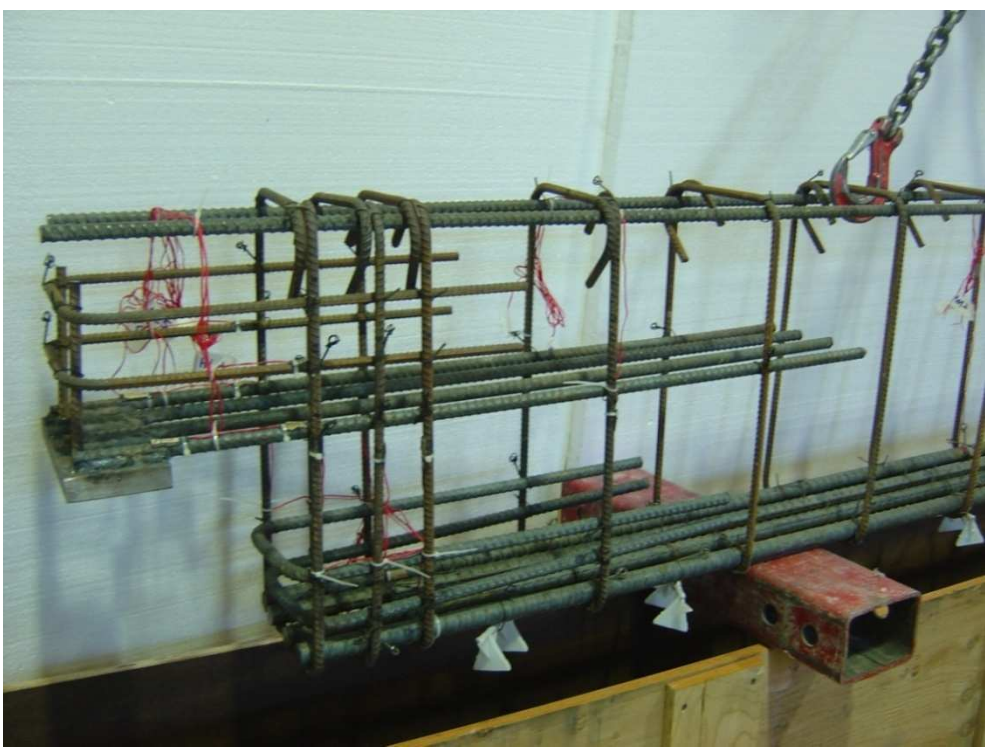

Figure 2.16 Reinforcement details at north side dapped end of DB1

Figure 2.17 Reinforcement details at south side dapped end of DB1

Figure 2.18 Reinforcement cage end view at north side dapped end of DB1

Figure 2.19 Reinforcement cage end view at north side dapped end of DB1

Figure 2.20 Overall view of reinforcement cage of DB2

Figure 2.21 Reinforcement details at north side dapped end of DB2

Figure 2.22 Reinforcement details at south side dapped end of DB2

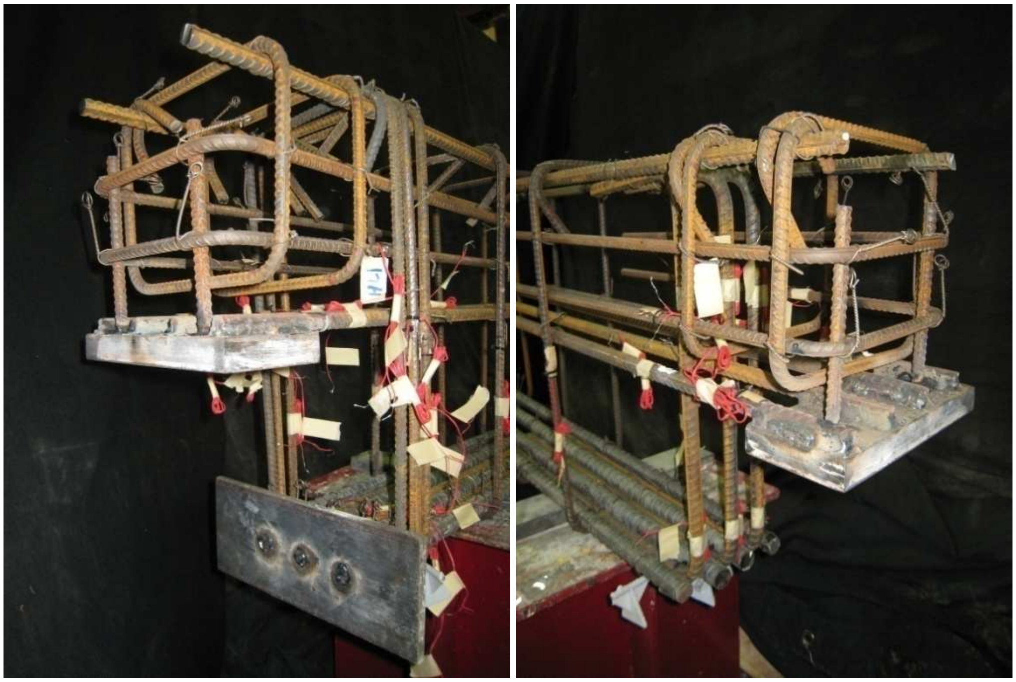

(a) north side (b) south side

Figure 2.23 Reinforcement cage end view at dapped end of DB2

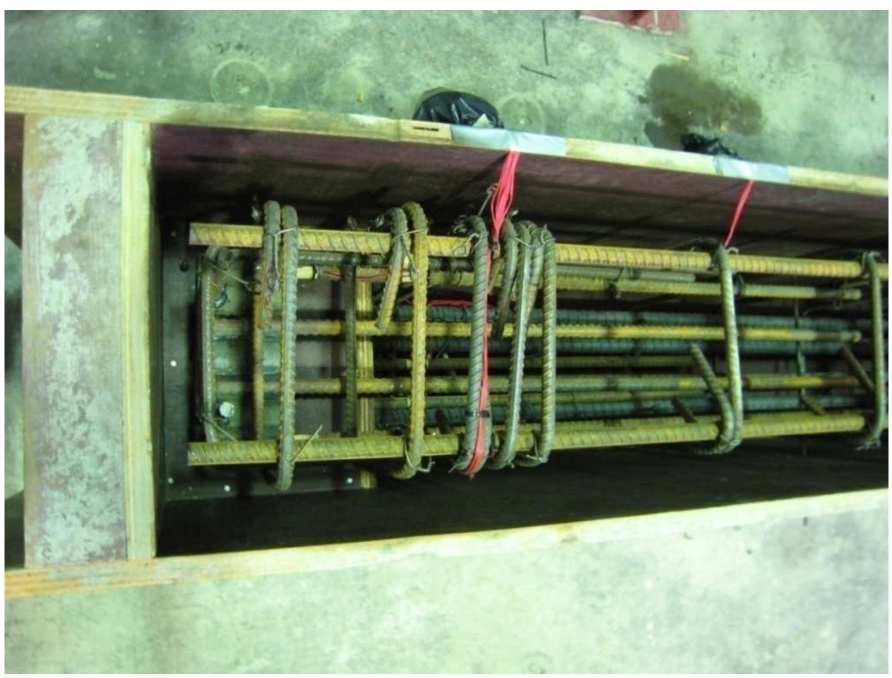

Figure 2.24 Reinforcement cage in formwork at north side of dapped end of DB2

Figure 2.25 Reinforcement cage in formwork at dapped end of DB2-S

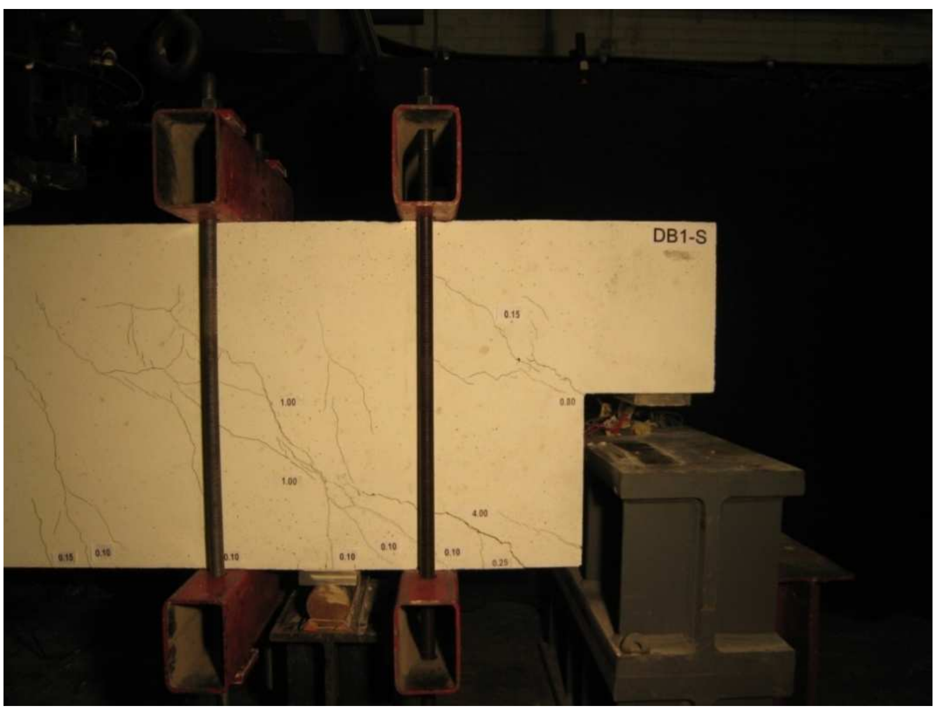

Figure 2.26 Retrofit of DB1at south end

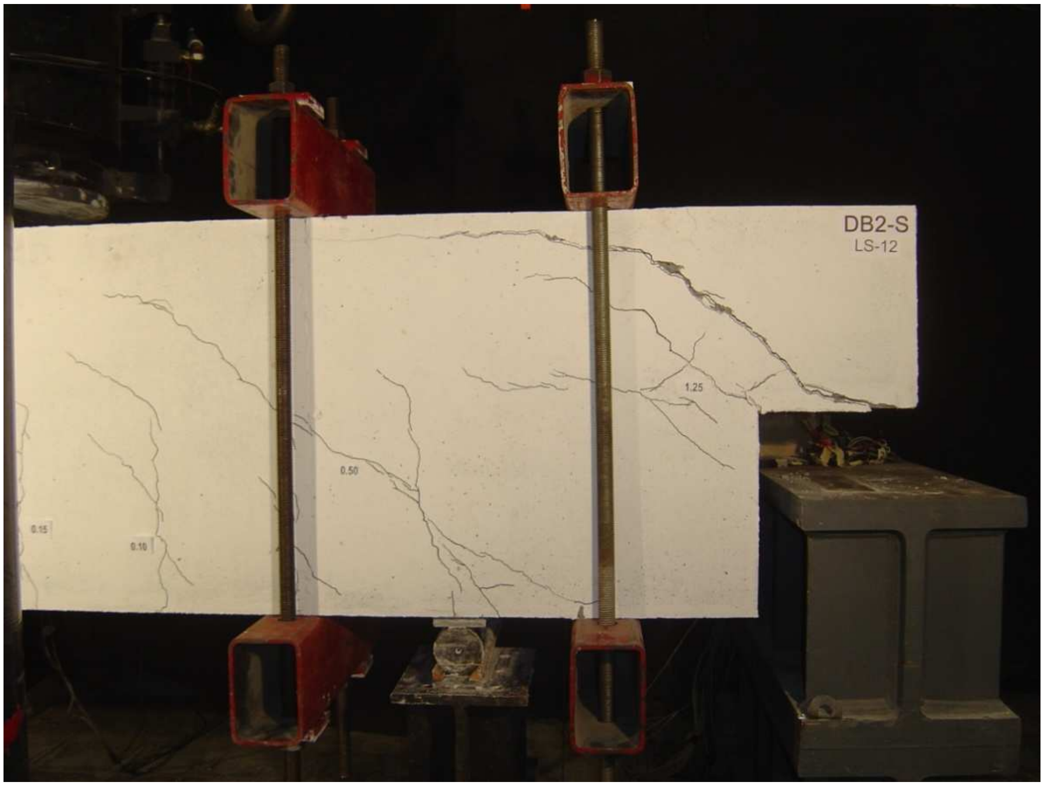

Figure 2.27 Retrofit of beam DB2 at south end

CHAPTER 3

Test Results

In this chapter, the experimental responses of the two dapped-end beams are presented. The load control of tests was the same for the two beams (DB1 and DB2). Both beams were tested starting with load control at a rate of 25 kN/min until the total applied load reached 300 kN, and then further testing was carried out in deflection control at a rate of 0.5 mm/min until the end of the test. During the test, loading stages (LS) were taken at 50 kN intervals up to a total load of 300 kN at LS-7, after that, loading stages were taken when there were new cracks, yielding of reinforcing bars, or crushing of the concrete. The shear loads at both supports were calculated based on the shear spans for the different loading setups. The deflection reported for all of the tests is the deflection at the end of the full-depth section, corrected for support settlement.

3.1 Beam DB1

Beam DB1 has two dapped ends, the north end (DB1-N) and the south end (DB1-S). Since the south end had the poorer reinforcing details as described in Chapter 2, it is much weaker than the north end of the beam DB1. The first loading (loading 1) was ended when the south end failed at LS-10 with a shear of 118.5 kN and a displacement of 2.46 mm at the end of the full-depth section. The beam was unloaded after loading 1. To permit further loading of the north end, DB1-N, the support was moved inwards and external post-tensioned stirrups were added at the south end (see Fig. 2.26). The support at DB1-S was moved inwards a distance of 600 mm. Thus, the second loading started after the retrofit of the failed end. The second loading (loading 2) was carried out to study the effectiveness properly anchored bottom longitudinal bars, and proper hanger reinforcement details. Loading 2 was stopped at LS-17 with a maximum shear crack width of 6 mm, a shear load of 206 kN and displacement of 4.34 mm.

Figure 3.1 shows the total applied load versus the net measured displacement from the LVDT at midspan for Loading 1 and Loading 2 (after strengthening DB1-S). This figure also shows the relationship between the total applied load and the shear for both of the loading setups.

3.1.1 Response of DB1-S

Table 3.1 summarizes the major events for DB1-S and Fig. 3.2 shows the shear versus deflection measured at the end of the full-depth section. There was no cracking was found at loading stage 1. The first hairline crack initiated at the re-entrant corner at a shear of 42.5 kN. As the load was further increased, the crack propagated at approximately 45 degree to the horizontal. At LS-3, the first flexure crack occurred at the bottom of the beam in the midspan region. At LS-4, at a shear of 75 kN, these cracks grew to 0.05 mm wide and the crack length at the re-entrant corner extended a distance of 120 mm beyond the face of full depth beam (see Fig. 3.3). At a shear of 100 kN, the crack width increased to 0.1 mm. As the loading increased, the crack width increased and additional diagonal tension cracks occurred in the nib and in the full depth beam. At LS-7, at a shear of 162 kN, the outmost closed stirrups of the hanger bars reached yielding and the crack width at the re-entrant corner was 0.50 mm (see Fig. 3.4). The load control was then changed to a deflection control at 0.5 mm/min for the remainder of the test. The maximum shear was reached at LS-8, at a shear of 193 kN with corresponding deflection of 2.75 mm. With the further loading in deflection control, a new tension-shear crack, 1.25 mm wide, suddenly appeared at LS-9, at a shear of 140 kN and a deflection of 2.11 mm, and extended to a location, 110 mm from the end of the full depth beam (see Fig. 3.5). This occurred because of the lack of proper hanger reinforcement anchorage at the bottom of the full-depth beam. This crack widened with increased loading. DB1-S failed at LS-10, at a shear of 118.5 kN, and a displacement of 2.29 mm (see Figs. 3.6 and 3.7). Thus, the testing of DB1-S was terminated, the maximum crack widths were 4.00 mm for the tension-shear crack, 0.80 mm for the shear crack at the re-entrant corner, and 0.25 mm for the flexural crack at midspan. The loading ended with failure of DB1-S and is referred to as Loading 1. The beam was unloaded and reset (including retrofit and support movement) to continue the testing of DB1-N.

Table 3.1 Summary of events for DB1-S

Loading stages	shear (kN)	Deflection (mm)	Events
LS-1	25	0.09	No cracks were found
LS-2	42.5	0.23	Hairline crack at re-entrant corner
LS-3	50	0.30	First flexural crack at midspan
LS-4	75	0.66	Crack at re-entrant corner increased to 0.05 mm, and extend to 120 mm beyond the face of full-depth beam
LS-7	150	1.91	Load control switch to deflection control at a rate of 0.5 mm/min. The outermost hanger reinforcement yielded at a shear of 162 kN
LS-8	193	2.75	Reached the maximum shear
LS-9	140	2.11	A new tension-shear crack suddenly occurred with a width of 1.25 mm, and formed to an inclined diagonal tension crack
LS-10	118.5	2.29	DB1-S failed, the first loading ended

Figure 3.8 shows the response of the shear versus the measured strains in the strain gauges (VR5, VR6, and VR8) located on the vertical hanger reinforcement and the stirrup which is closest to these hanger bars. The first yielding of the outermost leg of the hanger reinforcement occurred at a shear load of 162 kN, while the other leg did not yield. Figures 3.9 and 3.10 give the shear versus the measured strain on the horizontal 15M tension bars anchored in the nib. None of these bars yielded during loading. Figures 3.11 and 3.12 show the shear versus strains on the bottom flexure bars. No flexural yielding occurred in these bottom bars.

3.1.2 Response of DB1-N

Table 3.2 gives the summary of events for DB1-N and Fig. 3.13 shows the shear versus deflection measured at the end of the full-depth section. The first hairline shear crack appeared at the re-entrant corner at a shear of 42.5 kN at LS-2. At LS-4, the crack extended at about 45 degrees to the horizontal and was 150 mm long (see Fig. 3.14). At LS-7, additional diagonal tension cracks occurred in the nib and in the full depth beam (see Fig. 3.15). At LS-8, the first flexure-shear crack in the full-depth section formed at a location about 750 mm from the end of the full-depth section and extended to form an inclined diagonal tension crack towards the top of the midspan beam region (see Fig. 3.16). A second flexure-shear crack appeared at a location, 400 mm away from the end of the full- depth section of the beam at LS-10 (see Fig.3.17), at a shear of 118.5 kN, corresponding to the failure load of DB1-S, no significant distress was observed in DB1-N. Further loading of DB1-N was carried out after the retrofit of DB1-S. Because the support at the DB1-S end was relocated, the shears differed at each end. The ratio of the shear span is 1500:900 for DB1-N to DB1-S. After these modifications, the beam was reloaded in Loading 2. Upon reloading, the shear crack at the re-entrant corner rapidly increased to 0.60 mm at LS-14. At this stage, the inclined crack width in the nib increased to 0.25 mm. As loading increased further, additional cracks were formed and existing cracks lengthened and widened. The maximum shear was reached at LS-15, at a shear of 273 kN with corresponding deflection of 4.49 mm, a new crack at the corner of the full-depth section occurred, and a diagonal crack of 0.15 mm width occurred 50 mm above this crack (see Fig. 3.18). These inclined cracks are indicative of the diagonal compressive stresses in the concrete that are anchored by the horizontal U-bars at this corner (see Fig. 2.2). At this load stage, the shear crack at the re-entrant corner had a width of 0.8 mm. At LS-16, the shear crack at the corner of the full-depth section along the flexure bars suddenly opened to 1.00 mm wide, and increased quickly to 6.00 mm wide at LS-17 of shear of 206 kN, with a corresponding deflection of 2.92 mm (see Fig.

3.19). The testing was stopped at this stage.

Table 3.2 Summary of events for DB1-N

Loading stages	shear load (kN)	Deflection (mm)	Events
LS-1	25	0.08	No cracks were found
LS-2	42.5	0.21	Hairline crack at re-entrant corner
LS-3	50	0.27	First flexural crack at midspan
LS-4	75	0.61	Crack at re-entrant corner increased to 0.05 mm, and extended to 150 mm beyond the face of full depth beam
LS-7	150	1.76	Load control switch to deflection control at a rate of 0.5 mm/min. Additional diagonal tension cracks occurred in the nib and full depth beam
LS-8	175	2.26	First flexure-shear crack appeared at about 750 mm from the end of full depth beam
LS-11	4.7	--	The beam was unloaded (only self-weight)
LS-12	190	2.94	Reloaded for further loading at DB1-N
LS-14	243	3.70	The shear crack at re-entrant corner increased to 0.6 mm. The inclined crack at nib increased to 0.25 mm
LS-15	273	4.49	The maximum shear was reached A new crack at corner of full depth beam occurred. A diagonal crack at a width of 0.15 mm appeared 50 mm above the new crack The shear crack at re-entrant corner had a width of 0.8 mm
LS-16	225	4.40	The crack at full depth beam corner opened to a width of 1.0 mm
LS-17	206	2.92	The crack at full depth beam corner increased rapidly to 6.0 mm. The testing of DB1-N ended

Figures 3.20 show the response of the shear versus the strain of the hanger reinforcement (gauges VL1, VL3 and VL5) and the stirrup (VL7) closest to the hanger bars. No yielding was found during Loading 1, and all the three hanger reinforcing bars yielded in Loading

2. (VL1 yielded at a shear of 185 kN. VL3, VL5 yielded at a shear of 231 kN and 254 kN, respectively). Figures 3.21 and 3.22 give the shear versus the measured strain of the horizontal 15M tension bars anchored in the nib. The tension bar in the nib, near the steel plate yielded at a shear of 238 kN. Figure 3.23 shows the shear versus strain curves for the bottom flexure bars near the hanger bars. No yielding of the flexural reinforcement occurred.

3.2 Beam DB2

The second beam DB2 also has two different dapped ends: DB2-N (north side) and DB2-S (south side). In the disturbed region of DB2-N, the hanger bars were tied as close as practically (see Fig. 2.4). For DB2-S, the hanger bars was designed and detailed (see Fig. 2.4) according to the alternative details shown in the 1999 PCI Design Handbook. Moreover, to provide crack control reinforcement in the nib, two vertical 10M stirrups were used in the nib. The purpose of testing beam DB2 is to study the behaviour of these two different details at the two ends. The south end, DB2-S, failed at a shear of 108.5 kN and a deflection of 9.57 mm at the end of the full-depth end where Loading 1 was ended. For further loading of DB2-N, the retrofit of DB2 was done similar to that for beam DB1 and the support at the south end was moved. Loading 2 was stopped when beam had flexure distress at midspan at LS-21, at a shear of 281 kN and a deflection of 6.84 mm. the test of DB2-N ended.

Figure 3.24 shows the total applied load versus the measured displacement from the MTS displacement LVDT for Loading 1, Loading 2. It can be seen that the maximum total applied load for Loading 1 is 460 kN, for Loading 2 is 659 kN.

3.2.1 Response of DB2-S

Table 3.3 summarizes the major events for DB2-S and Fig. 3.25 shows the shear versus deflection measured at the end of the full-depth section. The initial hairline crack at the re-entrant corner appeared at LS-3, a shear of 50 kN and a deflection of 0.30 mm. At LS-4, six hairline flexure cracks occurred near the bottom of full-depth beam in the midspan region. The flexural cracks occurred at the stirrup locations (see Fig. 3.26). At LS-5, at a shear of 100 kN, the crack at the re-entrant corner increased up to 0.10 mm wide (see Fig. 3.27). As the loading increased, the crack at the re-entrant corner propagated at approximately 45 degree to the horizontal. At LS-7, the crack grew to a width of 0.30 mm. At LS-8, the first flexure-shear crack occurred and formed at a location about 700 mm from the end of full-depth section (see Fig. 3.28). At LS-9, a shear of 181.5 kN and a deflection of 2.31 mm, the crack width at the re-entrant corner increased to 0.70 mm. At this load stage, a new diagonal crack at full-depth beam appeared, and the flexure-shear crack width rapidly increased to 0.25 mm (see Fig. 3.29). At LS-10, the maximum shear was reached at a shear of 273 kN with corresponding deflection of 4.03 mm, and a new inclined crack at nib appeared with a width of 0.20 mm (see Fig. 3.30). This crack lengthened and widened as loading increased further and increased to 1.00 mm wide at LS-11. The loading ended at LS-12 where the crack in the dapped end propagated to the top of the15M horizontal bars, resulting in severe splitting cracks at the top and the bottom at a shear of 108.5 kN with corresponding deflection of 9.47 mm (see Fig. 3.31). The further loading of DB2-N was carried out after moving the support of DB2-S and strengthening DB2-S.

Table 3.3 Summary of events for DB2-S

Loading stages	shear load (kN)	Deflection (mm)	Events
LS-3	50	0.30	Hairline crack at re-entrant corner and flexure crack at middle span
LS-4	75	0.54	Six hairline flexure cracks appeared near the bottom of full-depth beam in the midspan region
LS-5	100	0.82	The diagonal crack at re-entrant corner increased to 0.1 mm wide
LS-7	150	1.55	The diagonal crack at re-entrant corner increased to 0.3 mm wide
LS-8	175	2.01	The first flexure-shear crack occurred
LS-9	181.5	2.31	The crack at re-entrant corner increased to 0.7 mm wide. A new diagonal crack appeared at full depth beam. The flexure-shear crack increased to 0.25 mm wide.
LS-10	228.3	4.03	Maximum shear was reached A new inclined crack at nib appeared with a width of 0.2 mm
LS-12	108.5	9.47	The inclined crack at nib propagated to the top hook and resulted in splitting cracks. The test of DB2-S ended.

Figure 3.32 presents the response of the shear versus the strains in the vertical hanger reinforcement. The first hanger bar close to the re-entrant corner yielded during Loading 1. Figure 3.33 shows the response of the shear load versus the strain in the horizontal 15M tension bars. The gauges which were close to the steel plate reached the yielding strain at a shear load of 218.4 kN for HR1 and 197.8 kN for HR2. Figure 3.34 gives the shear versus strain response for the horizontal U-bars in the nib. Figure 3.35 presents the shear versus strain in the bottom horizontal 15M tension bars, with no yielding detected. Figure 3.36 shows that the strains in the bottom flexure reinforcement at midspan are close to yield.

3.2.2 Response of DB2-N

Table 3.4 gives the summary of the major events for DB2-N and Fig. 3.37 shows the shear versus deflection measured at the end of the full-depth section as well as the different loading setups. The initial crack at the re-entrant corner appeared at LS-3, at a shear of 50 kN and a deflection of 0.26 mm. At LS-5, a new crack at the re-entrant corner occurred just below the first crack (see Fig. 3.38). Both cracks extended and opened to 0.10 mm wide at LS-6. At LS-8, the first flexure-shear crack appeared and formed at a location 250 mm away from the end of full depth section (see Fig. 3.39). At LS-10, a shear crack appeared above the steel plate at the end of full-depth section and propagated at approximately 45 degree (see Fig. 3.40). These inclined cracks are indicative of the diagonal compressive stresses in the concrete that are anchored by the steel plate anchorage at this corner (see Fig. 2.4). At LS-12, Loading 1 was ended when the south end, DB2-S, failed. The maximum crack widths were 0.50 mm for shear crack at full depth section, and 0.40 mm for shear crack at re-entrant corner. After the first loading, the beam was unloaded and the support at DB2-S was moved inward at a distance of 600 mm. At LS-14, the beam was reloaded and a new inclined crack at dapped end occurred with a width of 0.10 mm. The flexure crack extended and opened as loading increased. At LS-18, the shear crack width in the full-depth section increased to 1.0 mm, and the shear crack at the re-entrant corner had a width of 0.50 mm. At this load stage, a new inclined crack occurred at the top of the nib (see Fig. 3.41). At LS-20, the maximum shear was reached at a shear of 329 kN and a deflection of 7.18 mm, the maximum flexure crack width at midspan was 2.5 mm. Flexural distress occurred at midspan at LS-21(see Fig. 3.42). The testing of beam DB2 was ended at a shear of 281 kN and a deflection of 7.13 mm.

Table 3.4 Summary of events for DB2-N

Loading stages	shear load (kN)	Deflection (mm)	Events
LS-3	50	0.26	Hairline crack at re-entrant corner and flexure crack at midspan
LS-5	100	0.82	A new crack at re-entrant corner occurred just below the first crack
LS-6	125	1.14	The two cracks at re-entrant corner increased to 0.1 mm wide
LS-8	175	1.97	The first flexure-shear crack occurred
LS-10	200	2.40	Inclined rack formed just above the anchorage steel plate at the end of full-depth section and propagated at about 45 degree
LS-12	227	3.39	The first loading was ended
LS-13	4.7	-	The beam was unloaded (only self-weight)
LS-14	227	3.78	Reloaded for further loading at DB2-N
LS-18	268	4.40	The shear crack at full depth beam increased to 1.0 mm The shear crack at re-entrant corner had a width of 0.5 mm A new inclined crack occurred at the top of the nib
LS-20	329	7.18	Maximum shear was reached The maximum flexure crack at midspan was 2.5 mm
LS-21	281	7.13	Flexure distress occurred at midspan The second loading was ended

Figure 3.43 gives the response of the shear versus the measured strain in vertical hanger reinforcement and the stirrup closet to these hanger bars. During the first loading, the outermost hanger bar reached the yielding point of 2470 microstrain. All of the other hanger bars and the stirrup yielded during Loading 2. Figure 3.44 gives the shear versus the measured strain in the horizontal 15M tension bars anchored in the nib. This figure shows that the strain in the horizontal 15M tension bars in the nib near the steel plate reached their yield stress during Loading 2. Figure 3.45 gives the shear versus the measured strain in the horizontal U-bars in the nib. These 15M bars did not yield. Figure

3.46 shows the shear versus strains in the legs of hanger bars at the level of flexure reinforcement (gauges HL7, HL8 and HL9). This figure shows that HL9 yielded during Loading 2.

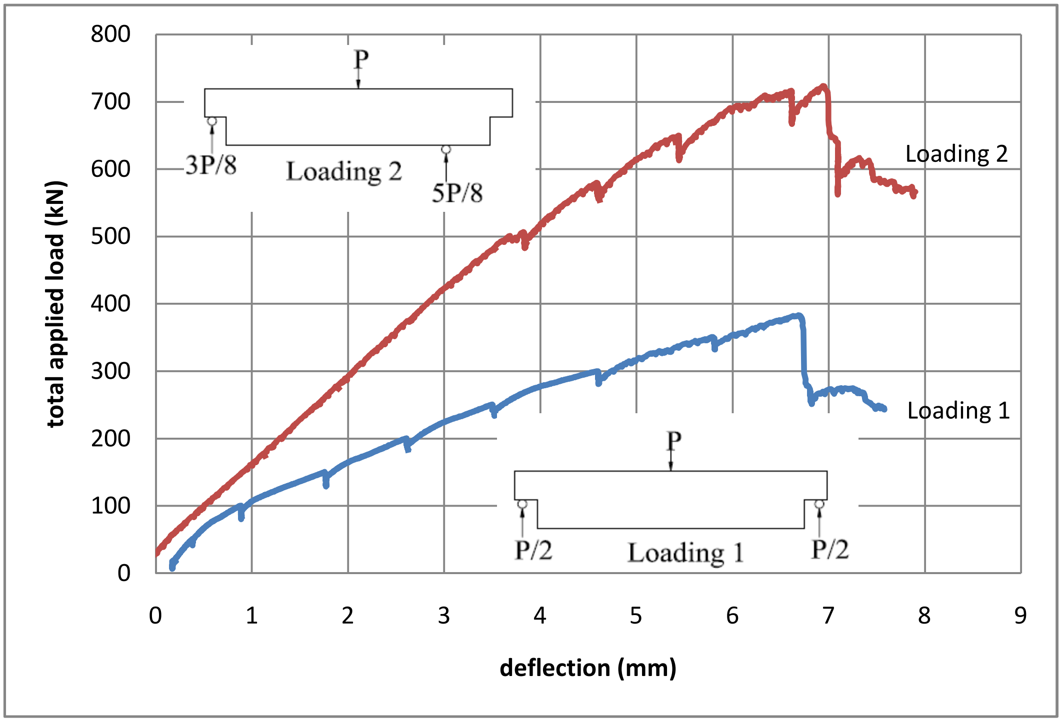

Figure 3.1 Total applied load versus net deflection at midspan for loading 1

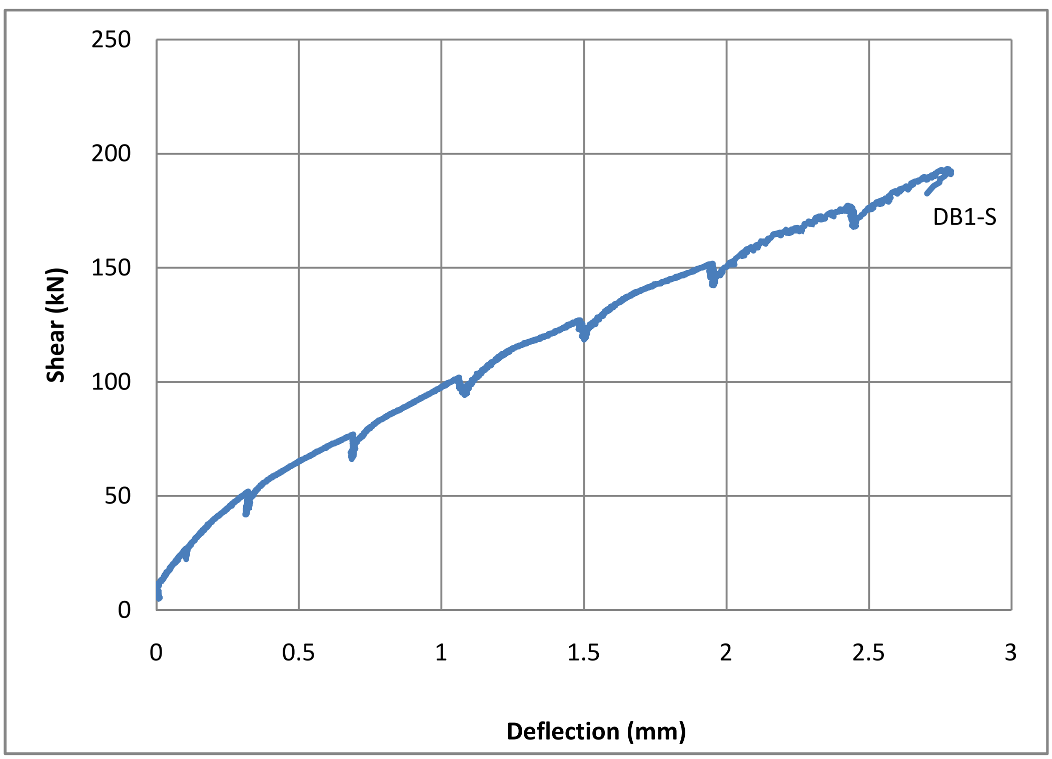

Figure 3.2 Shear versus deflection at the end of full-depth section of DB1-S

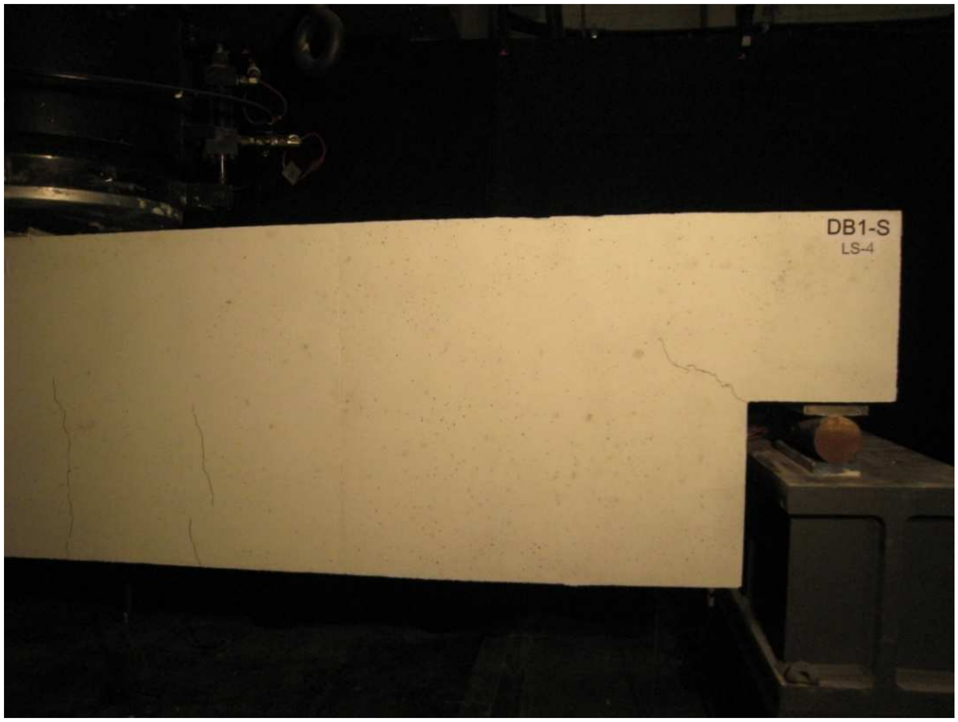

Figure 3.3 Crack pattern at LS-4 of DB1-S

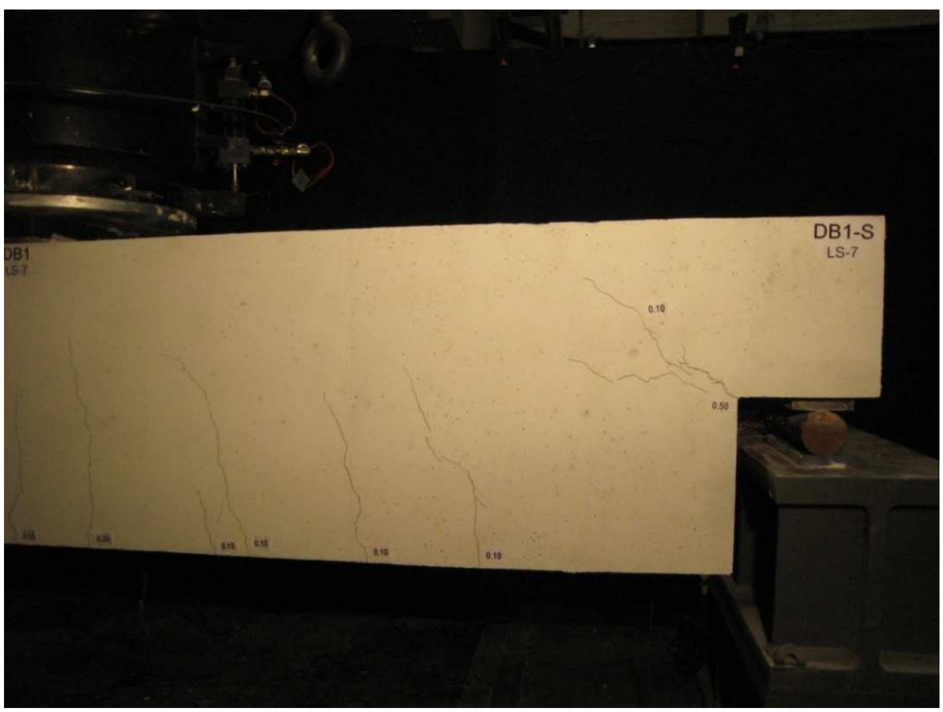

Figure 3.4 Crack pattern at LS-7 of DB1-S

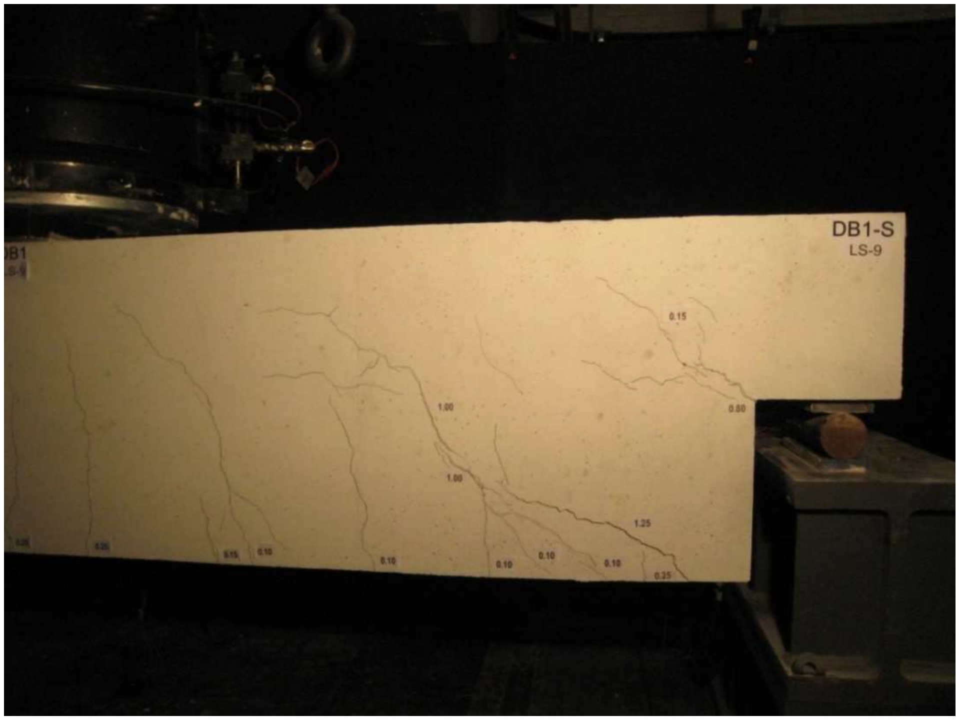

Figure 3.5 Crack pattern at LS-9 of DB1-S

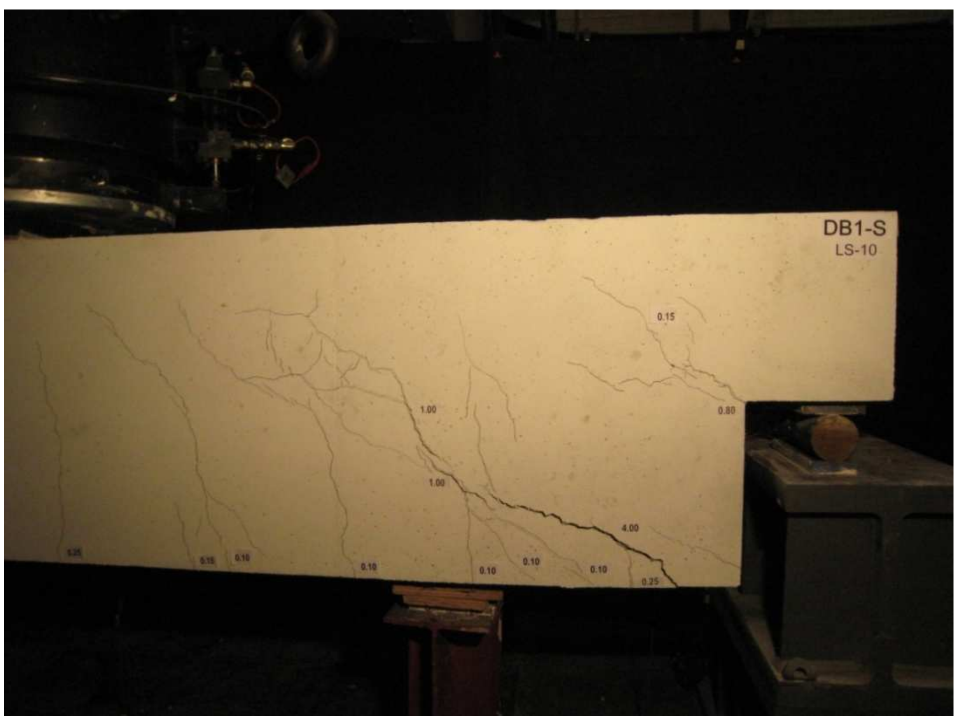

Figure 3.6 Crack pattern at LS-10 of DB1-S

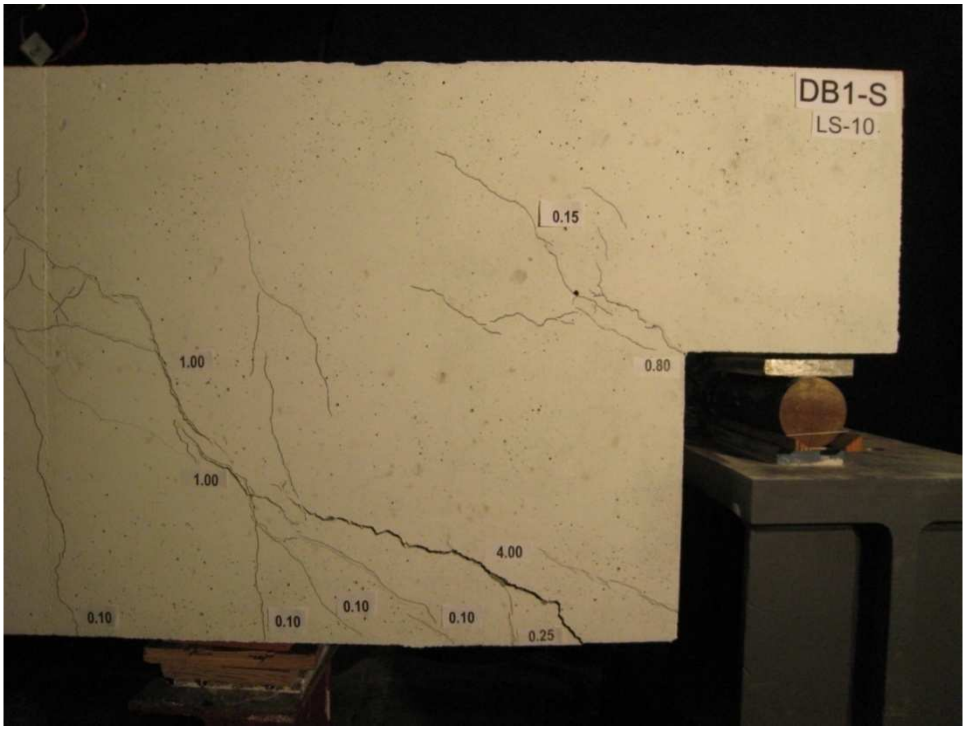

Figure 3.7 Closer view of crack pattern at LS-10 of DB1-S

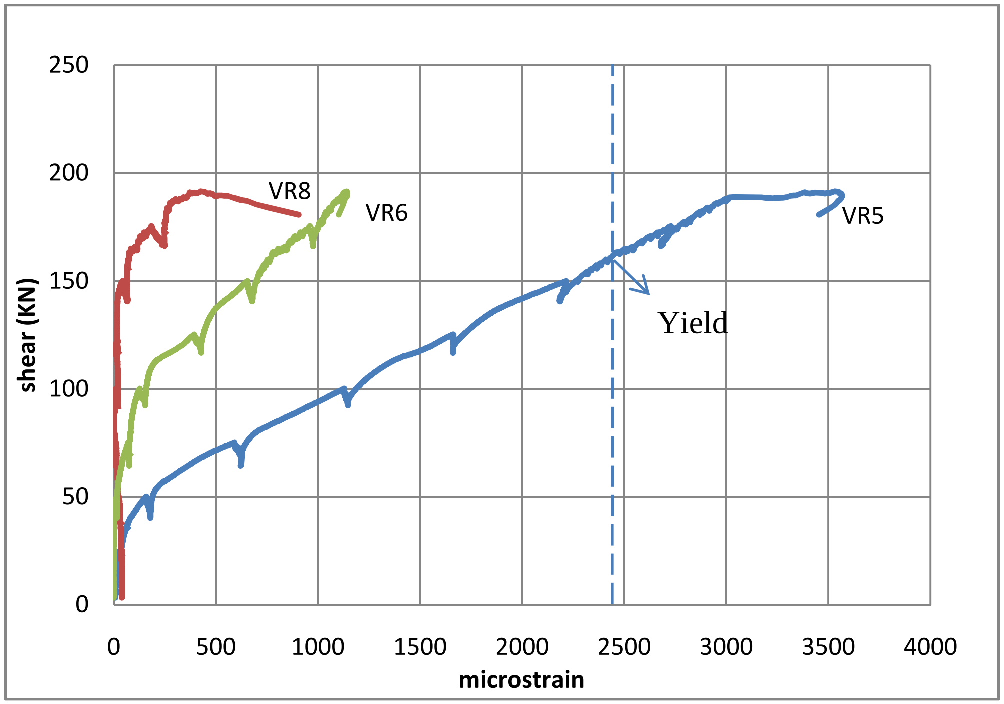

Figure 3.8 Shear versus strain in stirrups for DB1-S

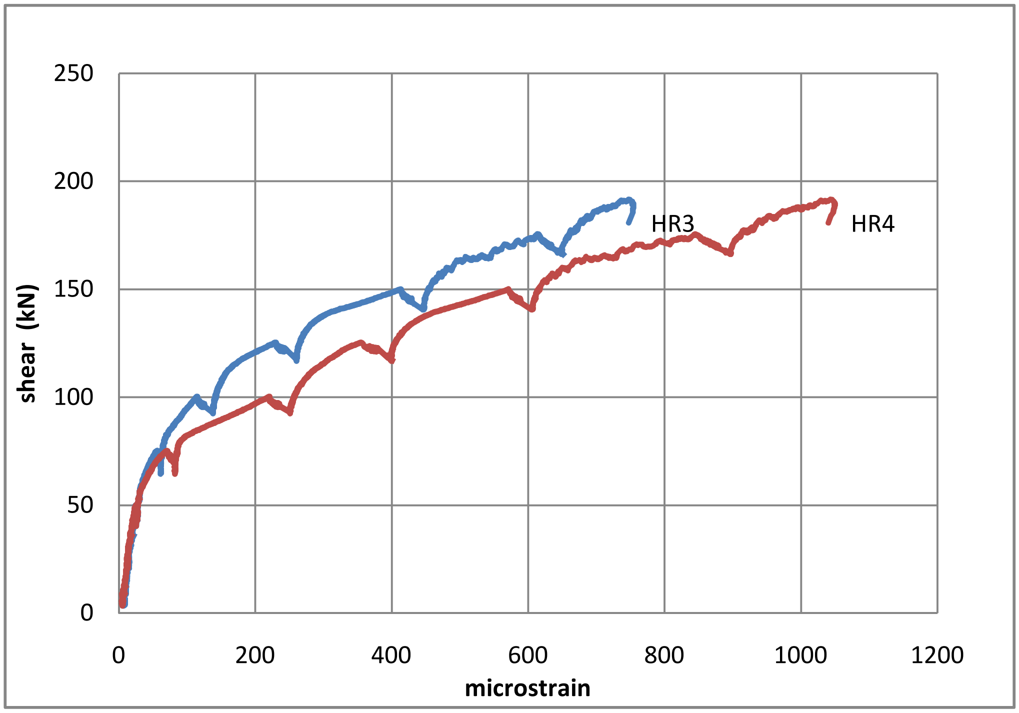

Figure 3.9 Shear versus strain in horizontal 15M tension bars near re-entrant corner for DB1-S

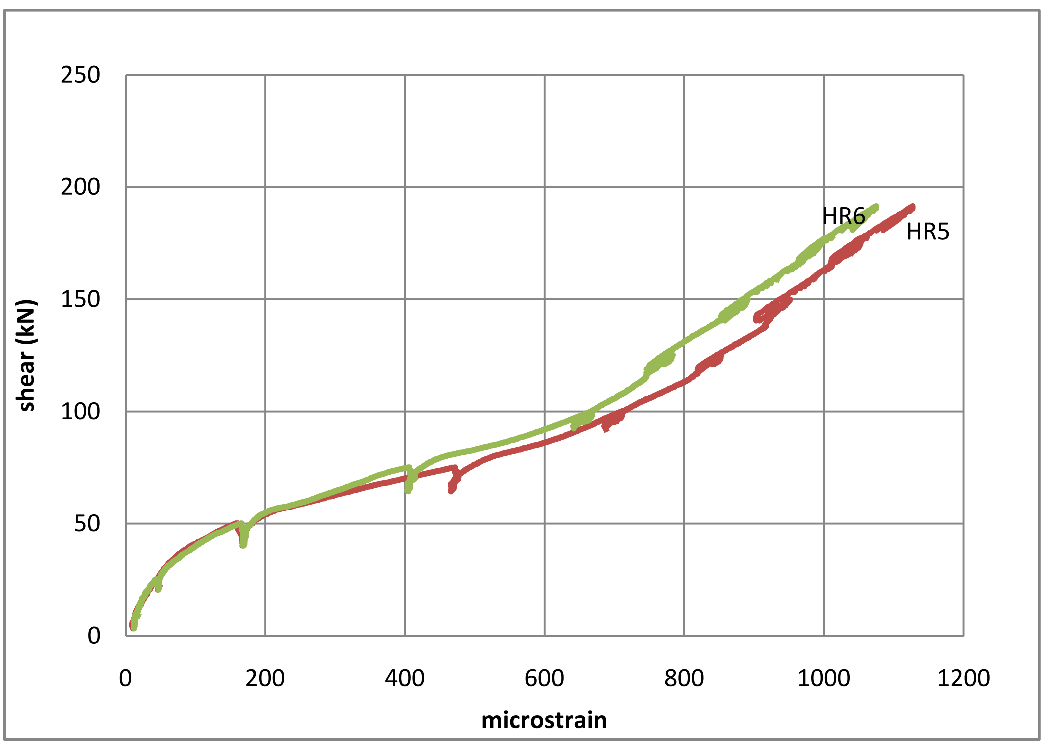

Figure 3.10 Shear versus strain in horizontal 15M tension bars for DB1-S

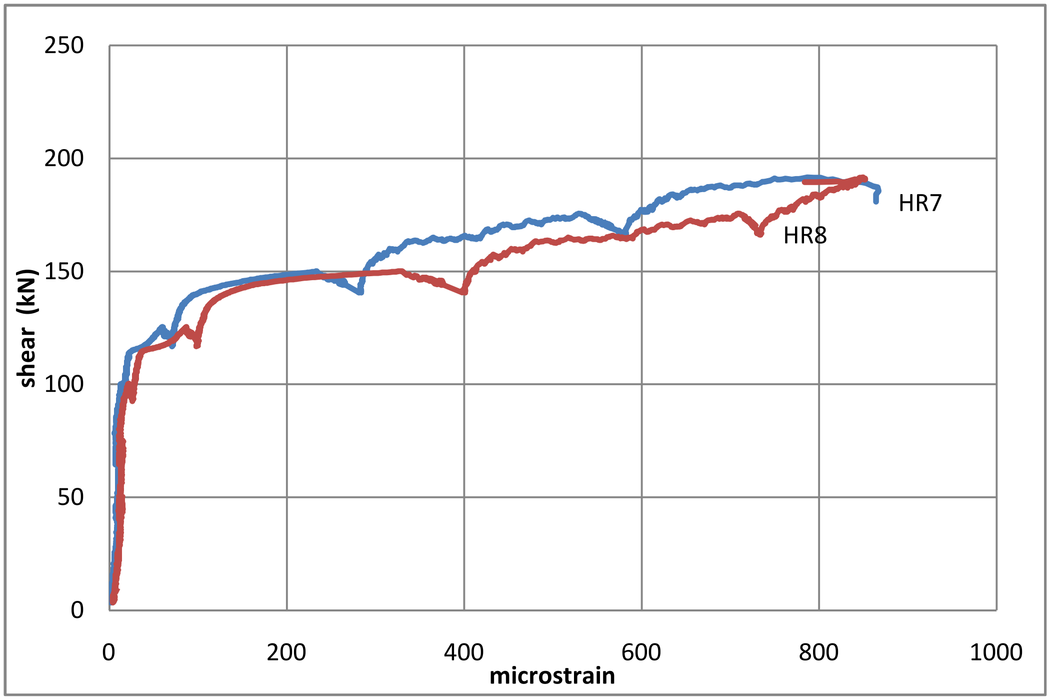

Figure 3.11 Shear versus strain in bottom flexure bars near hanger bars for DB1-S

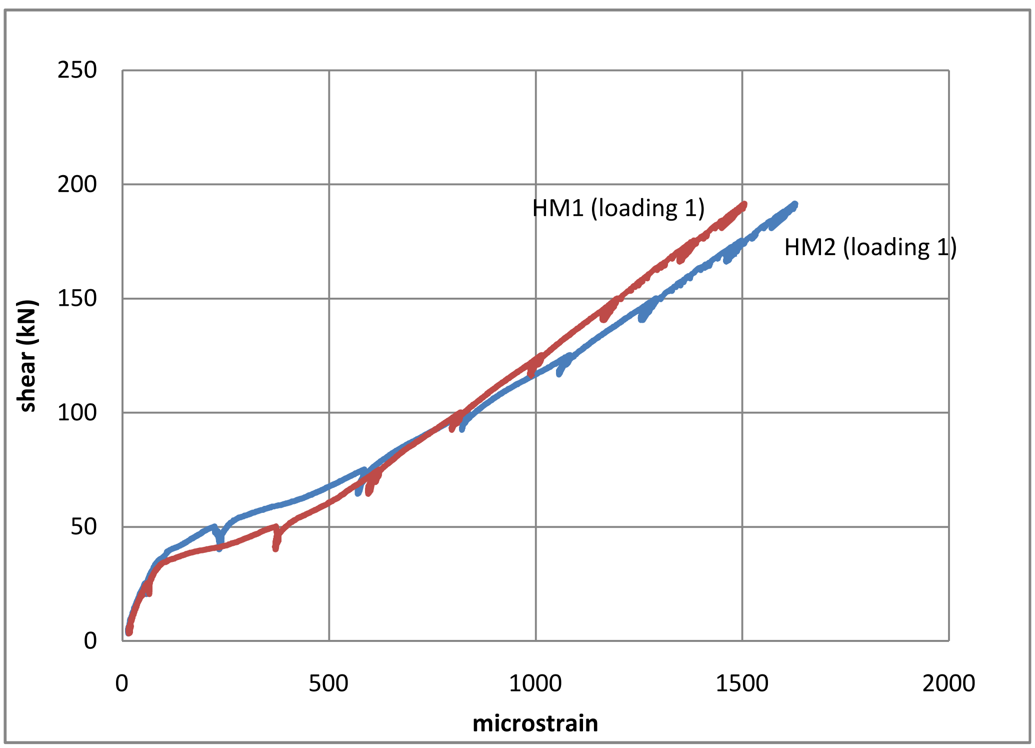

Figure 3.12 Shear versus strain responses of bottom flexure bars at midspan

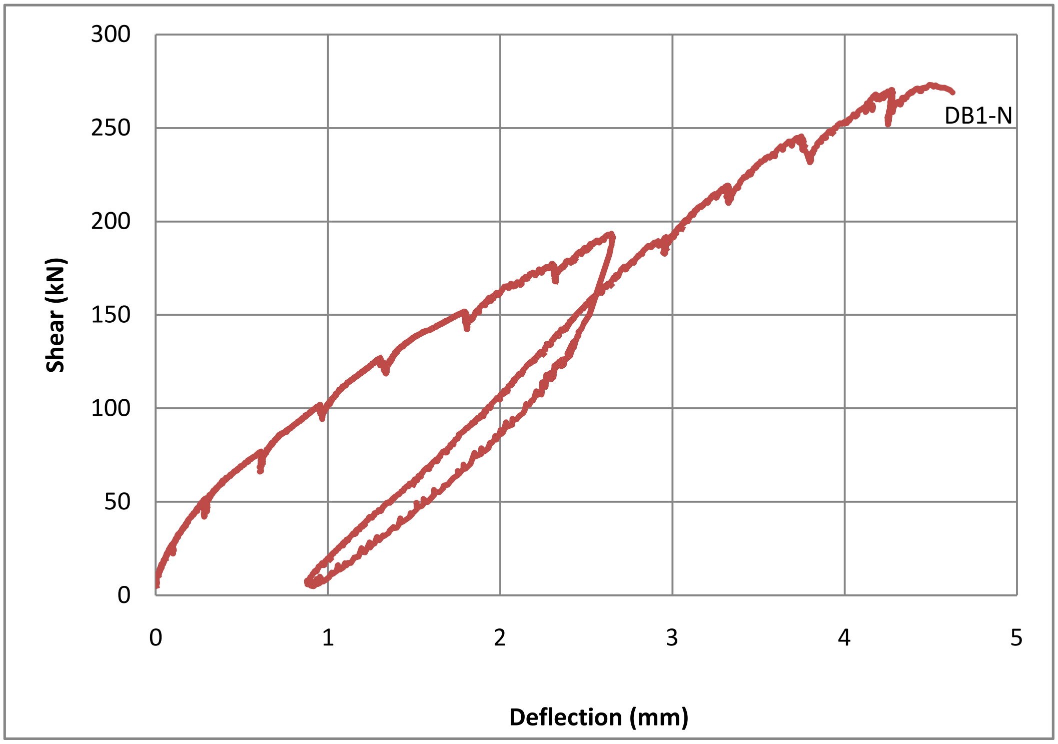

Figure 3.13 Shear versus deflection at the end of full-depth section for DB1-N

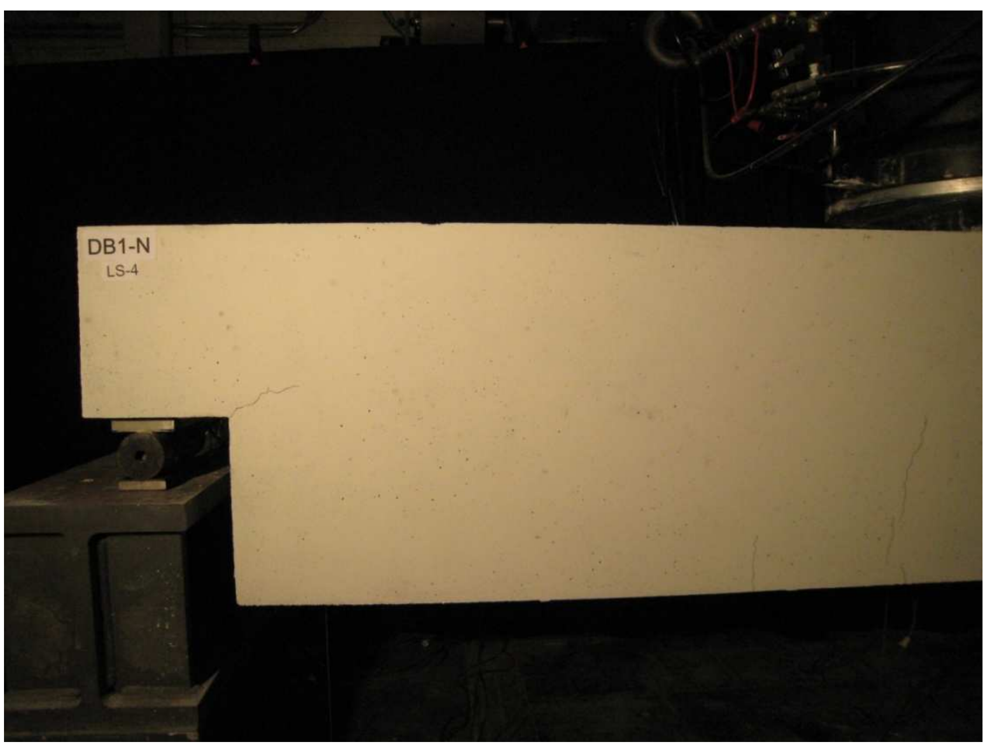

Figure 3.14 Photo of crack pattern at LS-4 for DB1-N

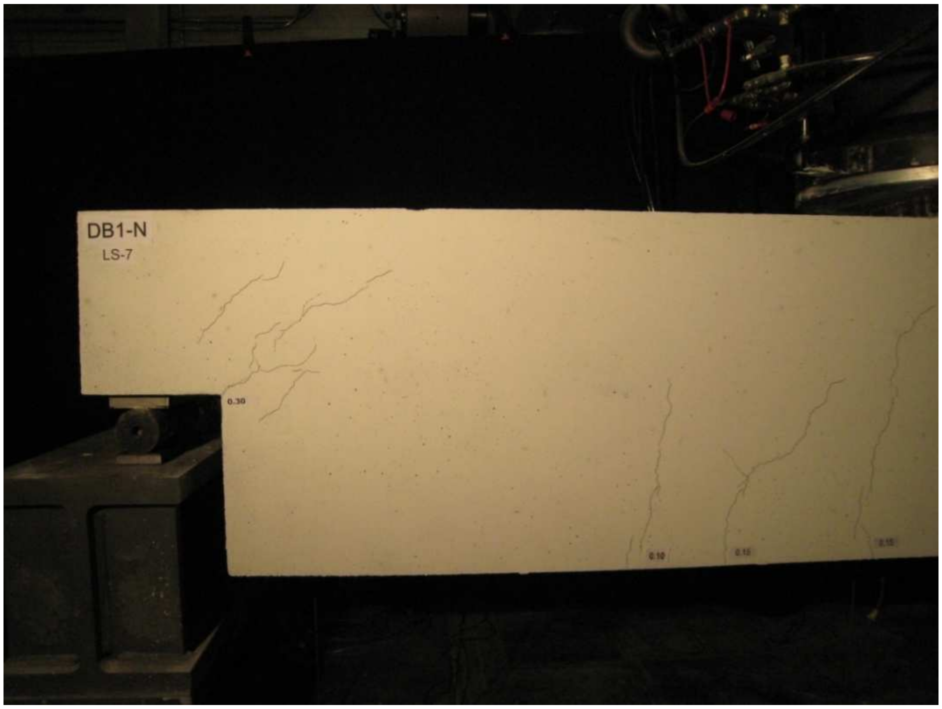

Figure 3.15 Photo of crack pattern at LS-7 for DB1-N

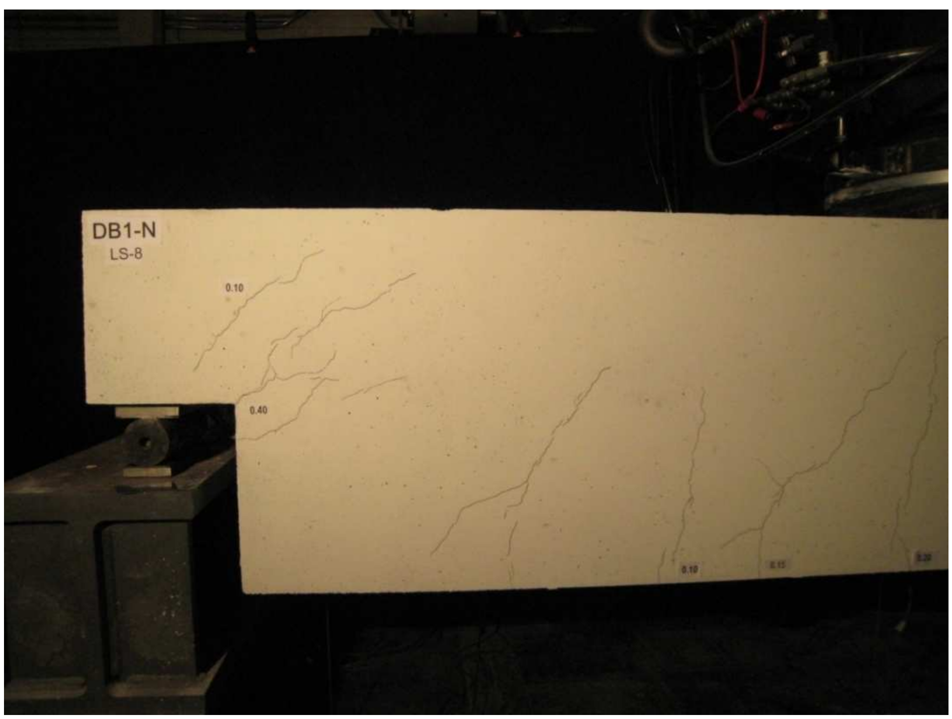

Figure 3.16 Photo of crack pattern at LS-8 for DB1-N

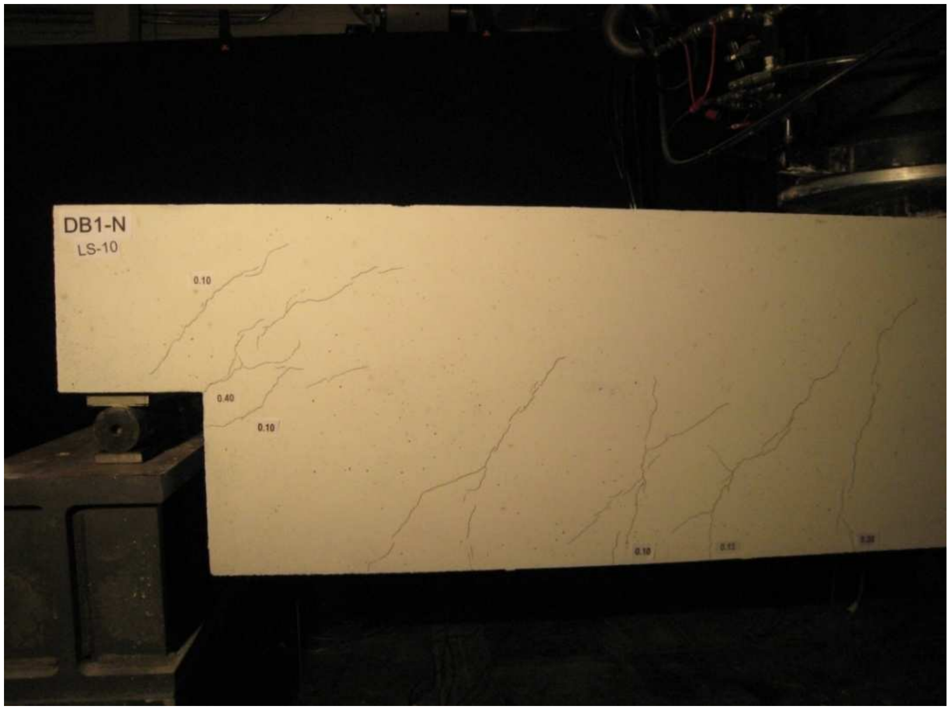

Figure 3.17 Photo of crack pattern at LS-10 for DB1-N

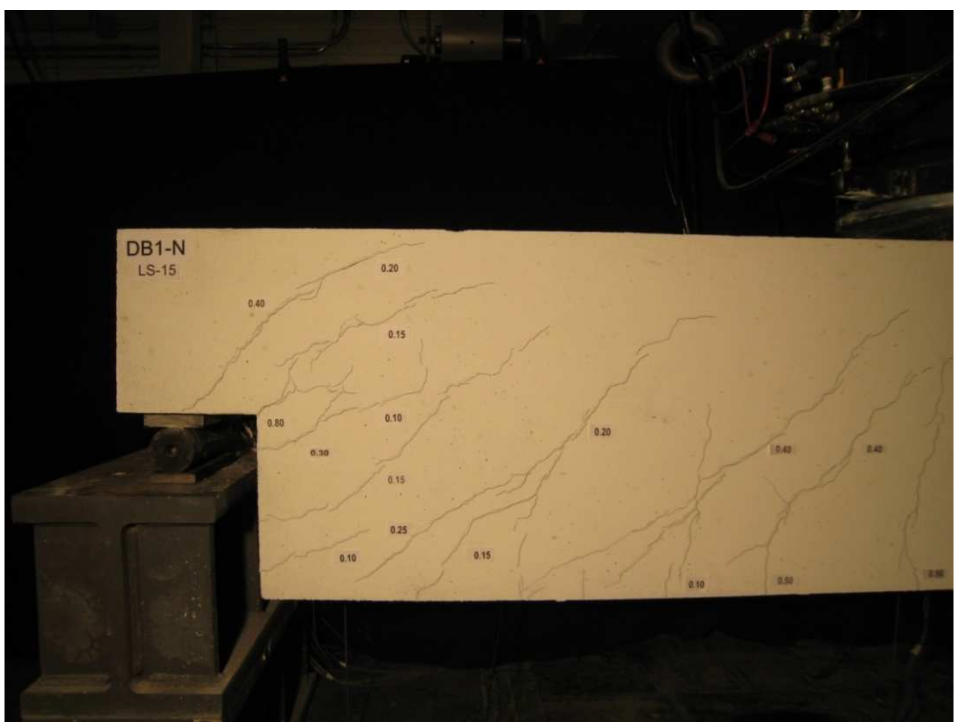

Figure 3.18 Photo of crack pattern at LS-15 for DB1-N

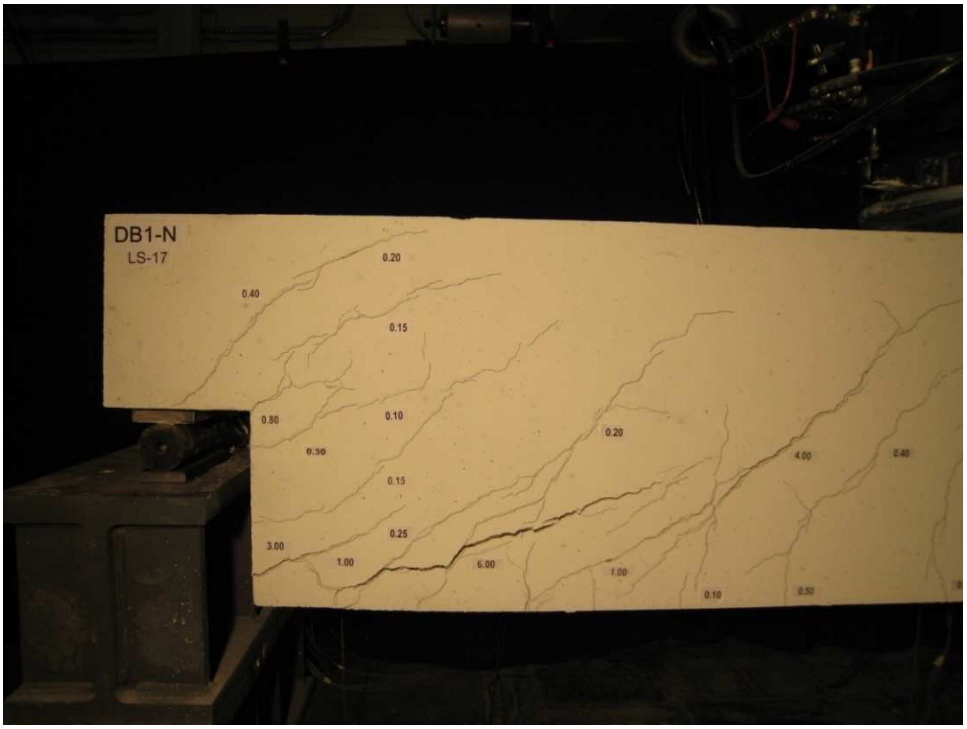

Figure 3.19 Photo of crack pattern at LS-17 for DB1-N

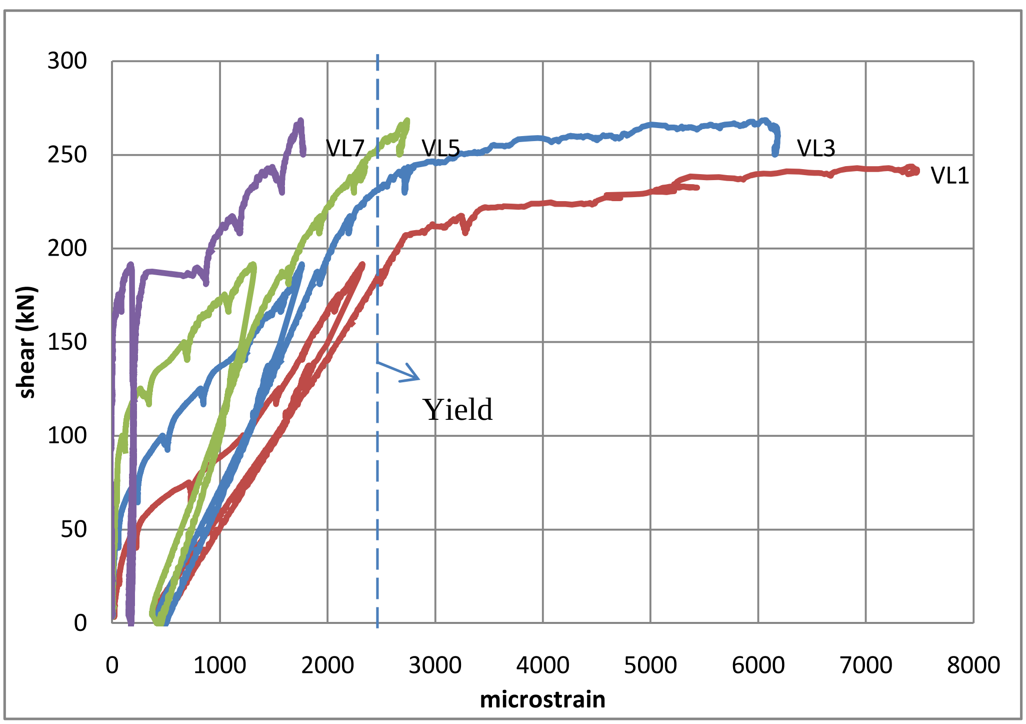

Figure 3.19 Shear versus strain responses of stirrups for DB1-N

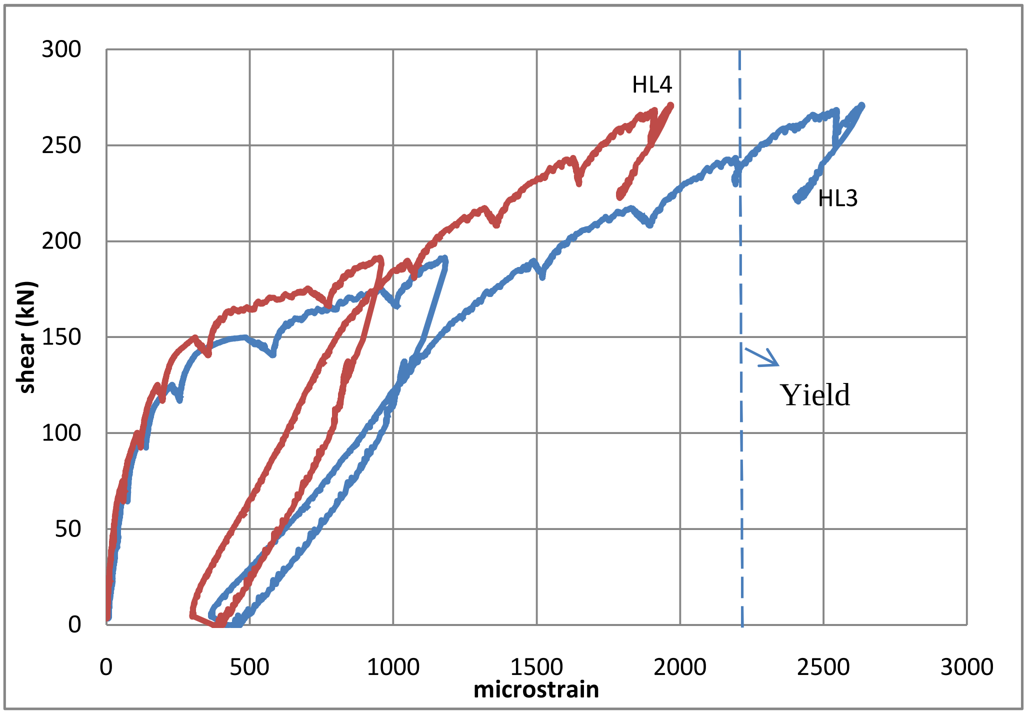

Figure 3.201 Shear versus strain responses of horizontal 15M tension bars near the re-entrant corner for DB1-N

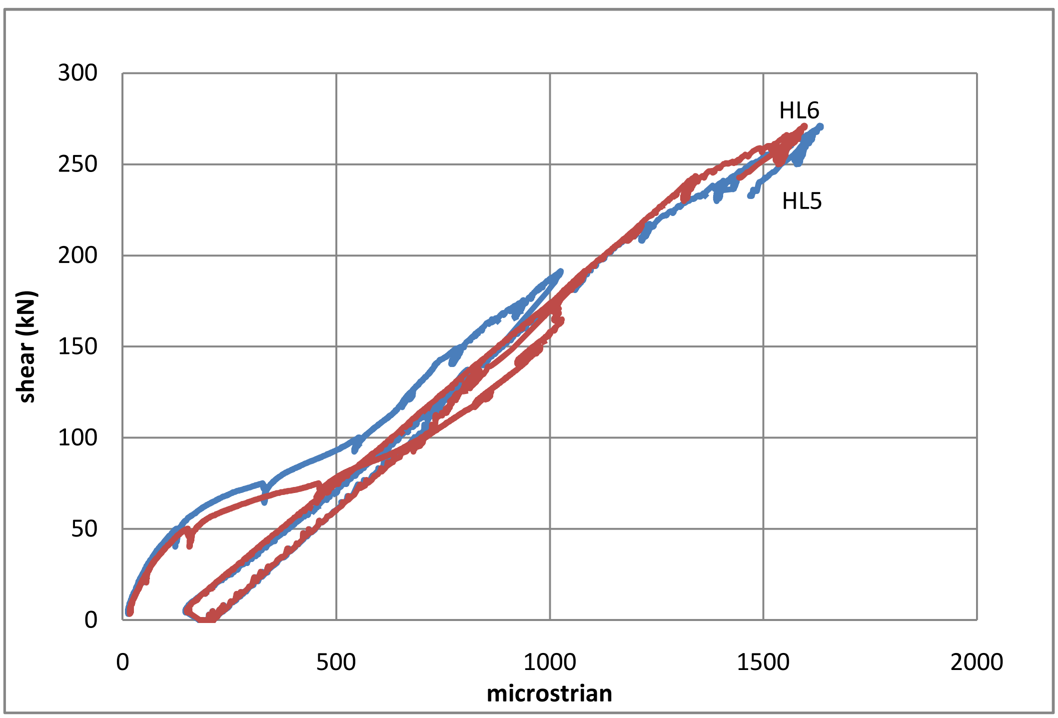

Figure 3.212 Shear versus strain responses of horizontal 15M tension bars for DB1-N

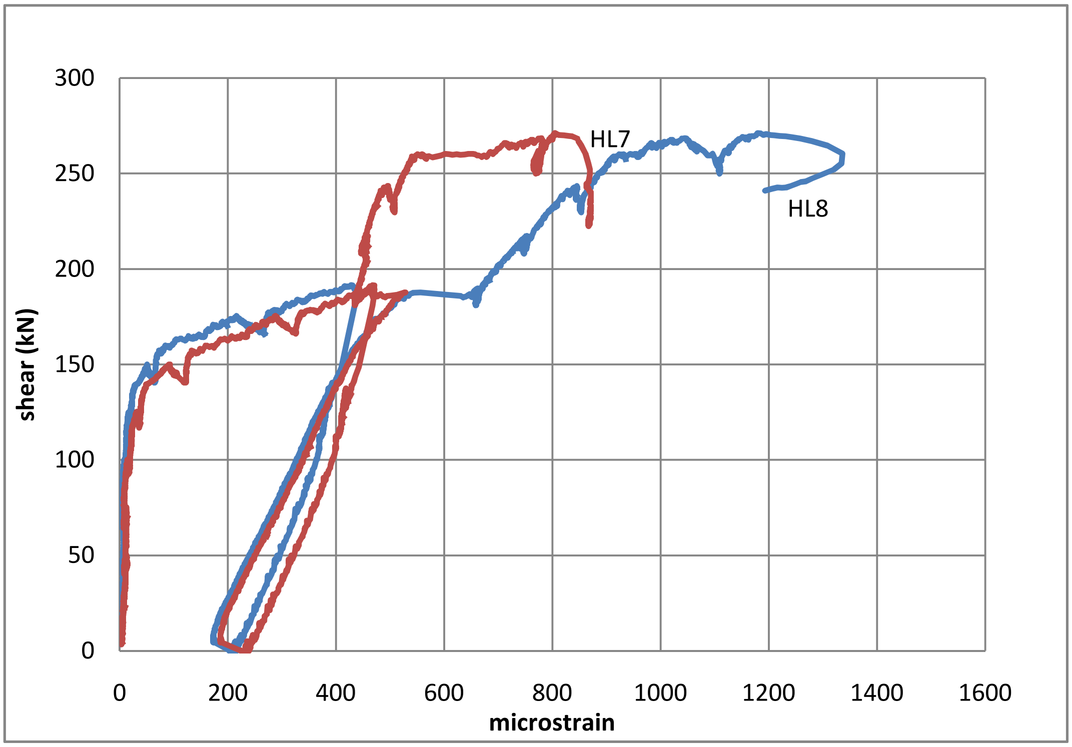

Figure 3.22 Shear versus strain responses of bottom flexure bars near hanger bars for DB1-N

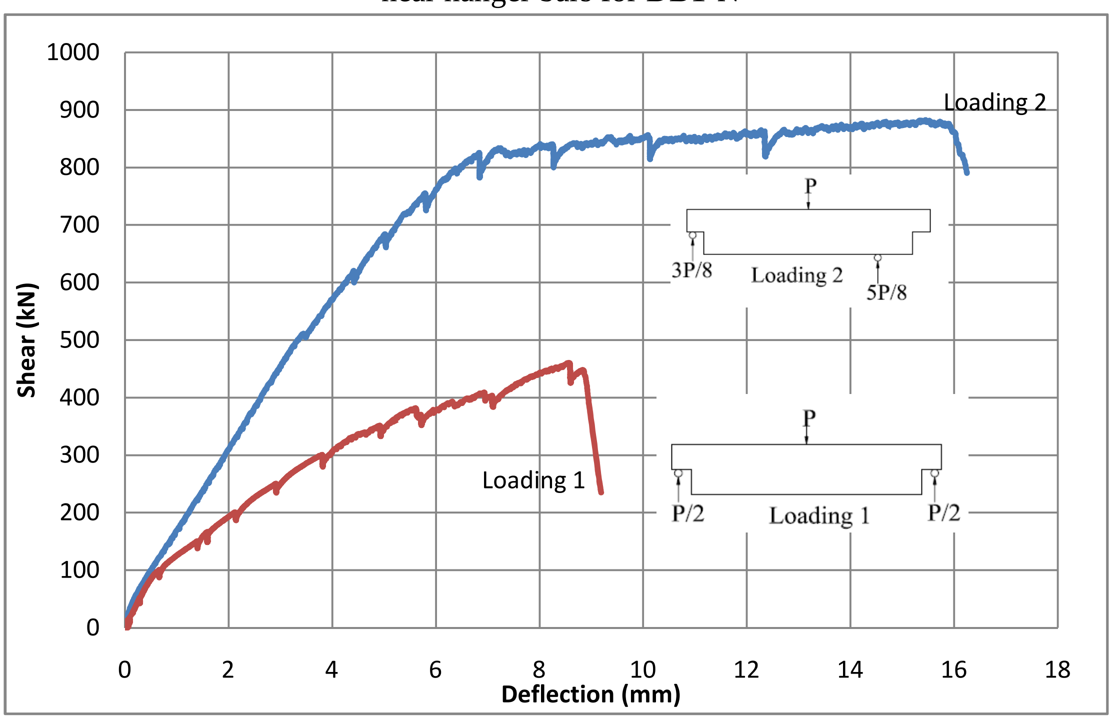

Figure 3.23 Total applied load versus net deflection at midspan for DB2 (loading1&2)

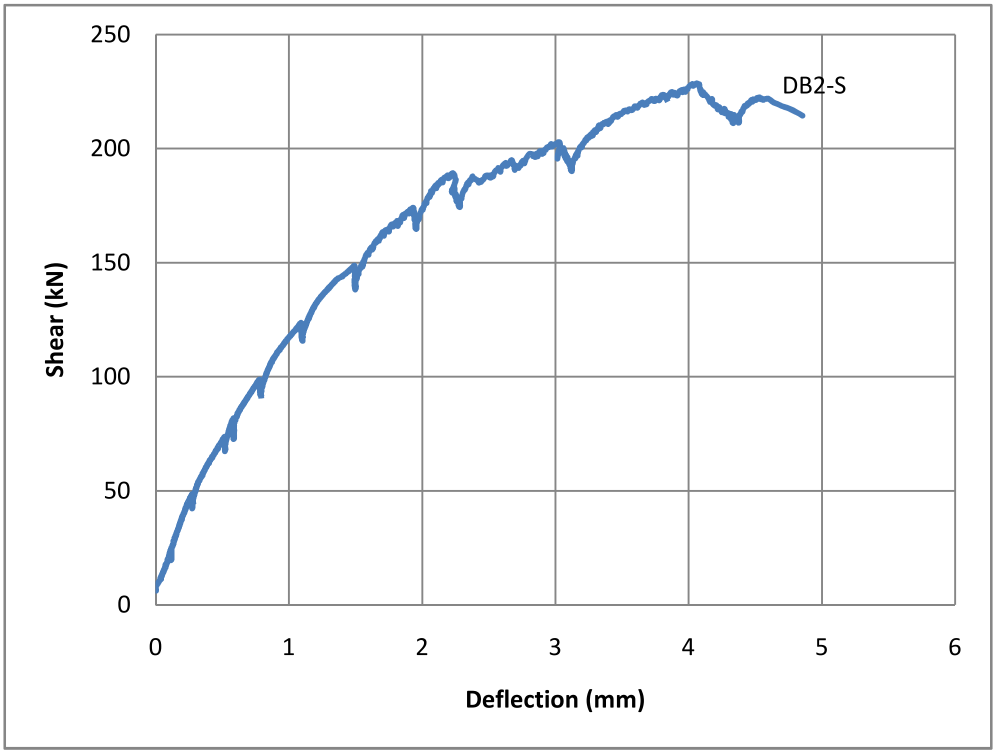

Figure 3.24 Shear versus deflection at the end of full-depth section for DB2-S

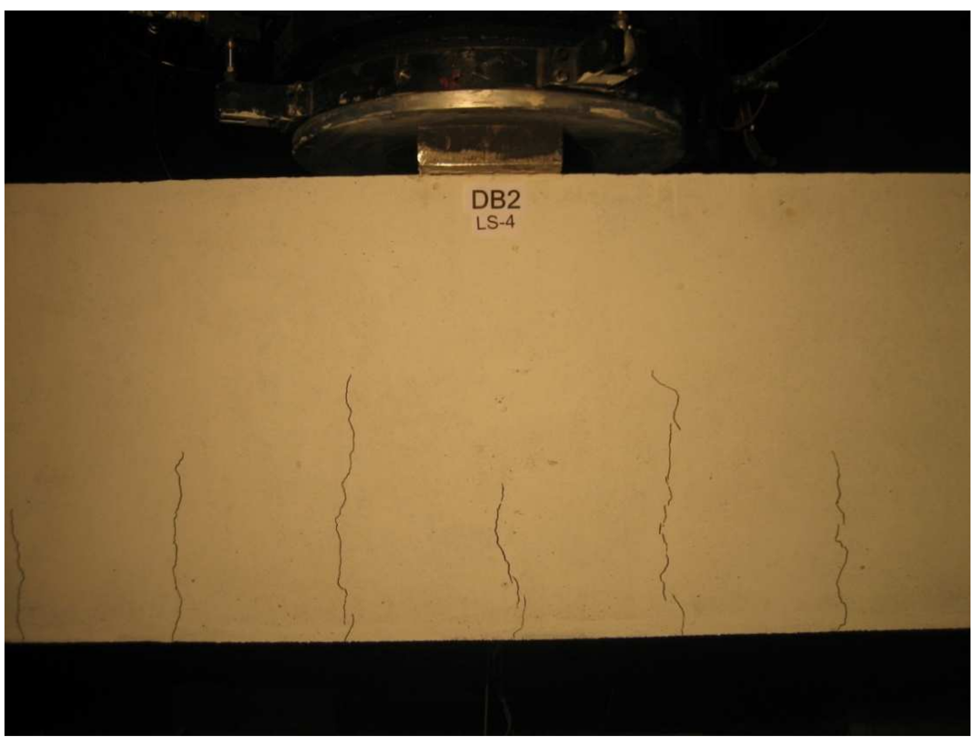

Figure 3.25 Photo of crack pattern at LS-4 for DB2 at midspan

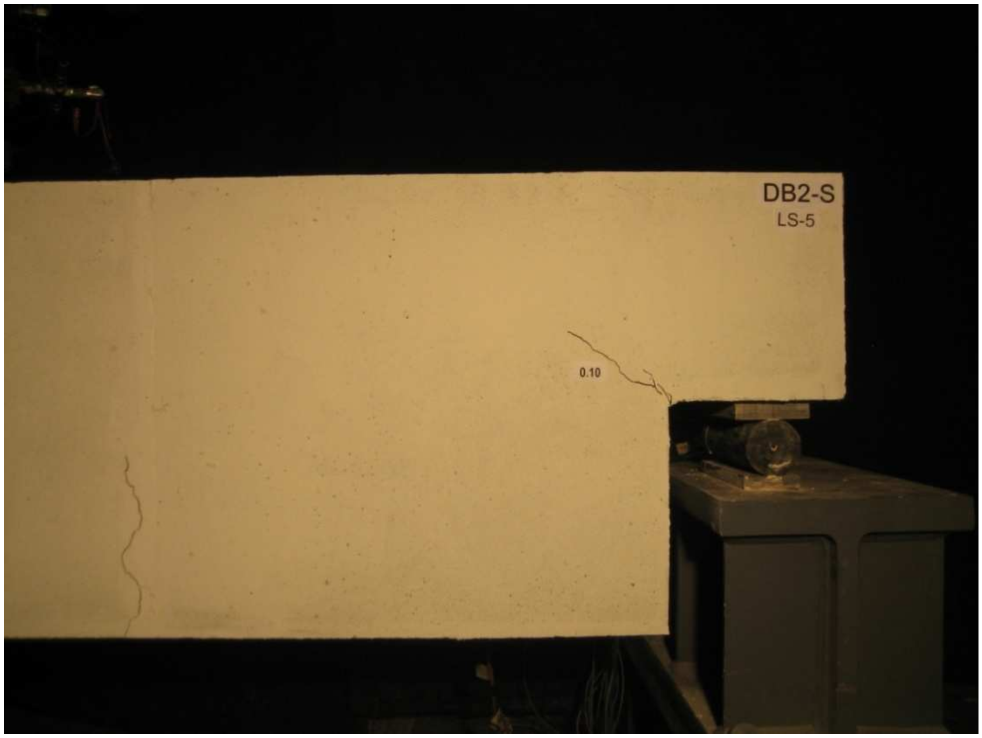

Figure 3.267 Photo of crack pattern at LS-5 for DB2-S

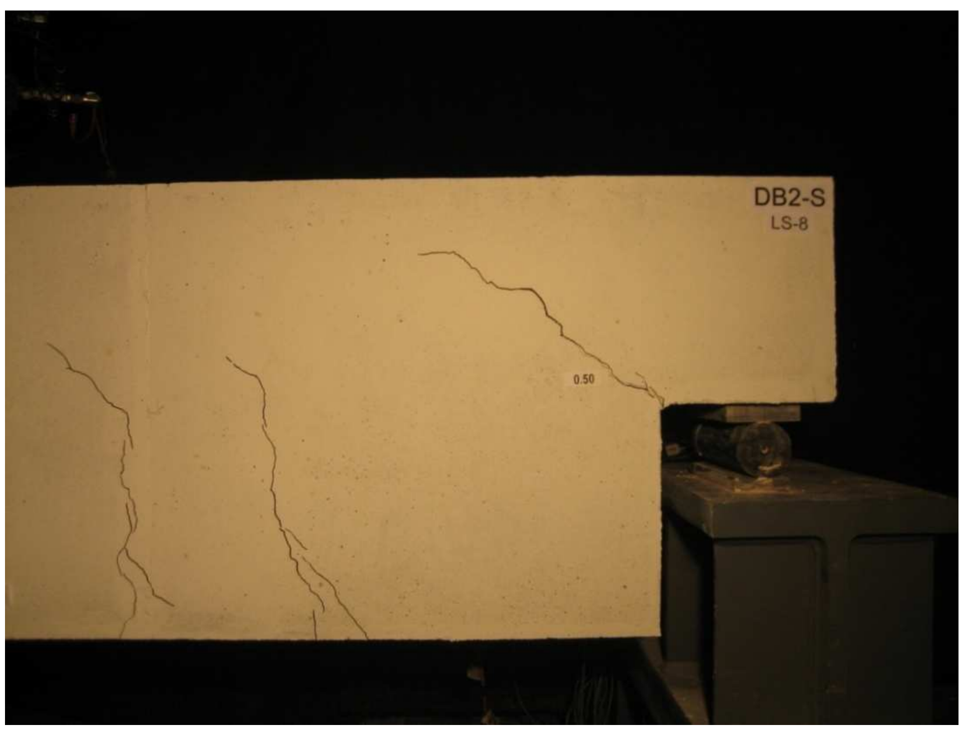

Figure 3.27 Photo of crack pattern at LS-8 for DB2-S

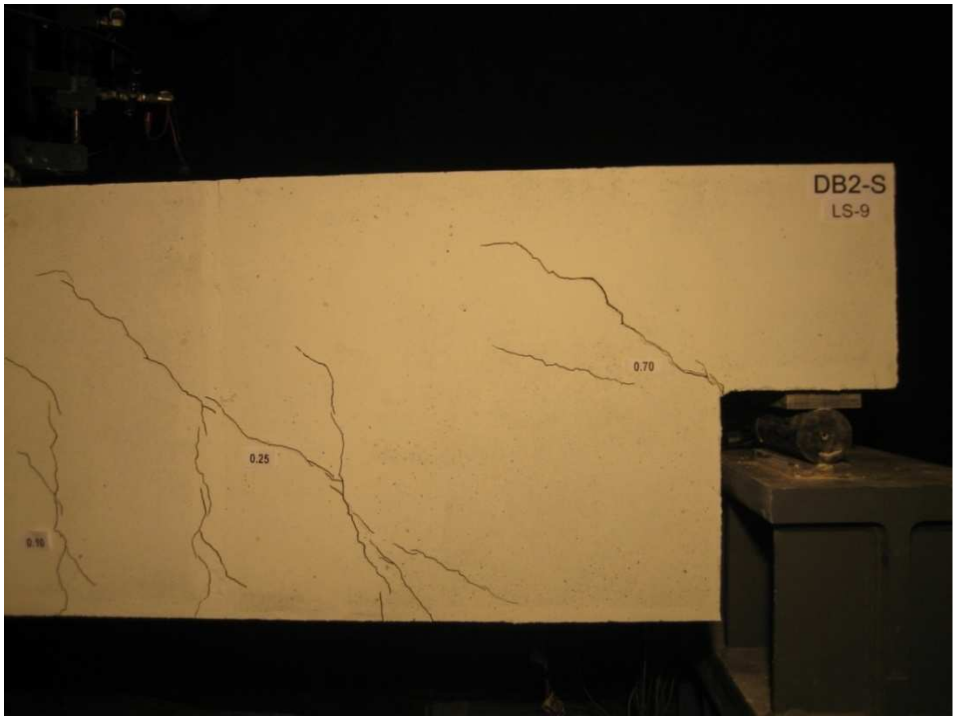

Figure 3.29 Photo of crack pattern at LS-9 for DB2-S

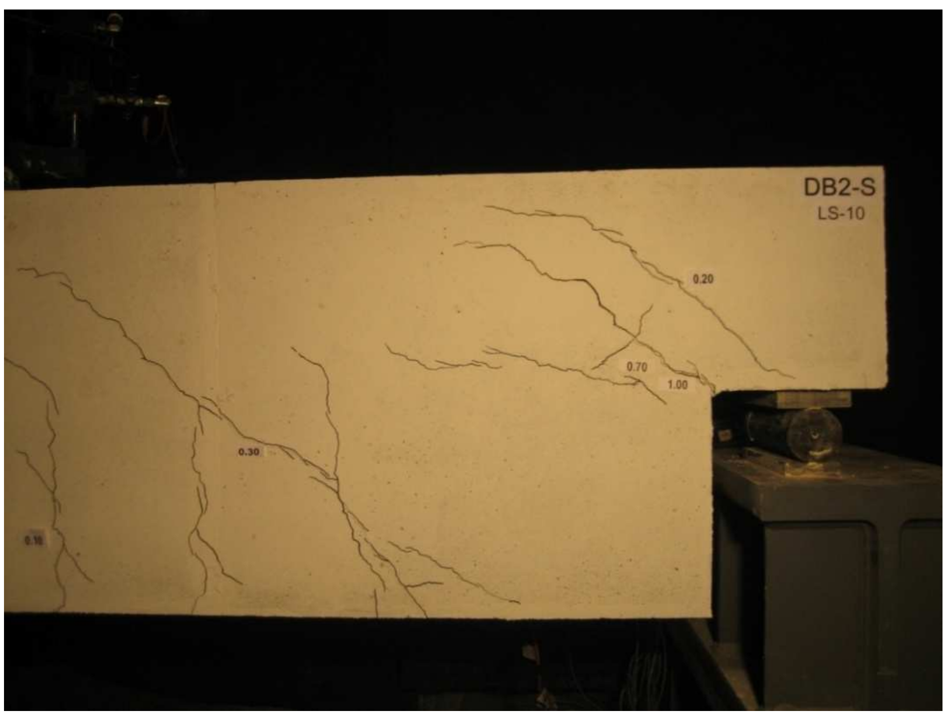

Figure 3.30 Photo of crack pattern at LS-10 for DB2-S

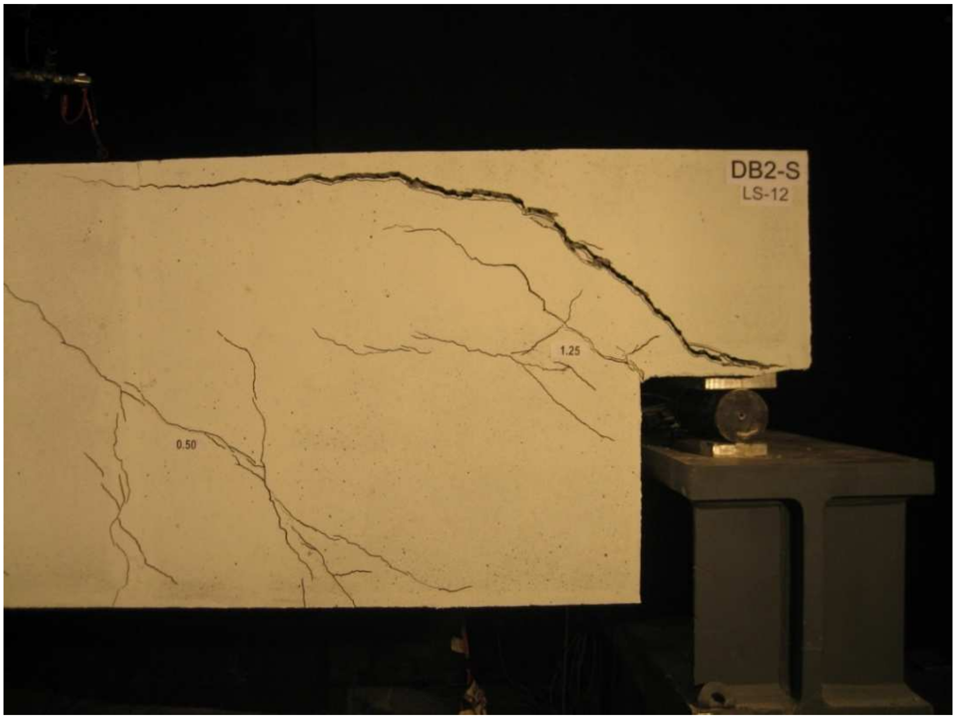

Figure 3.28 Photo of crack pattern at LS-12 for DB2-S

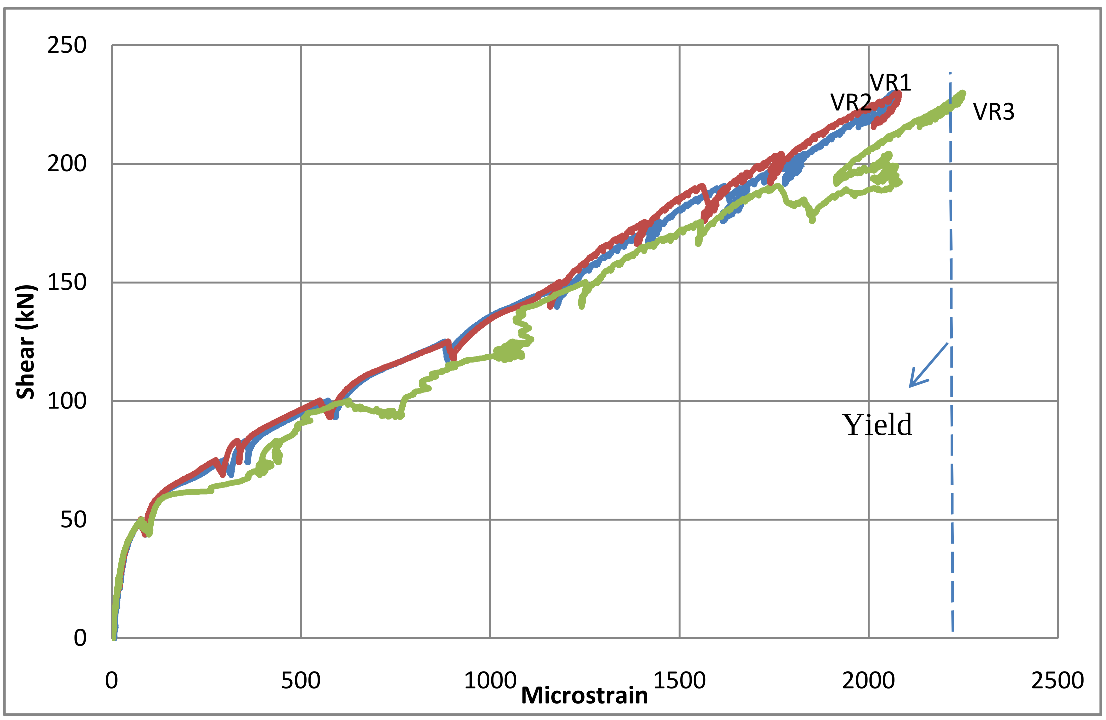

Figure 3.29 Shear versus strain response of hanger reinforcement for DB2-S

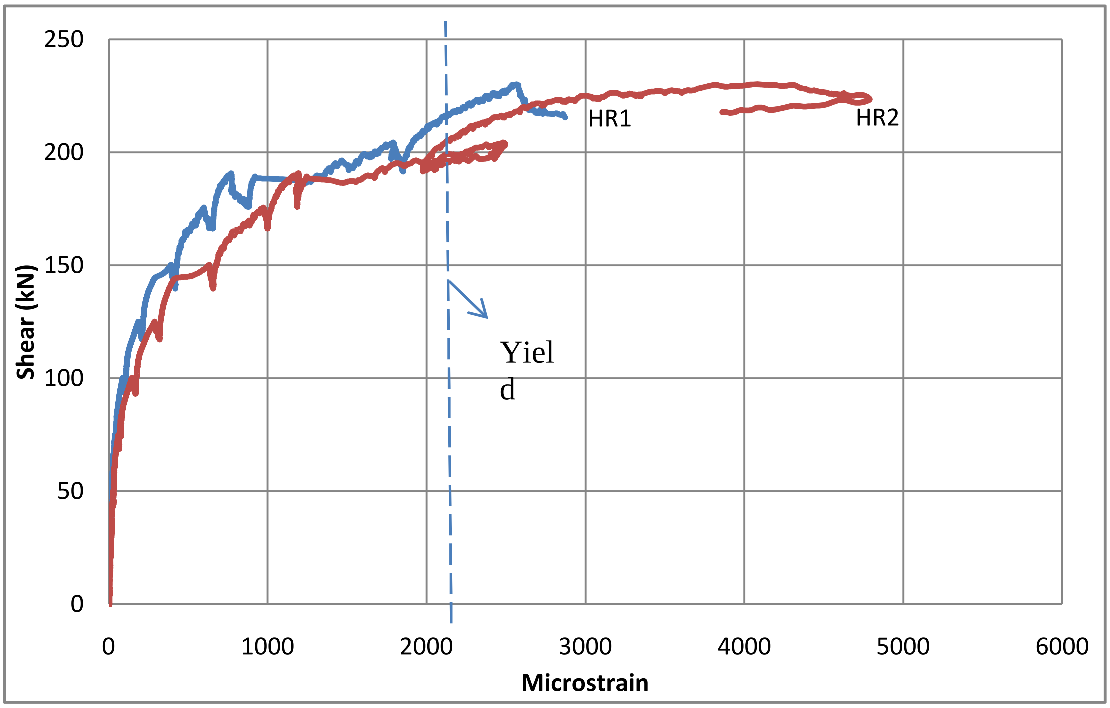

Figure 3.30 Shear versus strain response of horizontal 15M tension bars near the steel plate for DB2-S

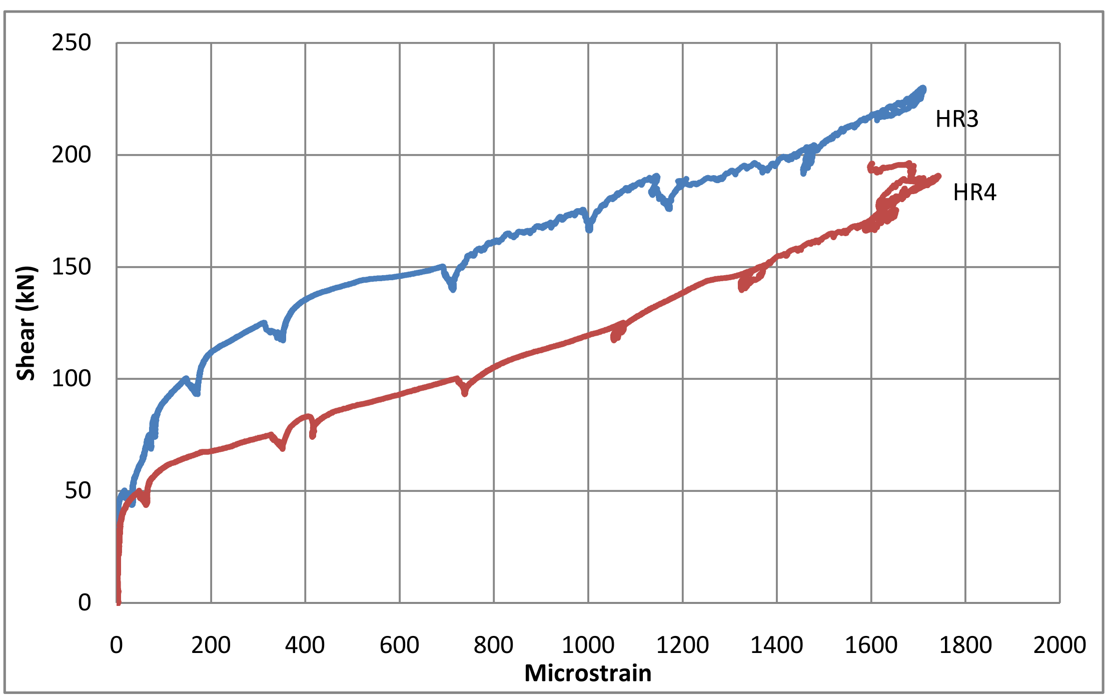

Figure 3.31 Shear versus strain response of horizontal U-bars at nib for DB2-S

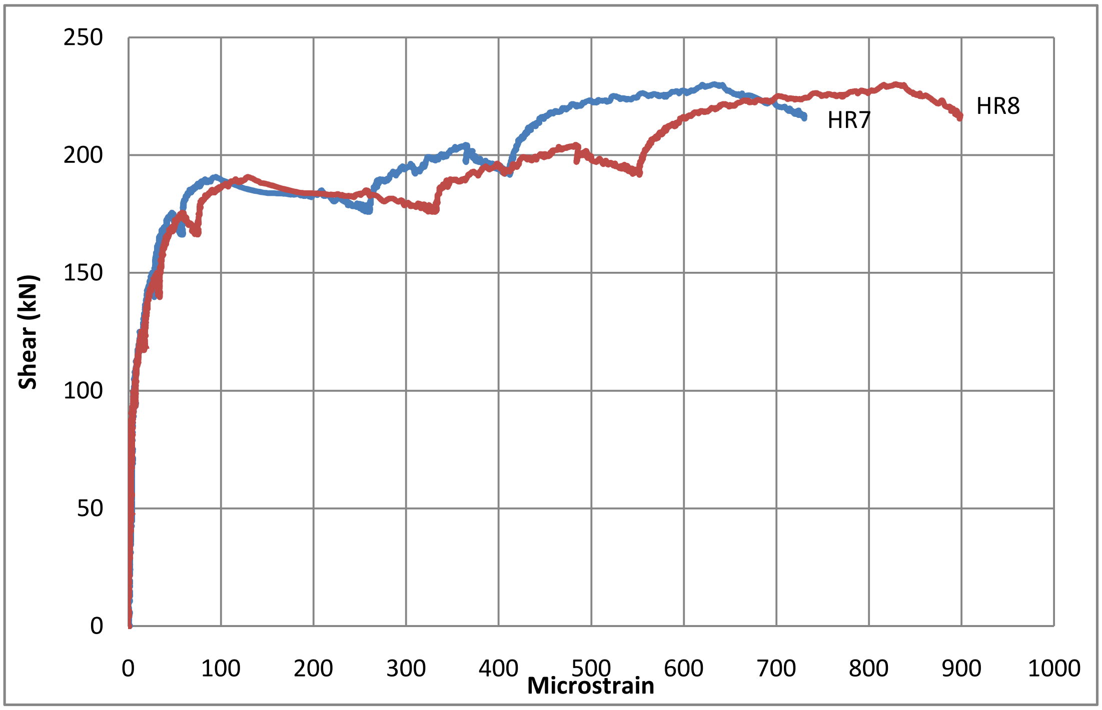

Figure 3.325 Shear versus strain response of the bottom anchorage bars near hanger bars for DB2-S

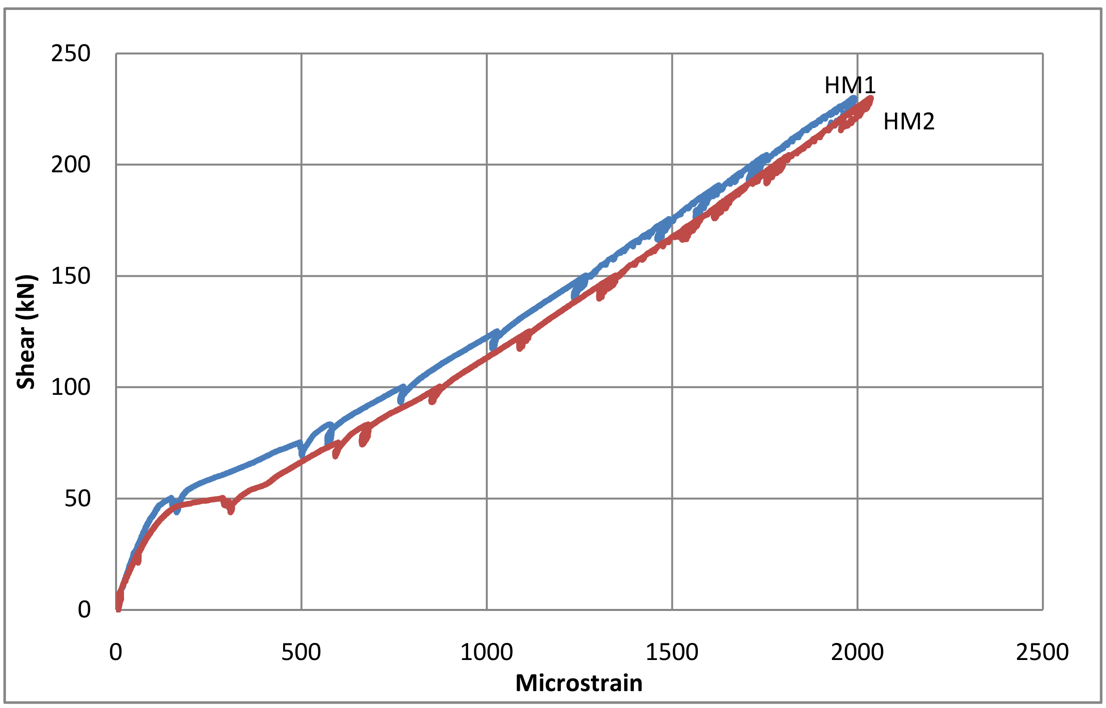

Figure 3.33 Shear versus strain response of the bottom flexure bars at midspan for DB2-S

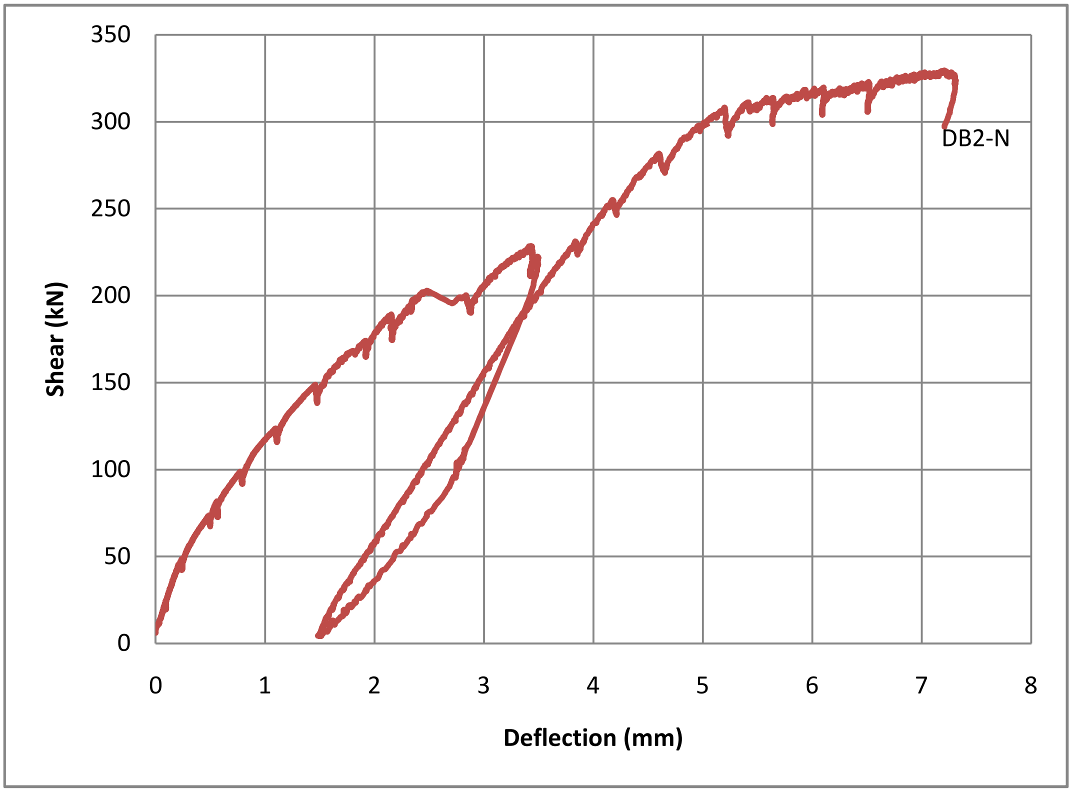

Figure 3.34 Shear versus deflection at the end of full-depth section for DB2-N

Figure 3.35 Photo of crack pattern at LS-5 for DB2-N

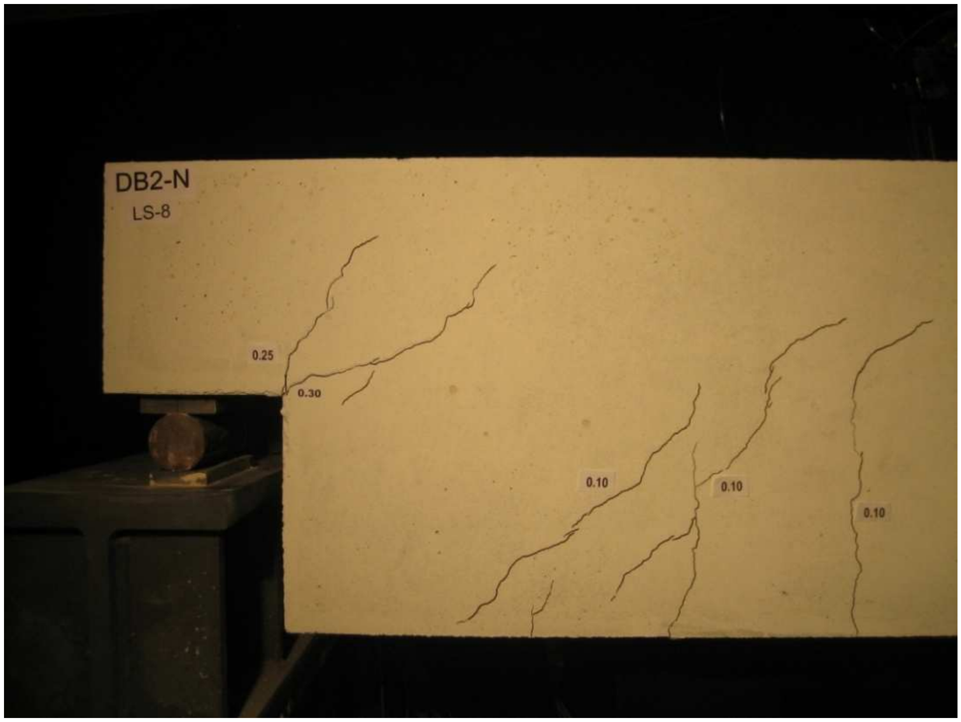

Figure 3.39 Photo of crack pattern at LS-8 for DB2-N

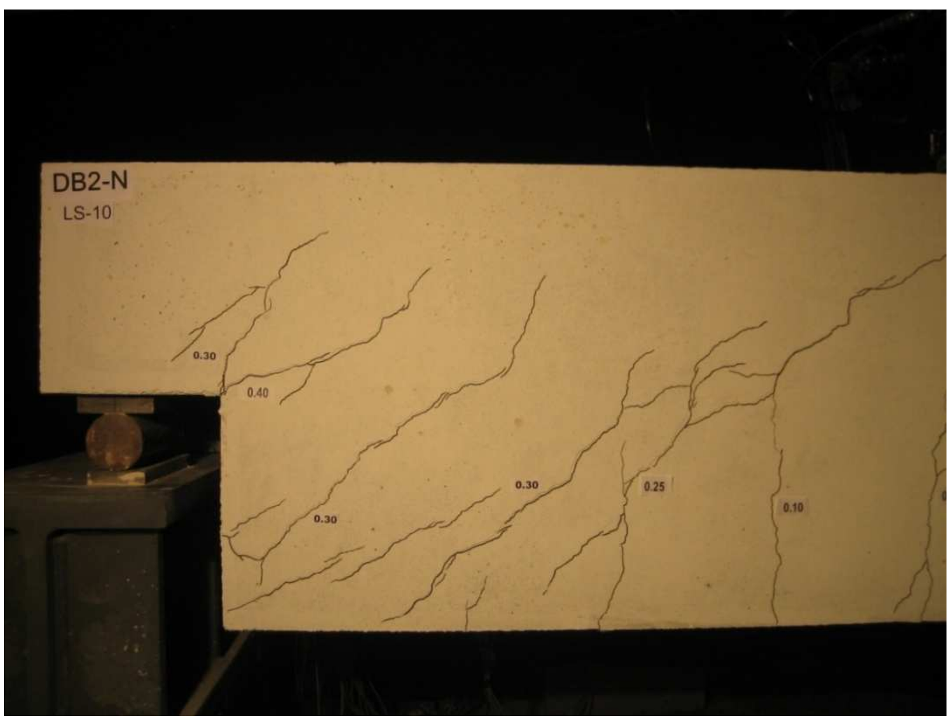

Figure 3.36 Photo of crack pattern at LS-10 for DB2-N

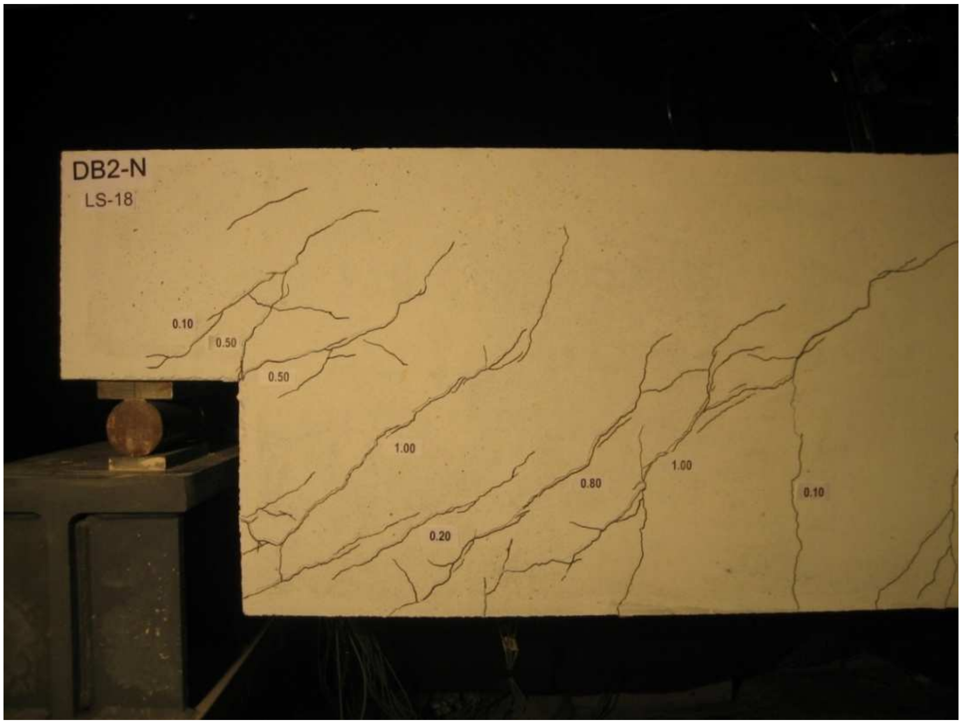

Figure 3.37 Photo of crack pattern at LS-18 for DB2-N

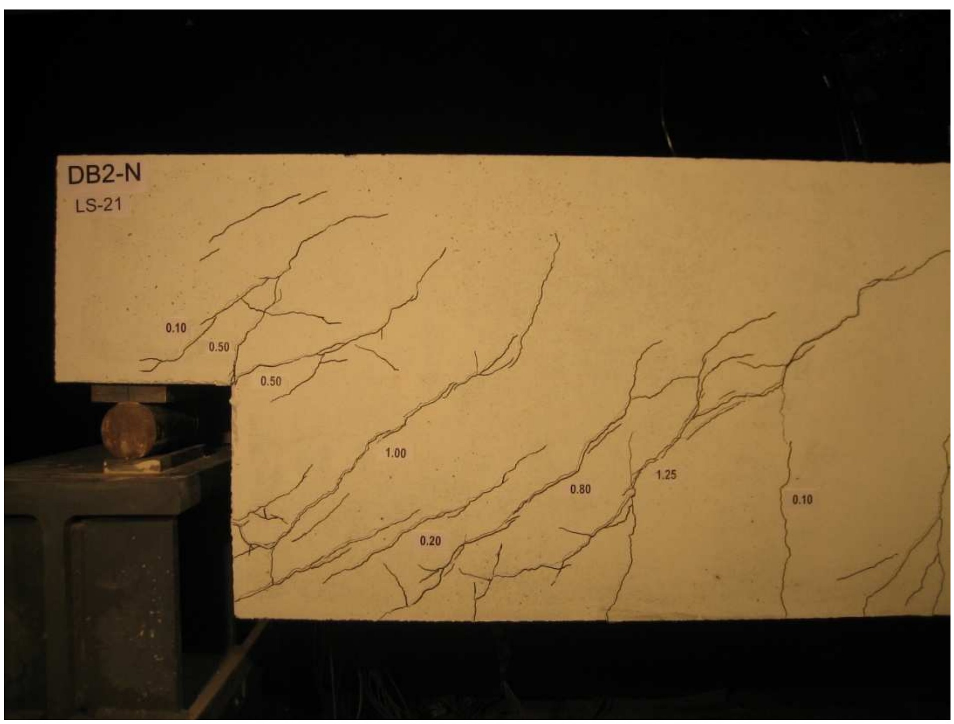

Figure 3.38 Photo of crack pattern at LS-21 for DB2-N

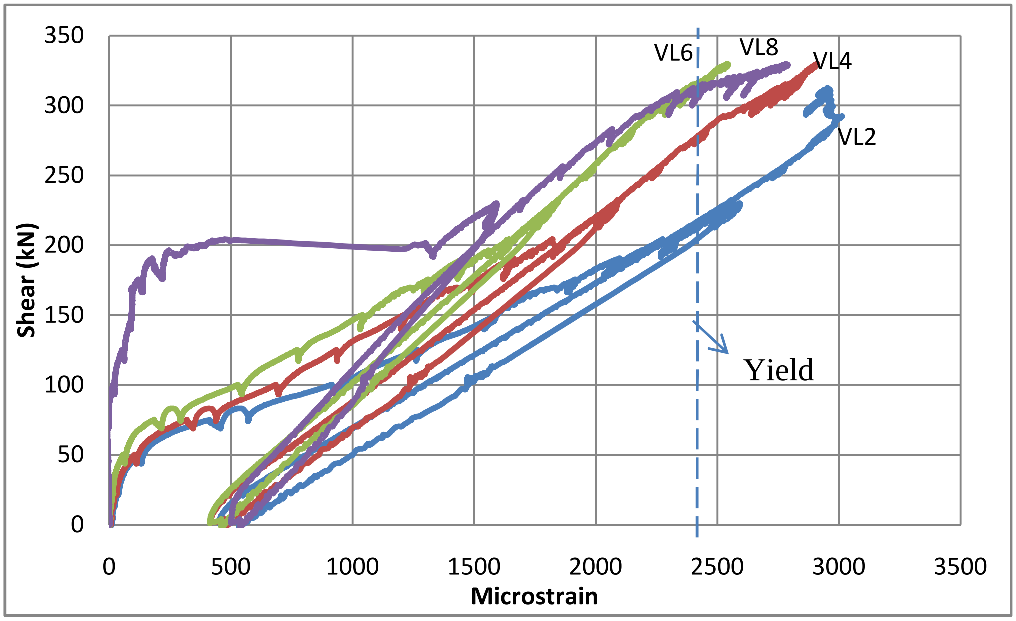

Figure 3.39 Shear versus strain in the hanger reinforcement and stirrup closest to the hanger bars at DB2-N (Loading 1&2)

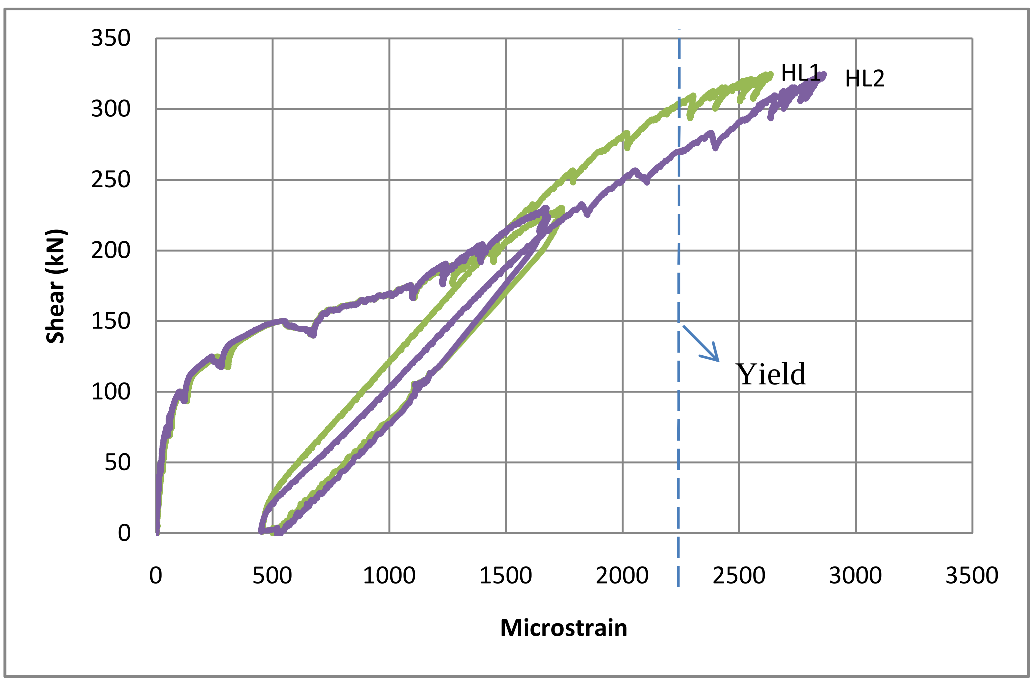

Figure 3.40 Shear versus strain in the horizontal 15M tension bars near the steel plate at DB2-N

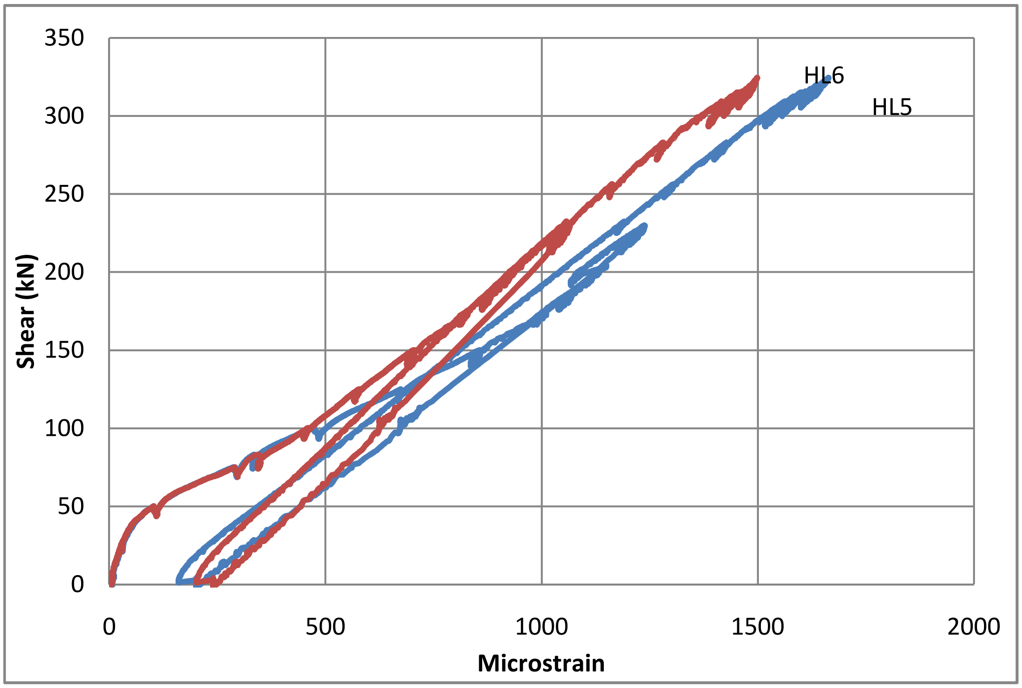

Figure 3.41 Shear versus strain in the horizontal 15M tension bars near the re-entrant corner at DB2-N

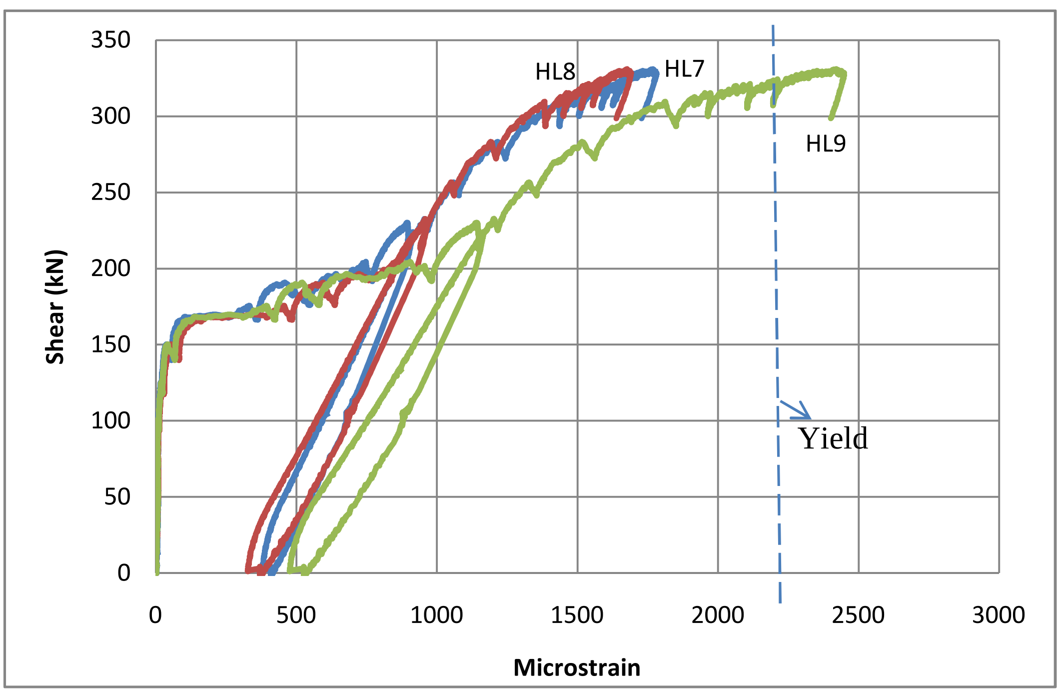

Figure 3.42 Shear versus strain in the bottom bend of hanger bars near the bend corners at DB2-N

CHAPTER 4

Analysis and Comparisons of Results

In this chapter, the analysis of the experimental results is presented. The shears and corresponding deflections are compared for the key load stages for dapped ends DB1-S, DB1-N, DB2-S and DB2-N. This chapter also discusses the failure modes and compares the strut-and-tie model prediction with the experimental results.

Table 4.1 summarizes the four different reinforcement details in the disturbed regions of dapped ends DB1-S, DB1-N, DB2-S and DB2-N. Figure 4.1 shows the photos of the reinforcing details of these specimens.

Table 4.1 Summary of differences in reinforcing details

	Differences in detailing
DB1-S	➢ The vertical hanger bars were not anchored around longitudinal reinforcing bars at both top and bottom ➢ Improper anchorage of bottom flexure reinforcement at the end of full-depth section
DB1-N	➢ The vertical hanger bars, with a 75 mm spacing, were anchored at both top and bottom by bending around longitudinal reinforcing bars, ➢ 2-15M U-bars (anchorage reinforcement) were located above the bottom flexure bars with a 50 mm spacing at the end of full-depth section
DB2-S	➢ The hanger bars with 90 degree hooked ends, with the hooks parallel to the longitudinal reinforcement, at the top and the bottom ➢ Two additional 10M vertical stirrups (shear reinforcement) in the nib
DB2-N	➢ The three vertical hanger bars were tied as close as practical and were anchored around the top and bottom longitudinal reinforcement ➢ Two additional 10M vertical stirrups (shear reinforcement) in the nib ➢ Three 15M horizontal tension bars anchored by welding to a steel plate in the end of full-depth section at the same level of bottom flexure reinforcement

4.1 Comparison of Experimental Results

4.1.1 Overall behaviour

Table 4.2 provides the measured shear and the corresponding deflections at first cracking, first yielding of the hanger reinforcement, and the maximum shear for the dapped ends. Figure 4.2 shows the comparison of the shear versus deflection responses of the four dapped ends. Figures 4.3 and 4.4 compare the responses of dapped ends DB1-S and DB1-N as well as DB2-S and DB2-N, respectively.

From the comparison shown in Table 4.2 and Fig. 4.2, it is apparent to see that the shear capacity is much higher with for those specimens with proper anchorage of both the vertical hanger reinforcement and the horizontal flexural reinforcement. The ultimate shear reached was 271.2 kN for DB1-N, which is 41.5% higher than the maximum shear reached in DB1-S (see Fig. 4.3). For DB2, The ultimate shear reached was 331.0 kN fro DB1-N, which is 43.9% higher than the maximum shear reached in DB1-S (see Fig. 4.4).The first cracking of all the dapped ends occurred at the re-entrant corner and Table 4.2 compares the shears and the deflections at first cracking. From Fig. 4.2, it is clear that the two dapped ends having the hanger reinforcement replaced close to the dapped end, had the higher initial stiffness than the other two dapped ends. DB2-N gave the smallest deflection with highest shear at first cracking. Dapped end DB2-N had the highest capacity and displayed some ductility after yielding of the hanger reinforcement. DB1-N with proper anchorage of the hanger steel exhibited yielding of this steel but failed in shear in the beam region due to the fact that the beam region contained only 4 stirrups, whereas DB2-N had 5 stirrups.

Table 4.2 The summary of the key shear and deflections during the test

		DB1-S	DB1-N	DB2-S	DB2-N
First cracking	Shear (kN)	42.5	42.5	50.0	50.0
	Deflection* (mm)	0.23	0.21	0.30	0.26
First yielding of hanger reinforcement	Shear (kN)	156.4	185.2	226.1	218.1
Maximum shear	Shear (kN)	193	273	228	329
	Deflection* (mm)	2.75	4.49	4.03	7.18

* The deflection at the end of full-depth section

4.1.2 Comparison of failure modes

Table 4.3 summarizes the failure modes for the four different dapped ends (DB1-S, DB1-N, DB2-S and DB2-N). The behaviour of DB1-S and DB2-S were unsatisfactory. For DB1-S, due to the improperly anchored hanger steel and bottom flexural reinforcement, only the outermost legs of the hanger reinforcement, closest to the nib, yielded. For DB2-

S, due to the improperly anchored hanger reinforcement where the 90 degree hooked ends of the hanger steel were paralleled to the longitudinal reinforcement at the top and the bottom, diagonal tension cracks occurred at the level of the top hooks, and first yielding occurred in the horizontal tension bars prior to yielding of the hanger reinforcement. Both DB1-N and DB2-N exhibited yielding of the hanger reinforcement and they both behaved as expected, with maximum shears considerably above the strut-and-tie model predictions.

Table 4.3 Summary of the failure mode of each detailing ends

	Failure mode comparison
DB1-S	➢ A combined bond and diagonal tension failure occurred in the end of full-depth section below the improperly anchored hanger steel ➢ Before failure, only the outermost legs, nearest the nib, of the vertical hanger reinforcement reached yielding
DB1-N	➢ A combined bond and diagonal tension failure occurred in the full-depth beam section adjacent to the dapped end after yielding occurred in the hanger reinforcement ➢ All of the three vertical hanger reinforcement yielded during Loading 2
DB2-S	➢ A diagonal tension failure occurred at the level of the top hooks of the improperly anchored hanger steel ➢ The horizontal 15M tension bars in the nib yielded prior to the vertical hanger reinforcement
DB2-N	➢ Significant yielding of the vertical hanger steel occurred as well as the stirrup closest to the hanger steel ➢ The well anchored longitudinal reinforcement yielded

Figures 4.5 and 4.6 compare the cracking at first yielding and close to maximum load level for the four different dapped ends. It is evident that the proper anchorage and proper hanger reinforcement details had a profound effect on the type of failure.

4.2 Comparisons with Strut and Tie Model Prediction

The strut and tie models (following the design example in the 2005 CAC Concrete Design Handbook) used for the design of DB1 and DB2 are presented in Fig. 2.1 and Fig. 2.3. The following assumptions were made for the design of both beams: the tension tie BC in the strut and tie models would yield before the yielding of all other steel tension ties; and crushing of the concrete compressive struts would not occur. It is noted that for each dapped end, the tension tie BC had the same area and yield force. Three 10M double-legged stirrups (600 mm^2 cross-sectional area) were used for DB1-S, DB1-N and DB2-N and three 15M reinforcing bars with 90 degree hooked ends (600 mm^2 cross-sectional area) were used for DB1-S.

In order to predict the strength using a strut-and-tie model, the vertical tension force in tie BC is taken as the yield force of 494 × 6 × 100 = 294.6 kN. Using this force and the strut-and-tie model, the predicted shear at yielding of the hanger steel was determined for specimens DB1-N and DB2-N (see Tables 4.4 and 4.5). These predictions are close to the shear corresponding to first yielding measured in the hanger steel. The forces of the entire truss were obtained using the CAST software (Kuchma and Tjhin, 2005). Figures 4.7 and 4.8 present the resulting forces in the strut and tie in the model for this analysis. Table 4.6 also shows the predictions if it is assumed that the vertical hanger steel reaches its ultimate stress. It is noted that very high strains were measured in the hanger steel of both of these well detailed dapped ends. It was also assumed that the stirrup closest to the hanger steel also contributed to the hanger reinforcement. As can be seen from Table 4.6, the predicted ultimate capacities are slightly higher than the test capacities.

From Table 4.6, it is clear that measured shears at first yield are greater than the predicted shears at yield by 2.4% for DB1-N and 7.0% for DB2-N. The measured maximum shears exceed the predicted shears, assuming an ultimate stress in the hanger reinforcement by 13.7% for DB1-N and 3.3% for DB2-N.

Table 4.4 Forces in the strut-and-tie truss members for DB1

Reaction force: 189.7 kN			
Truss member	Forces (kN)	Truss member	Forces (kN)
AB	-309.0	DE	-268.3
AD	243.9	CF	296.4
BD	-173.8	EF	189.7
BC	296.4	EG	-296.4
BE	-106.7	FG	-351.9
CD	-419.2	FH	592.8

Table 4.5 Forces in the strut-and-tie truss members for DB2

Reaction force: 203.9 kN			
Truss member	Forces (kN)	Truss member	Forces (kN)
AB	-295.3	DE	-289.9
AD	213.6	CF	299.5
BD	-151.6	EF	203.9
BC	296.4	EG	-299.5
BE	-93.4	FG	-394.5
CD	-421.4	FH	637.2

Table 4.6 Comparison of shear between the prediction and experimental results

	Predicted shear at yield (kN)	Shear at first yield of hanger tension bars (kN)	Predicted shear at ultimate stress in hanger bars (kN)	Maximum shear (kN)
DB1-N	189.7	185.2	316.4	273.0
DB2-N	203.9	218.1	340.1	329.0

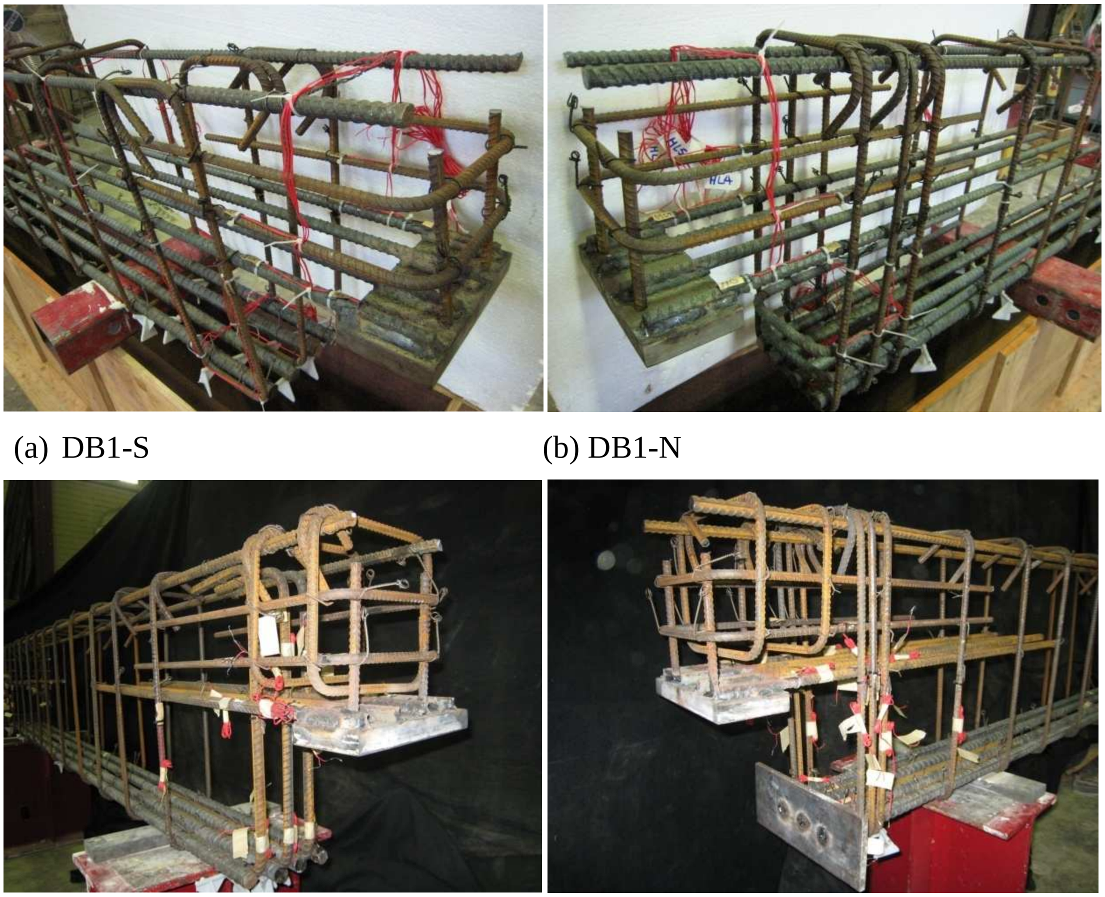

(a) DB1-S (b) DB1-N

(c) DB2-S (d) DB2-N

Figure 4.1 The reinforcing details at disturbed regions

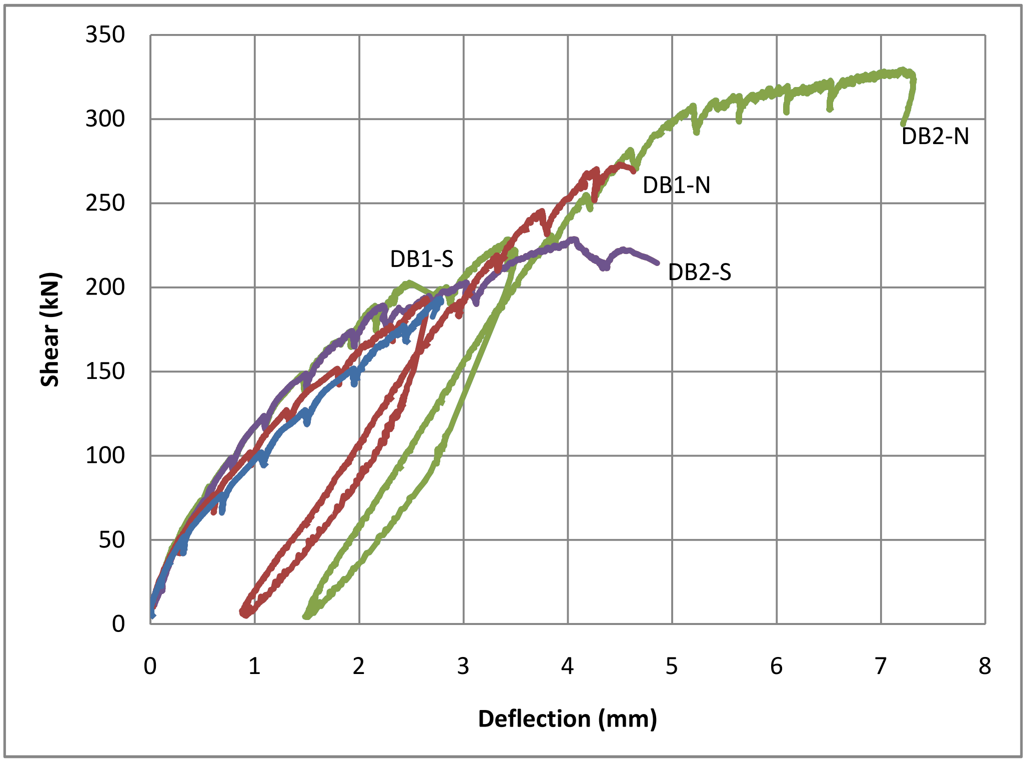

Figure 4.2 The shear versus deflection response for the four dapped ends

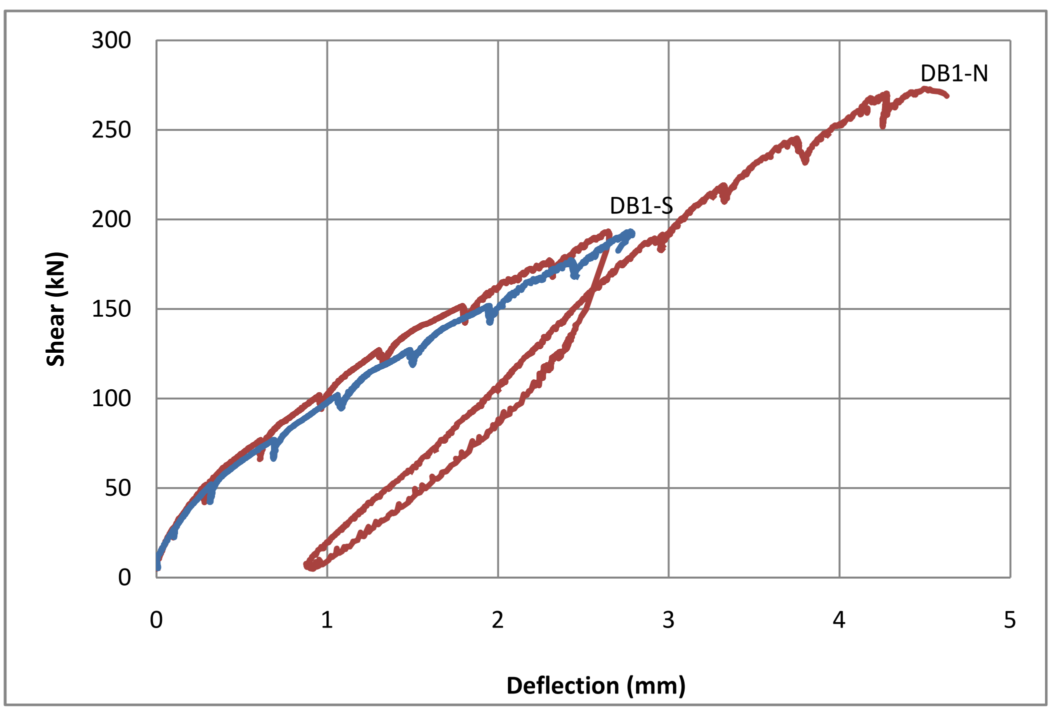

Figure 4.3 The shear versus deflection response for DB1-S and DB1-N

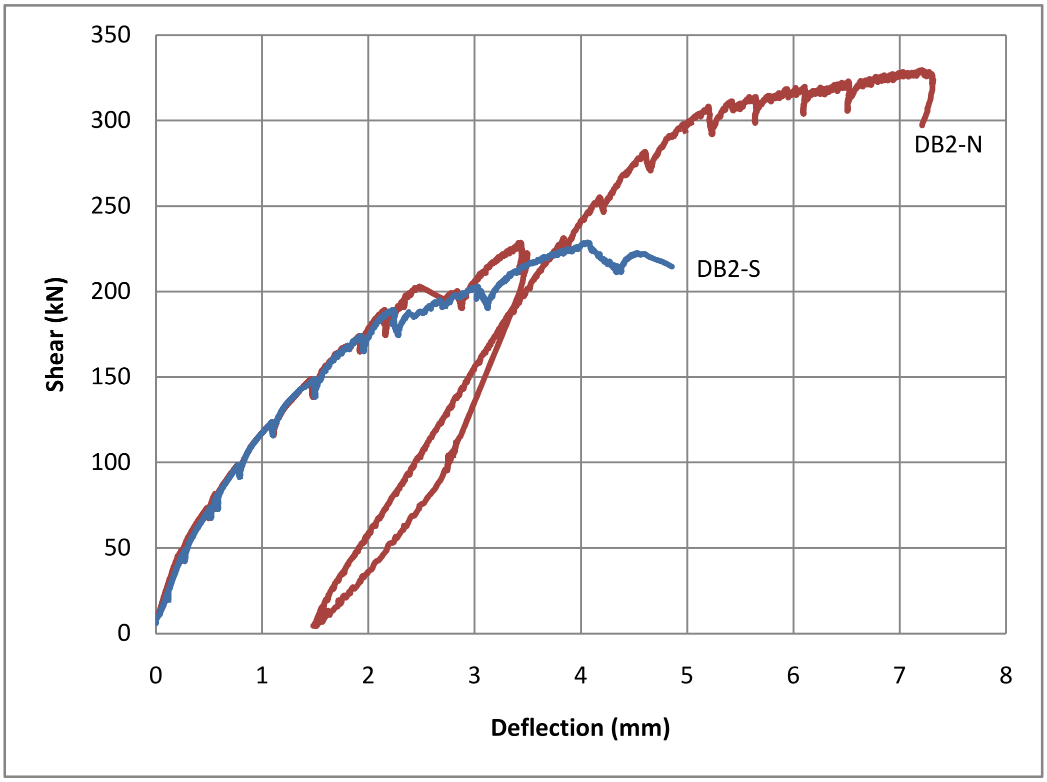

Figure 4.4 The shear versus deflection response for DB2-S and DB2-N

(a) DB1-S (b) DB1-N

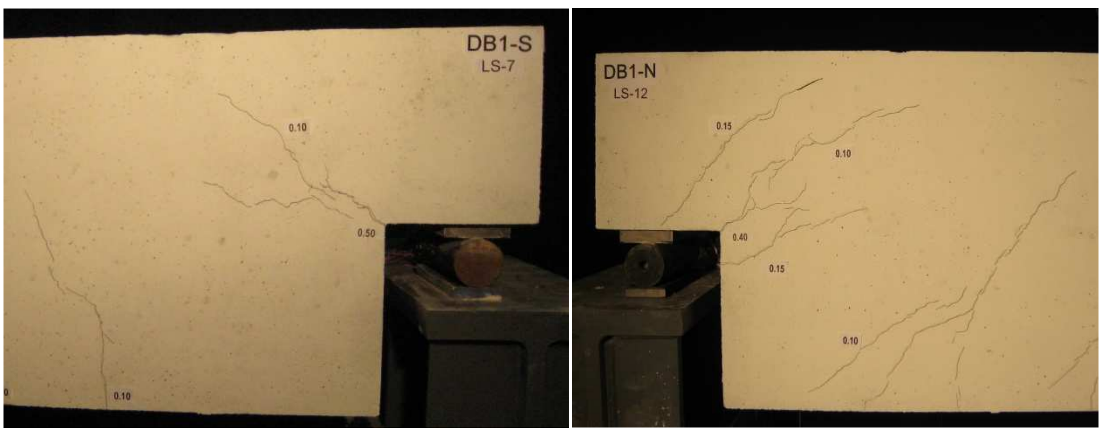

(c) DB2-S (d) DB2-N

Figure 4.5 The photos of cracking at first yielding for four different ends

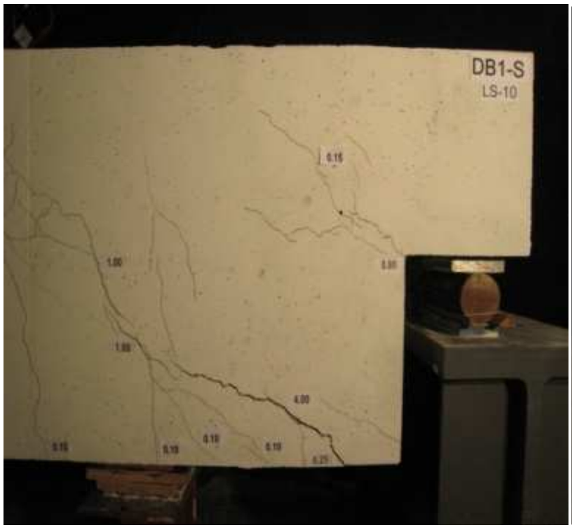

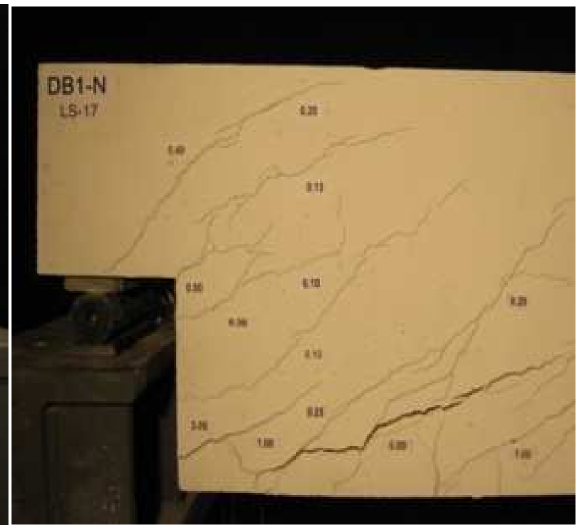

(a) DB1-S (b) DB1-N

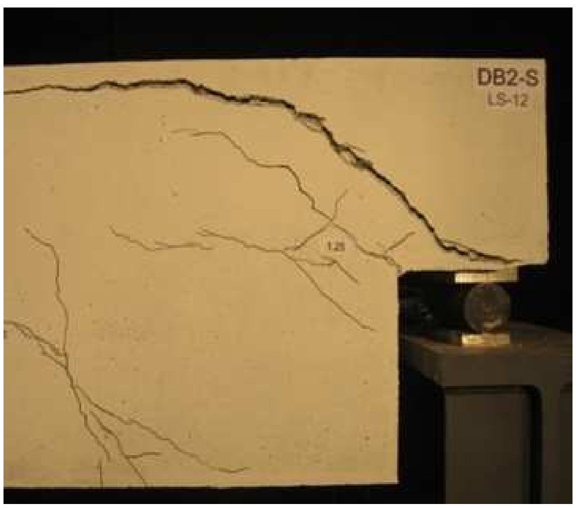

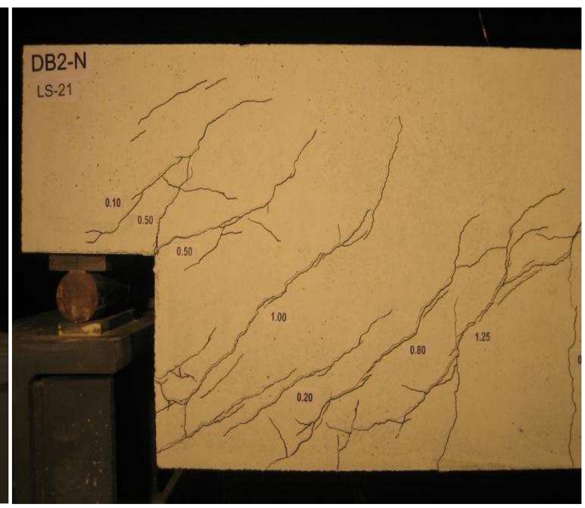

(d) DB2-S (d) DB2-N

Figure 4.6 The photos of cracking close to maximum shear for four different ends

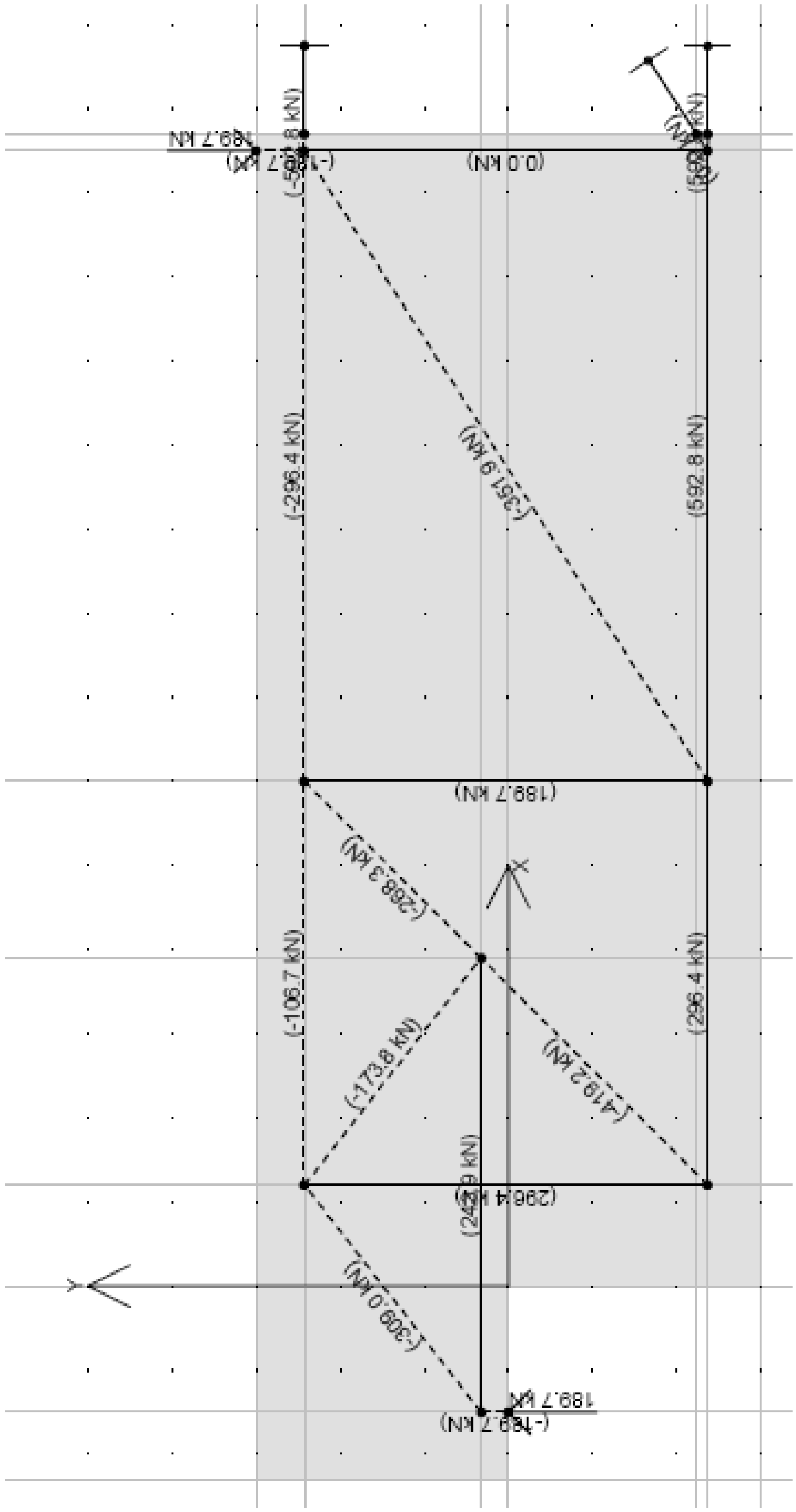

Figure 4.7 The results from CAST for DB1-N

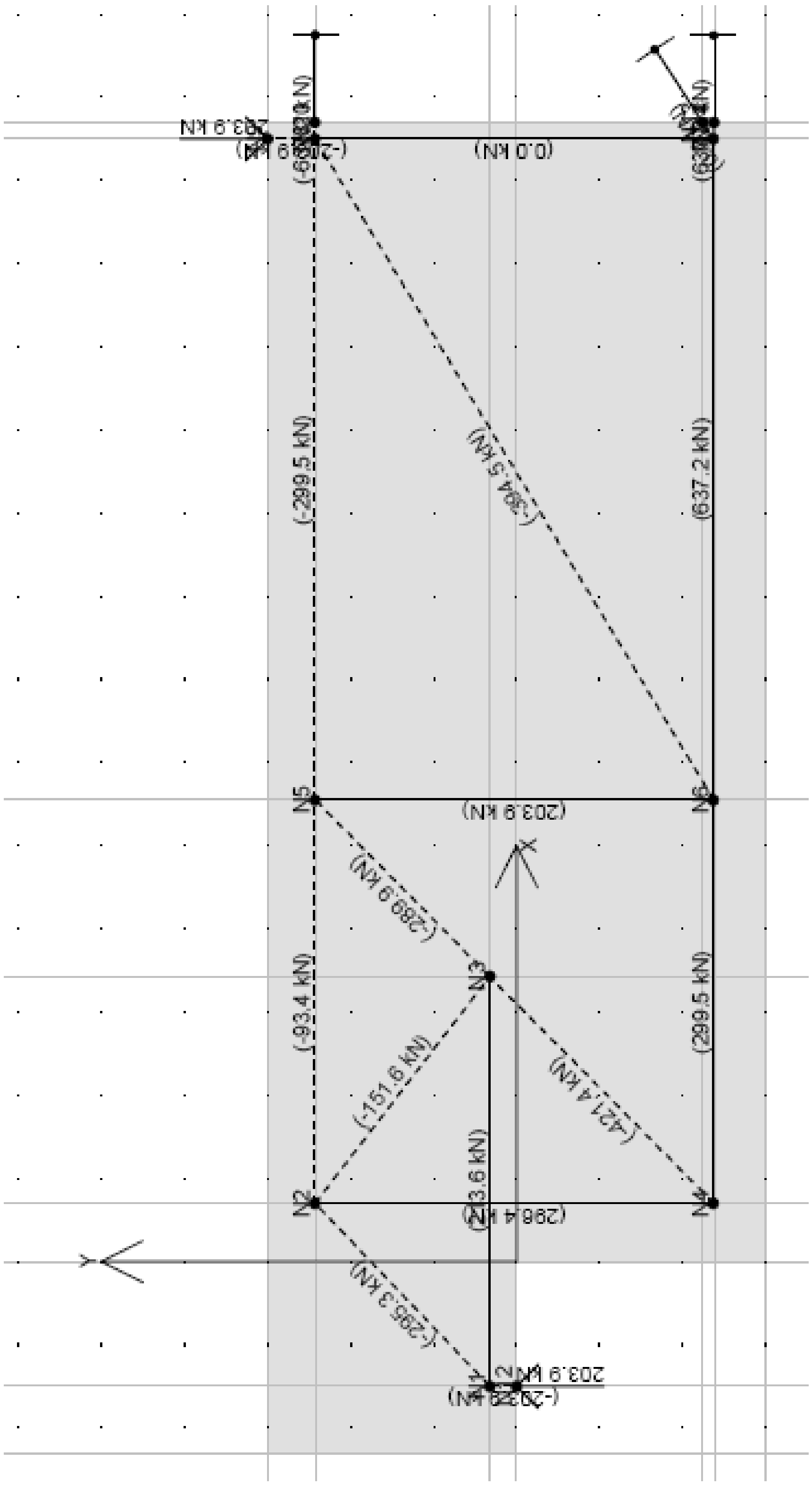

Figure 4.8 The results from CAST for DB2-N

CHAPTER 5

Conclusions

The following conclusions were drawn from the results of this experimental programme:

1. The two dapped ends with proper anchorage and hanger reinforcement details had maximum shears that were 42% and 44% higher than the other dapped ends having improper anchorage and hanger reinforcement details.
2. The dapped ends with proper anchorage and hanger reinforcement resulted in a higher capacity and some ductility after yielding of the hanger reinforcement.
3. It is evident that the proper anchorage and proper hanger reinforcement details had a profound effect on the type of failure. The dapped ends with poor anchorage details failed in a brittle manner without yielding of all of the hanger reinforcement.
4. It was found that anchorage details recommended in the 1971 PCI Design Handbook and the alternative anchorage details in the 1999 PCI Design Handbook are deficient and result in brittle failure modes.
5. The hanger reinforcement placed close to the dapped ends provides higher shear capacity.
6. The anchorage of the flexural reinforcement by welding the bars to a steel plate at the end of full-depth section provides excellent end anchorage.
7. The measured shears at first yield are greater than the predicted shears using strut-and-tie models by 2% for DB1-N and 7% for DB2-N. The measured maximum shears exceeded the predicted shears, assuming ultimate stress in the hanger reinforcement (by 14% for DB1-N and 3% for DB2-N). It was found that the stirrup closest to the hanger reinforcement also served as hanger reinforcement.

REFERENCES

AASHTO, 1994, "AASHTO LRFD Bridge Specifications for Highway Bridges," American Association of Highway and Transportation Officials, 1^{st} edition, Washington, DC, 1091 pp.

AASHTO, 2004, "AASHTO LRFD Bridge Specifications for Highway Bridges," American Association of Highway and Transportation Officials, 2^{nd} edition, Washington, DC, 1116 pp.

ACI Committee 318, 1977, "Building Code Requirements for Reinforced Concrete (ACI 318-77)," American Concrete Institute, Detroit, MI.

ACI Committee 318, 1983, "Building Code Requirements for Reinforced Concrete (ACI 318-83)," American Concrete Institute, Detroit, MI.

ACI Committee 318, 1995, "Building Code Requirements for Reinforced Concrete (ACI 318M-95) and Commentary (ACI 318M-95)-Appendix A," American Concrete Institute, Detroit, MI, pp. 369-384.

ACI Committee 318, 2002, "Building Code Requirements for Reinforced Concrete (ACI 318M-02) and Commentary (ACI 318R-02)," American Concrete Institute, Farmington Hills, MI, 443 pp.

ASCE-ACI Committee 445 on Shear and Torsion, 1998, "Recent Approaches to Shear Design of Structural Concrete", Journal of Structural Engineering, ASCE, V. 124, No. 12, pp. 1375-1417.

CAC, 2005, Third Edition, "Concrete Design Handbook," Cement Association of Canada, Ottawa, ON.

Collins, M.P., and Mitchell, D., 1986, "A Rational Approach to Shear Design – The 1984 Canadian Code Provisions," ACI Journal, Vol.83, No. 6, pp. 925-933.

Commission of Inquiry, 2007, "Report – The Collapse of a Portion of the de la Concorde Overpass", Montreal, QC, 222 pp.

Cook, W.D. and Mitchell, D., 1988, "Non-linear Analysis of Disturbed Reinforced Concrete Regions", Journal of the American Concrete Institute, Vol. 85, No. 2, pp. 206-216.

CPCA, 1985, “Concrete Design Handbook,” Canadian Portland Cement Association, Ottawa, ON.

CSA Technical Committee A23.3, 1984, “Design of Concrete Structures,” CAN3-A23.3-M84, Canadian Standard Association, Rexdale, ON, 281 pp.

CSA Technical Committee A23.3, 1994, “Design of Concrete Structures,” CSA A23.3-04, Canadian Standard Association, Rexdale, ON, 199 pp.

CSA Technical Committee A23.3, 2004, “Design of Concrete Structures,” CSA A23.3-04, Canadian Standard Association, Mississauga, ON, 214 pp.

Collins, M.P., Bentz, E., and Mitchell, D., 2006, “Chapter 4 – Shear and Torsion”, Concrete Design Handbook, Cement Association of Canada, Ottawa, ON, pp. 4-1 - 4-42.

Hamondi, A. A. and Phang, M. K. S., 1974, “Shear Strength of Post-tensioned Daps in Prestressed Concrete Beams,” Journal of Structural Engineering, Vol. 100, No. 12, pp. 2403-2418.

Kuchma D. and Tjhin T., 2005, “CAST (Computer Aided Strut-and-Tie),” University of Illinois, Urbana, IL.

Kupfer, H., 1964, “ Erweiterung der Morsch schen Fachwerkanalogie mit Hilfe des Prinzips vom Minimum der Formanderungsarbeit (Generation of Mörsch’s Truss Analogy Using the Principle of Minimum Strain Energy),” Comite Euro-International du Beton, Bulletin d’Information, No. 40, CEB, Pairs, pp. 44-57.

Marchand, J. and Mitchell D., 2007, “Rapport sur les causes techniques de l’effondrement du viaduct de la Concorde”, Rapport principal, Commission d’enquete sur le viaduc de la Concorde, 184 pp.

Marti, P., 1985, “Basic Tools of Reinforcement Concrete Beam Design,” ACI Journal, Proceedings, Vol. 82, No. 1, pp. 45-56.

Mattock A. H., 1976, “Design Proposals for Reinforced Concrete Corbels,” PCI Journal, Vol. 21, No. 3, pp. 18-42.

Mattock, A. H. and Chan, T. C., 1979, “Design and Behaviour of Dapped-End Beams,” PCI Journal, Vol. 24, No. 6, pp. 25-45.

Mattock, A. H. and Theryo, T. S., 1986, "Strength of Precast Prestressed Concrete Members with Dapped Ends," PCI Journal, Vol. 31, No. 5, pp. 58-75.

Mitchell, D. and Collins, M. P., 1990, "Prestressed Concrete Structures," Prentice Hall, New York, 747 pp.

Mitchell, D., Collins, M. P., Bhide, S. B., and Rabbat, B. G., 2004, "AASHTO LRFD Strut-and-Tie Model Design Examples," Portland Cement Association, 60 pp.

Mitchell, D. and Cook, W.D., 2007, "Evaluation of Structural Design – de la Concorde and de Blois Bridges", Annex 7, Inquiry on the Collapse of the de la Concorde Bridge., 46 pp.

Mitchell, D. and Cook, W.D., 2007, "Experimental Simulation of Cantilever - de la Concorde Bridge", Annex 8, Inquiry on the Collapse of the de la Concorde Bridge., 50 pp.

Mitchell, D. and Cook, W.D., 2007, "Non-Linear Analysis of Cantilever - de la Concorde Bridge", Annex 9, Inquiry on the Collapse of the de la Concorde Bridge., 40 pp.

Mörsch, E., 1909, "Concrete-Steel Construction (Der Eisenbetonbau)," Translation of the 3rd German Edition by E. P. Goodrich, McGraw Hill Book Co., New York, 368 pp.

PCI Design Handbook (First Edition), 1971, "Precast and Prestressed Concrete", Prestressed Concrete Institute, Chicago.

PCI Design Handbook (Second Edition), 1978, "Precast and Prestressed Concrete", Prestressed Concrete Institute, Chicago.

PCI Design Handbook (Third Edition), 1985, "Precast and Prestressed Concrete", Prestressed Concrete Institute, Chicago.

PCI Design Handbook (Forth Edition), 1999, "Precast and Prestressed Concrete", Prestressed Concrete Institute, Chicago.

Prestressed Concrete Institute (CPCI), 1982, First Edition, "Metric Design Manual – Precast and Prestressed Concrete," Ottawa.

Ritter, W., 1899, "The Hennebique Design Method (Die Bauweise Hennebique)," Schweizerische Bauzeitung (Zurich), Vol. 33, No. 7, pp. 59-61.

Schlaich, J., Schäfer, K., 1984, "Konstruieren im Stahlbetonbau," Beton-Kalender, Wilhelm Ernst und Sohn, Berlin, pp. 787-1004.

Schlaich, J., Schäfer, K., and Jennewein, M., 1987, "Toward a Consistent Design of Structural Concrete," PCI Journal, Vol. 32, No. 3, pp. 74-150.

Schlaich, J., Schäfer, K., 1991, "Design and Detailing of Structural Concrete Using Strut-and-Tie Models," The Structural Engineer, Vol. 69, No. 6, pp. 113-125.

Thurlimann, B., Marti, P., Pralong, J., Ritz, P., and Zimmerli, B., 1983, "Application of the theory of Plasticity of Reinforced Concrete (Anwendung der Plastizitaetstheorie auf Stahlbeton)," Institute for Structural Engineering, ETH Zurich, 252 pp.

Werner, M. P., and Dilger, W. H., 1973, "Shear Design of Prestressed Concrete Stepped Beams," PCI Journal, V.18, No. 4, pp. 33-49.